UNIVERSIDADE ESTADUAL DE CAMPINAS

INSTITUTO DE BIOLOGIA

VALQUIRIA APARECIDA MATHEUS

“Ação anti-diabetogênica do butirato de sódio e seu efeito protetor sobre a barreira epitelial intestinal em camundongos alimentados com dieta hiperlipídica."

“Anti-diabetogenic action of sodium butyrate and its protective effect on the intestinal epithelial barrier in mice fed a high-fat diet”

Campinas, 2020

VALQUIRIA APARECIDA MATHEUS

“Ação anti-diabetogênica do butirato de sódio e seu efeito protetor sobre a barreira epitelial intestinal em camundongos alimentados com dieta hiperlipídica."

“Anti-diabetogenic action of sodium butyrate and its protective effect on the intestinal epithelial barrier in mice fed a high-fat diet”

Tese apresentada ao Instituto de Biologia da Universidade Estadual de Campinas como parte dos requisitos exigidos para a obtenção do título de Doutora em Biologia Celular e Estrutural, na área de Biologia Tecidual.

Thesis presented to the Biology Institute of the University of Campinas in partial fulfillment of the requirements for of PhD in Cellular and Structural Biology, subarea Tissue Biology.

ORIENTADORA: CARLA BEATRIZ COLLARES BUZATO

ESTE ARQUIVO DIGITAL CORRESPONDE À VERSÃO FINAL DA TESE DEFENDIDA PELA ALUNA VALQUIRIA APARECIDA MATHEUS E ORIENTADA PELA PROFA. DRA. CARLA BEATRIZ

Campinas, 2020

Ficha catalográfica
Universidade Estadual de Campinas
Biblioteca do Instituto de Biologia
Mara Janaina de Oliveira - CRB 8/6972

Matheus, Valquiria Aparecida, 1977-
M421a Ação anti-diabetogênica do butirato de sódio e seu efeito protetor sobre a barreira epitelial intestinal em camundongos alimentados com dieta hiperlipídica / Valquiria Aparecida Matheus. – Campinas, SP : [s.n.], 2020.

Orientador: Carla Beatriz Collares Buzato.
Tese (doutorado) – Universidade Estadual de Campinas, Instituto de Biologia.

1. Junções íntimas. 2. Mucosa intestinal. 3. Butirato de sódio. 4. Diabetes mellitus tipo 2. 5. Obesidade. I. Collares Buzato, Carla Beatriz, 1965-. II. Universidade Estadual de Campinas. Instituto de Biologia. III. Título.

Informações para Biblioteca Digital

Título em outro idioma: Anti-diabetogenic action of sodium butyrate and its protective effect on the intestinal epithelial barrier in mice fed a high-fat diet
Palavras-chave em inglês:
Tight junctions
Intestinal mucosa
Sodium butyrate
Diabetes mellitus, Type 2
Obesity
Área de concentração: Biologia Tecidual
Titulação: Doutora em Biologia Celular e Estrutural
Banca examinadora:
Carla Beatriz Collares Buzato [Orientador]
Carolina Prado de França Carvalho
Elaine Minatel
Luciana Le Sueur Maluf
Valéria Helena Alves Cagnon Quitete
Data de defesa: 17-07-2020
Programa de Pós-Graduação: Biologia Celular e Estrutural

Identificação e informações acadêmicas do(a) aluno(a)
- ORCID do autor: https://orcid.org/0000-0001-8528-8004
- Currículo Lattes do autor: http://lattes.cnpq.br/9385542078624760

Campinas, 17 de julho de 2020

BANCA EXAMINADORA

Profa Dra Carla Beatriz Collares Buzato

Profa Dra Carolina Prado de França Carvalho

Profa Dra Elaine Minatel

Profa Dra Luciana Le Sueur Maluf

Profa Dra Valéria Helena Alves Cagnon Quitete

Os membros da Comissão Examinadora acima assinaram a Ata de Defesa, que se encontra no processo de vida acadêmica do aluno.

A Ata da defesa com as respectivas assinaturas dos membros encontra-se no SIGA/Sistema de Fluxo de Dissertação/Tese e na Secretaria do Programa de Pós-Graduação em Biologia Celular e Estrutural do Instituto de Biologia da Universidade Estadual de Campinas - UNICAMP.

AGRADECIMENTOS

Agradeço primeiramente a minha orientadora Professora Doutora Carla Beatriz Collares Buzato por ter me recebido em seu laboratório e pela oportunidade de desempenhar esse trabalho oferecendo todo apoio necessário para a execução do mesmo. Aos membros da banca que prontamente atenderam ao convite dedicando parte de seu tempo para ler e contribuir com a presente Tese.

Sou grata aos meus pais (*in memorian*) por me ensinarem o verdadeiro valor do trabalho, do respeito ao próximo e da honestidade acima de tudo. Sou grata a minha irmã com quem desde o início aprendi o que é compartilhar e a compreender as diferenças individuais (que existem até mesmo entre irmãos). Aos amigos os quais considero minha segunda família: Valdirene Barbosa, Mônica Mattielo, Leandro Canuto, Laura Penedos, Luis Gomez e Ariane de Sant'ana por estarem ao meu lado nos melhores e nos piores momentos de minha vida e por acreditarem em mim e no meu potencial. São nessas pessoas, juntamente com minha irmã, que encontro forças para continuar e me esforço para ver o lado positivo de qualquer situação.

Agradeço aos meus queridos companheiros de laboratório por terem me recebido tão bem e por terem compartilhado seus conhecimentos, em especial ao Ricardo Beltrame de Oliveira, pessoa que mais contribuiu para o meu aprendizado técnico durante minha passagem pelo laboratório. Aos colegas pesquisadores Gabriela Moreira Soares e Felippe Mousovich Neto que participaram diretamente na coleta de dados desta tese. Aos técnicos que, de alguma forma, contribuíram para a execução prática deste trabalho: Susy Tada, Fabiana Kuhne, Cláudio Zoppi, Emerielle Vanzela, Cinthia Rizoli, Thais Holtz e Luis Henrique (Kiko).

Aos professores Alexandre L. R. de Oliveira, Valéria H. A. C. Quitete, Sílvio Roberto Consonni, Elaine Minatel, aos seus alunos e ao Infabic, por facilitarem o acesso aos equipamentos necessários para a execução desse projeto. E as professoras Sarah e Lúcia pelo apoio e incentivo. Sou grata aos companheiros de departamento Monique Mendonça, Carolina Mantovani, Viviane Rosa, Bianca Castelucci e Paula Dellati pela amizade e apoio nos momentos de dificuldade.

O presente trabalho foi realizado com apoio da Coordenação de Aperfeiçoamento de Pessoal de Nível Superior - Brasil (CAPES) - Código de Financiamento 001. Agradeço às agências de fomento CNPq (Processo 141442/2018-2) e Fundação de Amparo a Pesquisa – São Paulo (FAPESP - Processo 2018/02118-2)**,** ao departamento de Bioquímica e Biologia Tecidual e ao Instituto de Biologia da Unicamp.

RESUMO

O trato intestinal, além de atuar no processo de absorção, desempenha importante função de barreira contra agentes nocivos, sejam eles microorganismos ou antígenos provenientes da alimentação. Alterações na morfologia e na função desta barreira parecem contribuir com a patogênese de várias doenças, incluindo o diabetes melito, doença metabólica crônica que afeta milhões de pessoas por todo o mundo. Estudos com o butirato de sódio, um ácido graxo de cadeia curta (AGCC), proveniente do metabolismo da microbiota intestinal, têm mostrado efeito positivo sobre o metabolismo e sobre a barreira intestinal em situações patológicas. A presente Tese de Doutorado tem como objetivo geral estudar a possível ação anti-diabetogênica do butirato de sódio e seu efeito protetor sobre a barreira epitelial intestinal mediada pelas junções de oclusão (JO) em modelos *in vivo* e *in vitro* de diabetes melito tipo 2 (DMT2). Camundongos machos adultos, da linhagem C57BL6J, foram distribuídos em quatro grupos experimentais: controle (C); controle+butirato (CB); dieta hiperlipídica (DHL); dieta hiperlipídica+butirato (DB) (n=36 animais/grupo), os quais foram mantidos num período de tratamento de 60 dias. A suplementação com butirato inibiu significativamente as disfunções metabólicas induzidas pela DHL (como intolerância à glicose e resistência à insulina, hiperglicemia jejum e pós-prandial e hiperinsulinemia), bem como reduziu significativamente o ganho de peso e aumentou de forma significativa o gasto energético (avaliado em câmara metabólica). Tais efeitos do butirato foram observados sem alteração da ingestão calórica diária, da expressão hipotalâmica de genes orexigênicos e anorexigênicos e da atividade locomotora. Ainda, em comparação com o grupo DHL, os animais do grupo DB apresentaram um aumento na função secretora de insulina (em ensaio *in vitro* de secreção estática em ilhotas isoladas), diminuição significativa na adiposidade e na razão massa gorda/massa magra (como avaliado por microtomografia computadorizada), preservação das características morfológicas do tecido adiposo marrom, aumento da expressão de UCP-1 nesse tecido e inibição significativa do quadro de esteatose hepática e de acúmulo de gordura no pâncreas. Quanto à avaliação da estrutura da barreira intestinal, mediada pelas proteínas da junção de oclusão (JO), o tratamento com butirato reverteu os efeitos deletérios da ingestão de DHL sobre a estrutura da JO, observada por imunomarcação juncional de claudinas -1 -2 -3 e de ZO-1 no epitélio de diferentes segmentos do intestino delgado e grosso, bem como reduziu a permeabilidade intestinal a marcadores paracelulares Ainda, esse AGCC não teve um efeito tóxico sistêmico, avaliado através de parâmetros hematológicos e bioquímicos séricos dos camundongos. No modelo *in vitro* de barreira intestinal, observamos que as células da linhagem Caco-2, expostas ao lavado do conteúdo luminal intestinal de animais que receberam a suplementação com butirato (CB e DB), apresentaram um reestabelecimento da estrutura e função da barreira epitelial mediada pela JO quando comparadas àquelas expostas ao conteúdo intestinal dos animais que receberam a dieta sem suplementação (C e DHL), o que corrobora os dados *in vivo*. Em conclusão, a suplementação com butirato inibe o efeito diabetogênico do consumo de DHL atenuando as disfunções bioquímicas, teciduais e metabólicas e reforçando a barreira intestinal mediada pela JO em modelos *in vitro* e *in vivo*.

ABSTRACT

The intestinal tract, besides acting in the nutrient absorption process, plays an important barrier function against harmful agents, whether they are microorganisms or food-derived antigens. Changes in the morphology and function of this barrier appear to contribute to the pathogenesis of several diseases, including diabetes mellitus, a chronic metabolic disease that affects millions of people worldwide. Butyrate, a short-chain fatty acid (SCFA) produced by the intestinal microbiota, has been shown to display a positive effect on metabolism and the intestinal barrier in pathological situations. This Ph.D. thesis aims to study the possible anti-diabetogenic action of sodium butyrate and its protective effect on the intestinal epithelial barrier mediated by tight junctions (TJ) in vivo and in vitro models of type 2 diabetes mellitus (T2DM). Adult male C57BL6J mice were distributed into four experimental groups, that were maintained in a 60-day treatment period: control (C), control + butyrate (CB), high-fat diet (HF), and HF diet + butyrate (HFB) groups (n = 36 animals/group). Butyrate supplementation significantly inhibited metabolic dysfunctions induced by HF diet (such as glucose intolerance, insulin resistance, fasting and postprandial hyperglycemia, and hyperinsulinemia), as well as significantly reduced weight gain while significantly increased energy expenditure (evaluated in the metabolic chamber). Such effects of butyrate were observed in the absence of significant alteration in daily caloric intake, hypothalamic expression of orexigenic and anorexigenic genes, or motor activity. Besides, in comparison with the HF group, the animals from the HFB group showed an increase in insulin secretory function (as assessed by *in vitro* static secretion assay in isolated islets), a significant decrease in adiposity and the fat mass/lean mass ratio (as assessed by microtomography), the preservation of the morphological characteristics of brown adipose tissue, increased expression of UCP-1 in this tissue accompanied by a significant inhibition of hepatic steatosis and accumulation of fat in the pancreas. Regarding the TJ-mediated intestinal barrier, butyrate treatment reversed the deleterious effects of HF diet ingestion on the TJ structure, evaluated by junctional immunostaining of claudins -1 -2 -3 and ZO-1 in the epithelium of different segments of the small and large intestine, as well as reduced the intestinal permeability to paracellular markers. Also, this SCFA did not seem to have a toxic effect, as revealed by the analysis of hematological and biochemical parameters. In the *in vitro* intestinal barrier model, we observed that Caco-2 cell monolayers, when exposed to the washing of the intestinal luminal content of animals that received butyrate supplementation (CB and HFB), showed a reestablishment of the structure and function of the TJ-mediated epithelial barrier as compared to those exposed to the intestinal content of animals that received the diet without supplementation (C and HF), which corroborates the *in vivo* data. In conclusion, butyrate supplementation inhibits the diabetogenic effect of HF diet consumption, attenuating biochemical, tissue, and metabolic dysfunctions and strengthening the intestinal barrier mediated by TJ *in vitro* and *in vivo* models.

LISTA DE ILUSTRAÇÕES

CAPÍTULO 1

CAPÍTULO 3

CAPÍTULO 4

CAPÍTULO 5

LISTA DE TABELAS

CAPÍTULO 2

CAPÍTULO 4

CAPÍTULO 5

LISTA DE ABREVIATURAS E SIGLAS

AGCC – Ácido graxo de cadeia curta
ALT – Alanina transaminase
AST – Aspartato aminotransferase
AgRP – Agouti-related protein
BAT – Brown adipose tissue
C – Controle
Caco-2 – Linhagem celular de adenocarcinoma colorretal
CB – Controle + Butirato
Cld – Claudina
CART – Cocaine- and amphetamine- regulated transcript
DHL – Dieta hiperlipídica
DMT1 – Diabetes melito tipo 1
DMT2 – Diabetes melito tipo 2
FFA – Free fat acid
FFAR – Free fat acid receptor
GRP – G receptor proteína (receptores acoplados à proteína G)
GTT – Teste de tolerância à glicose
HDAC – Histona deacetilase (enzima)
HDL – High-density lipoprotein
HF – High-fat diet
HFB – High-fat diet + butirato
IL – Interleucina
ITT – Teste de Tolerância à Insulina
JO – Junção de oclusão
LDL – Low-density lipoprotein
LPS – Lipopolissacarídeo
LY – Lucifer Yellow
NPY – Neuropeptide
RQ – Respiratory Quotient
Rt – Resistência transepitelial
SCFA – Short chain fatty acid
TEER – Transepithelial electrical resistance
TJ – Tight junction
TNF – Fator de necrose tumoral
T1DM – Type 1 diabetes mellitus
T2DM – Type 2 diabetes mellitus
UCP-1 – Uncoupling protein 1
VO_2 – Volume de oxigênio
ZO – Zonula occludens protein

Sumário

ESTRUTURA DA TESE

A presente Tese está estruturada em sete capítulos. O Capítulo 1 apresenta uma abordagem dos assuntos que estão relacionados ao tema desta Tese afim de trazer informações relevantes para a maior compreensão dos desafios e relevância apresentados nos capítulos seguintes. Para tal, há uma descrição do tubo digestório segundo sua anatomia e histologia com ênfase no epitélio intestinal, e da importância da função de barreira epitelial intestinal mediada pelas proteínas da junção de oclusão e como a disfunção dessa barreira pode estar envolvida na patogênese do *diabetes mellitus* tipo 2. Quanto ao butirato de sódio, traz pesquisas que demonstraram seu efeito em doenças intestinais inflamatórias possivelmente por meio do reforço da barreira epitelial intestinal, sua influência no crescimento e morte celular e também no metabolismo.

O Capítulo 2 traz a descrição detalhada das metodologias empregadas no desenvolvimento dessa Tese. Os resultados obtidos estão organizados na forma de artigos científicos redigidos na língua inglesa e apresentados nos Capítulos 3 a 5. No Capítulo 3, temos os resultados parciais, publicados em revista internacional indexada, que mostram o efeito protetor do butirato de sódio sobre a esteatose hepática e o acúmulo de gordura no pâncreas induzidos por DHL, que foram associados com melhora da função secretora da célula beta e reforço da barreira epitelial intestinal por meio do aumento do conteúdo juncional da proteína da junção de oclusão (JO), a Claudina-1, em animais pré-diabéticos. O Capítulo 4 traz os dados que demonstram um efeito anti-diabetogênico do butirato de sódio em disfunções metabólicas características da pré-diabetes tipo 2, como a hiperglicemia e a intolerância à glicose, juntamente com o seu efeito sobre o ganho de peso, adiposidade, gasto energético basal e consumo de oxigênio/estado funcional do tecido adiposo marrom. O Capítulo 5 mostra os resultados do efeito do butirato de sódio sobre a distribuição juncional e conteúdo proteico de outras proteínas do complexo juncional da JO (Claudinas -2, -3, Ocludina e ZO-1) no epitélio intestinal de animais controle e pré-diabéticos, bem como análises do grau de acetilação da Histonas 3 e 4 no epitélio intestinal e a concentração plasmática/intestinal de zonulina, LPS, e da citocina pró-inflamatória TNF-α, marcadores de quebra de barreira epitelial intestinal, endotoxemia e inflamação, respectivamente. No Capítulo 6 estão as considerações finais e conclusão e, por fim, o Capítulo 7 que traz a lista de referências citadas.

CAPÍTULO 1

1. INTRODUÇÃO AO TEMA DA TESE

1.1. BARREIRA EPITELIAL INTESTINAL E A JUNÇÃO DE OCLUSÃO

O intestino é um órgão tubular oco posicionado no abdômen, tendo seu início logo após a região pilórica do estômago (região proximal) e se estendendo até a região do ânus (região distal). É classificado em intestino delgado e grosso, levando em consideração o calibre que cada região apresenta, embora também difiram quanto ao seu aspecto anatômico, histológico e funcional (Dangelo & Fattini, 2011). O intestino delgado é subdivido em 3 regiões distintas: duodeno, jejuno e íleo. O ceco, o cólon, o reto e o ânus são subdivisões do intestino grosso (Kierszenbaum & Tres, 2012; Junqueira & Carneiro, 2013). A principal função do intestino delgado é a absorção de nutrientes, já o intestino grosso é especializado na absorção de água e eletrólitos, fermentação do quimo, formação de massa fecal e produção de muco.

Histologicamente, a estrutura geral da parede intestinal é similar sendo composta por 4 túnicas: mucosa, submucosa, muscular e serosa. A mucosa intestinal é revestida por epitélio simples colunar com borda estriada (Figura 1) que contém, principalmente, células absortivas (enterócitos) e células caliciformes. Essas células estão justapostas, firmemente unidas entre si e com a lâmina basal através de especializações de membrana plasmática denominadas junções celulares. Esse epitélio de revestimento da parede interna do intestino é contínuo com o epitélio glandular que compõe a porção secretora das criptas ou glândulas intestinais (Figura 1). Essas glândulas são compostas por células enteroendócrinas, células de Paneth e células tronco além dos enterócitos e células caliciformes. Uma característica histológica do intestino delgado é a presença de vilosidades. As vilosidades tratam-se da projeção da túnica mucosa em direção a luz do intestino e com isso aumentando a área de superfície intestinal. Entre as vilosidades, abrem-se as criptas ou glândulas intestinais classificadas morfologicamente como glândulas tubulares simples. As vilosidades são ausentes no intestino grosso o qual é caracterizado por criptas intestinais longas e por abundância de células caliciformes (Junqueira & Carneiro, 2013).

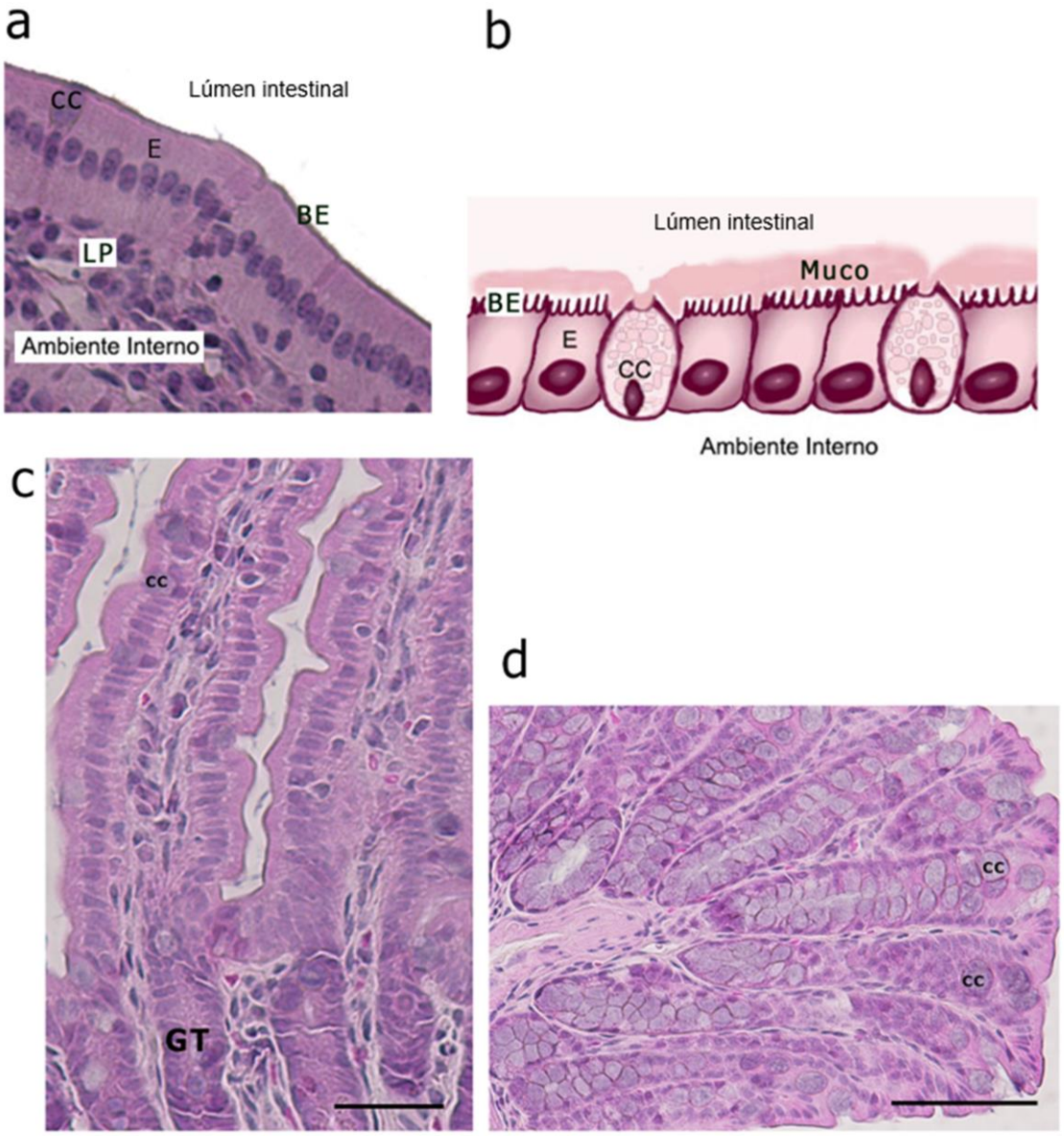

Figura 1. **Fotomicrografia e representação esquemática do epitélio intestinal**. **(a)** Fotomicrografia de corte histológico do intestino delgado de camundongo. **(b)** Esquema do epitélio simples colunar com borda estriada que delimita o lúmem intestinal do ambiente interno. **(c)** Fotomicrografia de corte histológico de vilosidade intestinal e glândula tubular (GT). **(d)** Fotomicrografia de corte histológico de intestino grosso – cólon. E: enterócito – CC: célula caliciforme – GT: glândula tubular (glândula intestinal) – LM: lâmina própria – BE: borda estriada. (Barra 50µm)

O duodeno é a primeira região do intestino delgado e se estende a partir do óstio pilórico até a flexura duodenojejunal. Por se tratar de uma região com a função de dar continuidade ao processo de digestão iniciado pelo estômago, é no duodeno que desembocam, através da papila duodenal maior, os produtos das glândulas anexas como a bile produzida

pelo fígado e trazida pelo ducto colédoco e as secreções do pâncreas trazidas pelo ducto pancreático (Dangelo & Fattini, 2011). Do ponto de vista histológico, o duodeno é caracterizado por possuir glândulas duodenais na camada submucosa responsáveis pela secreção mucosa alcalina afim de neutralizar o quimo ácido proveniente do estômago (Kierszenbaum & Tres, 2012; Junqueira & Carneiro, 2013).

O jejuno é a porção seguinte ao duodeno, tem seu início a partir da flexura duodenojejunal e, anatomicamente, não possui limite nítido em sua continuidade com o íleo que, por sua vez, abre-se na primeira porção do intestino grosso que é o ceco (Dangelo & Fattini, 2011). Já do ponto de vista histológico, o jejuno e o íleo podem ser diferenciados a partir da presença de placas de Peyer (nódulos linfoides) bastante desenvolvidas no íleo. Suas funções também são similares sendo responsáveis pela absorção dos nutrientes provenientes das porções anteriores. O segmento inicial do intestino grosso é o ceco, em fundo cego, local onde se intensifica a absorção de água. Os enterócitos do intestino grosso apresentam microvilosidades (borda estriada) apicais menos desenvolvidas e as células caliciformes aumentam em número no epitélio intestinal em comparação aos segmentos anteriores (Kierszenbaum & Tres, 2012; Junqueira & Carneiro, 2013).

O intestino está em constante contato com o conteúdo luminal, por este motivo, além de atuar no processo de absorção de nutrientes e água, desempenha importante função de barreira contra a entrada sistêmica de agentes nocivos, sejam eles microorganismos ou antígenos provenientes da alimentação. Várias são as barreiras que limitam o conteúdo luminal do ambiente interno. A barreira física é composta pelo próprio epitélio intestinal, já a barreira química inclui o muco secretado pelas células caliciformes. Ainda há a barreira imune, que compreende desde células especializadas em sintetizar e secretar agentes bacteriostáticos e bactericidas (como as células de Paneth) ou capazes de fagocitar antígenos do conteúdo luminal e “apresentá-los” às células do sistema imune (como as células M – *microfold cell*), até o tecido linfóide difuso situado abaixo do epitélio, na lâmina própria (conhecido como GALT, ou "Gut-Associated Lymphoid Tissue) (Schultz & Sartor, 2000; Garrett *et al*., 2010; Halpern & Denning, 2015). E a barreira molecular que compreende o complexo proteico que forma a estrutura da junção de oclusão situada na posição lateroapical dos enterócitos justapostos, regulando a via paracelular de moléculas (Figura 2) (Collares-Buzato, 2019).

Existem duas vias pelas quais íons e moléculas (incluindo os nutrientes) podem atravessar o epitélio intestinal, são elas: a via transcelular e a via paracelular (Groschwitz & Hogan, 2009). O transporte transcelular é mediado por canais, carreadores e transportadores localizados na membrana apical das células absortivas. A integridade da via paracelular, por sua vez, depende da regulação mediada por uma das junções intercelulares, conhecida como junção de oclusão (*tight junction* ou *zonula occludens*) (Figura 2). A junção de oclusão (JO) constitui, portanto, o elemento principal da barreira epitelial paracelular (Collares-Buzato, 2019). Acreditava-se que a JO formava uma barreira absoluta e inerte que impedia o tráfego de moléculas no espaço intercelular. Entretanto, nas últimas décadas, vários estudos experimentais comprovaram que essa junção intercelular é uma estrutura dinâmica e regulável, cuja permeabilidade pode se alterar em resposta a vários estímulos como nutrientes, sinalização humoral/neuronal ou mediadores inflamatórios, o que lhe atribui importante função no epitélio gastrointestinal, seja em condições experimentais, fisiológicas ou patológicas (Collares-Buzato *et al.*, 1994, 1998; Jepson *et al*., 2000; Mitic *et al*., 2000; Peixoto & Collares-Buzato, 2005; De Kort *et al*, 2011; Mongelli-Sabino *et al*., 2017; Collares-Buzato, 2019).

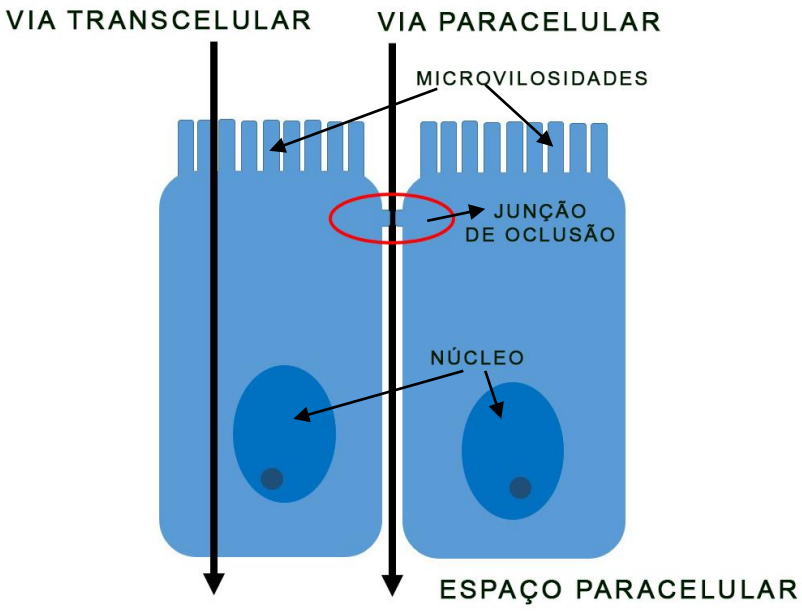

Figura 2. Representação das vias de transporte epitelial transcelular e paracelular.

O complexo da junção de oclusão (JO) (Figura 3) é composto por proteínas integrais de membrana como a ocludina e as claudinas (família de proteínas com 27 membros identificados). A interação *cis* e *trans* dessas proteínas integrais formam uma rede complexa de cordões anastomosantes na porção mais apical da membrana lateral que são visualizados em criofraturas do epitélio intestinal. A interação entre esses cordões situados em células adjacentes leva ao fechamento parcial do espaço intercelular que aparece como sítios de fusão das membranas plasmáticas identificados em secções ultrafinas da região da JO. As proteínas que formam a estrutura desses cordões de vedação (claudinas e ocludina), interagem indiretamente com o anel perijuncional do citoesqueleto de actina por meio de proteínas citoplasmáticas como a *zonula occludens* - ZO-1, ZO-2 e ZO-3, cingulina, simplequina, dentre outras (Van Itallie & Anderson, 2014; Salvador *et al.*, 2016).

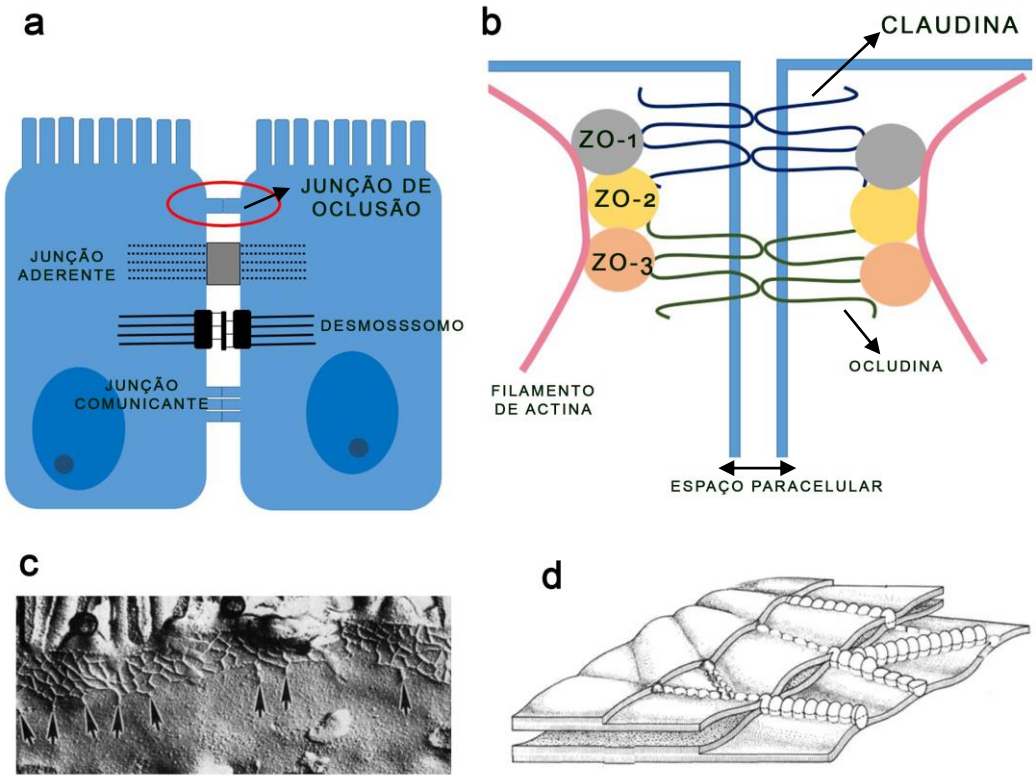

Figura 3. **Representações esquemáticas e criofatura da junção de oclusão**. **(a)** Esquema simplificado indicando a localização baso-apical da junção de oclusão, modificado a partir de (Collares-Buzato, 2019) **(b)** Esquema simplificado enfatizado as principais proteínas do complexo juncional (modificado a partir de (Fasano, 2008)). **(c)** Fotomicrografia de criofatura da rede de cordões de vedação que formam a junção de oclusão. **(d)** Representação dos cordões de vedação, formados por claudinas e ocludina, que constituem a estrutura da junção de oclusão. (c – d) (Anderson & Van Itallie, 2009).

Consideradas componentes chave para a função das JO, as claudinas possuem peso molecular entre 20-34kDa, são proteínas transmembranas tendo as regiões N- e Carboxi-terminal situadas no citoplasma das células formando dois *loops* extracelulares (ECL1 e ECL2) e um *loop* intracelular. As diferenças funcionais observadas entre suas isoformas está na grande heterogeneidade na cauda carboxi-terminal diversificando as regiões de fosforilação. A maioria das claudinas (exceto Cld-11, -12, -13 e -16) apresentam uma sequência tirosina-valina na cauda carboxi-terminal que atua como uma região de interação com domínio PDZ classe I encontrado em diversas proteínas citoplasmáticas que fazem a ponte entre as claudinas e os filamentos de actina do anel perijuncional, sendo a principal delas a ZO-1 (Furuse, 2010; Van Itallie & Anderson, 2014). Dentre as 27 isoformas de claudinas, existem as claudinas “formadoras de poro" (ex: Cld -2, -7, -12) e as “formadoras de barreira” (ex: Cld -1, -3, -4, -5, -8) (Markov *et al.*, 2010; Milatz *et al.*, 2010; Veshnyakova *et al.*, 2012; Gunzel & Yu, 2013; Lu *et al.*, 2013; Krug *et al.*,2014). As claudinas presentes no epitélio intestinal são as isoformas 1, 2, 3, 4, 5, 7, 8, 12, 14, 15 e 18, sendo que no intestino delgado há prevalência de claudinas permeável a íons ou como mencionado acima “formadoras de poro" (Cld-2 e -12). No intestino grosso a prevalência é de claudinas “formadoras de barreira” principalmente (Cld-1, -3 e -5).

A interação entre as diferentes isoformas de claudinas forma homodímeros ou heterodímeros capazes de determinar o grau de permeabilidade através da JO, regulando a maior ou menor permeabilidade paracelular do epitélio. Alteração da organização molecular da JO, por meio de modificações pós-traducionais das suas proteínas (por fosforilação, desfosforilação ou palmitoilação), bem como a contração dos filamentos de actina do citoesqueleto perijuncional podem regular a abertura ou o fechamento da junção de oclusão interferindo na permeabilidade paracelular intestinal (Arrieta *et al*., 2006; Hossain & Hirata, 2008; De Kort *et al*., 2011; Khan & Asif, 2015; Collares-Buzato, 2019). Um comprometimento estrutural dos microfilamentos de actina do citoesqueleto altera o arranjo do complexo da junção de oclusão, permitindo a passagem paracelular de antígenos e toxinas, podendo desencadear uma resposta imune local e sistêmica (De Kort *et al*., 2011).

Um importante mecanismo de regulação deste arranjo proteico no epitélio intestinal é mediado pelo sistema zonulina. A zonulina, é uma proteína endógena que atua como uma protease e é liberada por células do sistema imune (Fasano, 2011). A zonulina liga-se de forma direta aos receptores EGFR ou de forma indireta por meio da transativação dos

receptores $(PAR)_2$ distribuídos na região do jejuno, desencadeando uma cascata de eventos intracelulares que induz um rearranjo do citoesqueleto, e com isto, interfere na integridade do complexo proteíco da junção de oclusão, aumentando a permeabilidade paracelular intestinal (Sapone *et al.*, 2006; Fasano, 2008, 2011). Várias bactérias agem no sistema zonulina, produzindo uma proteína exógena, funcionalmente homóloga à zonulina (De Kort *et al*., 2011). Desta forma, as bactérias podem comprometer a barreira epitelial paracelular e ter acesso ao meio interno, desencadeando uma resposta imune sistêmica e possibilitando, inclusive, o início de doenças inflamatórias ou autoimunes (De Kort *et al*., 2011). Outros fatores, substâncias e/ou tratamentos experimentais podem influenciar na interação entre as proteínas da junção de oclusão e o citoesqueleto, induzir alteração na expressão de algumas proteínas associadas a este complexo ou mesmo no grau de fosforilação das mesmas (Fasano & Shea-Donohue, 2005; Collares-Buzato, 2019).

Além de influenciar na interação entre as proteínas da junção de oclusão e o citoesqueleto, fatores neurais, parácrinos e endócrinos podem regular a permeabilidade paracelular induzindo alteração na expressão gênica de algumas proteínas associadas a este complexo (Ulluwishewa *et al.*, 2011; Van Itallie & Anderson, 2014; Salvador *et al*., 2016; Collares-Buzato, 2019). Quanto à regulação epigenética das proteínas da JO, os estudos são raros. Alguns trabalhos recentes revelam a influência da regulação epigenética de genes codificadores de proteínas das JOs (Li *et al.*, 2016; Hichino *et al.*, 2017). Durante o desenvolvimento embrionário, a hipermetilação dos genes CTNNA1 e MYH2 (relacionados à via de sinalização da JO), durante os dois estágios iniciais do desenvolvimento do tubo neural, pode estar associada com risco de má-formação dessa estrutura (Wang *et al.*, 2017).

O aumento da permeabilidade intestinal mediada pelas JOs tem sido considerado um fator etiológico importante de várias doenças inflamatórias intestinais como a doença de Crohn e a colite ulcerativa (Odenwald & Turner, 2016). Pacientes com doenças intestinais inflamatórias apresentam diminuição de claudinas formadoras de barreira (Cld-1, -3, -4, -5, -7 e/ou -8) juntamente com aumento de Cld-2, formadora de poro, no intestino. Também há indícios da relação entre o aumento da permeabilidade intestinal com a etiologia de doenças metabólicas como o *diabetes mellitus* (Aron-Wisnewsky & Clément, 2016; Spiljar *et al*., 2017).

1.2 *DIABETES MELLITUS*

Diabetes mellitus é uma das doenças endócrino-metabólicas mais prevalentes no mundo, com estimativa atual de mais de 400 milhões de adultos afetados (World Health Organization, 2016). O *diabetes mellitus* é classificado em dois tipos principais, tipo 1 e tipo 2, os quais se distinguem pela sua etiologia e patogênese (Canivell & Gomis, 2014; American Diabetes Association, 2020). O *diabetes mellitus* tipo 1 é classificado como uma doença autoimune que tem como alvo as células-beta pancreáticas e, como resultado, a deficiência ou ausência da secreção de insulina. O *diabetes mellitus* tipo 2 (DMT2), por sua vez, é a forma mais frequente (aproximadamente 90% dos casos de *diabetes mellitus* diagnosticados), e está relacionada com a insensibilidade à ação da insulina em tecidos alvos, principalmente muscular esquelético, hepático e adiposo (Tripathy & Chavez, 2010; Wu *et al.*, 2014; Asmat *et al*., 2016; Chaudhury *et al.*, 2017).

Em nível celular, a ação da insulina inicia-se por meio da interação/ligação com seu respectivo receptor na superfície celular (Figura 4). O receptor de insulina (membro da família de receptores tirosinas cinase) é formado por duas subunidades α e duas subunidades β ligadas por pontes dissulfeto. A insulina interage com a subunidade α, ativando a subunidade β que se autofosforila em resíduos de tirosina. Uma vez ativado, o receptor de insulina fosforila resíduos de tirosina de seu substrato (IRS) que, por sua vez, desencadeia uma cascata de sinalização intracelular resultando na translocação de vesículas com isoformas do transportador de glicose, como por exemplo o GLUT4 (no caso do tecido adiposo e muscular), para a superfície da célula (membrana plasmática) (Pessin & Saltiel, 2000; Lee & Lee, 2014) aumentando, assim, a taxa de captação de glicose. No DMT2, a falha na resposta à insulina pode ocorrer em qualquer ponto dessa cascata de fosforilação/desfosforilação de proteínas associadas à essa via (Björnholm & Zierath, 2005). Níveis elevados de ácidos graxos livres, citocinas pró-inflamatórias e estresse do retículo endoplasmático podem interferir na resposta à insulina por meio da ativação de outras vias de sinalização intracelular ou ocasionando a fosforilação de resíduos de serina/treonina do receptor de insulina reduzindo sua funcionalidade (Lin & Sun, 2010; Tripathy & Chavez, 2010).

No DMT2, a falha na captação tecidual de glicose, como consequência do quadro de resistência periférica à insulina, resulta em hiperglicemia, ou seja, no aumento na concentração glicose no sangue. A hiperglicemia pode ser parcialmente compensada pela hiperplasia (aumento de massa das células beta pancreáticas) e/ou pelo aumento da síntese e

secreção de insulina pelo pâncreas endócrino (Oliveira *et al.*, 2014; Maschio *et al.*, 2016). Esses eventos compensatórios ocorrem principalmente durante a fase inicial, conhecida como pré-diabetes. Entretanto, a alta atividade secretora das células-beta, por um extenso período de tempo, pode resultar em sua exaustão funcional e sua morte por apoptose. Portanto, na fase tardia da DMT2, o paciente frequentemente necessita de reposição hormonal para controle da homeostase glicêmica.

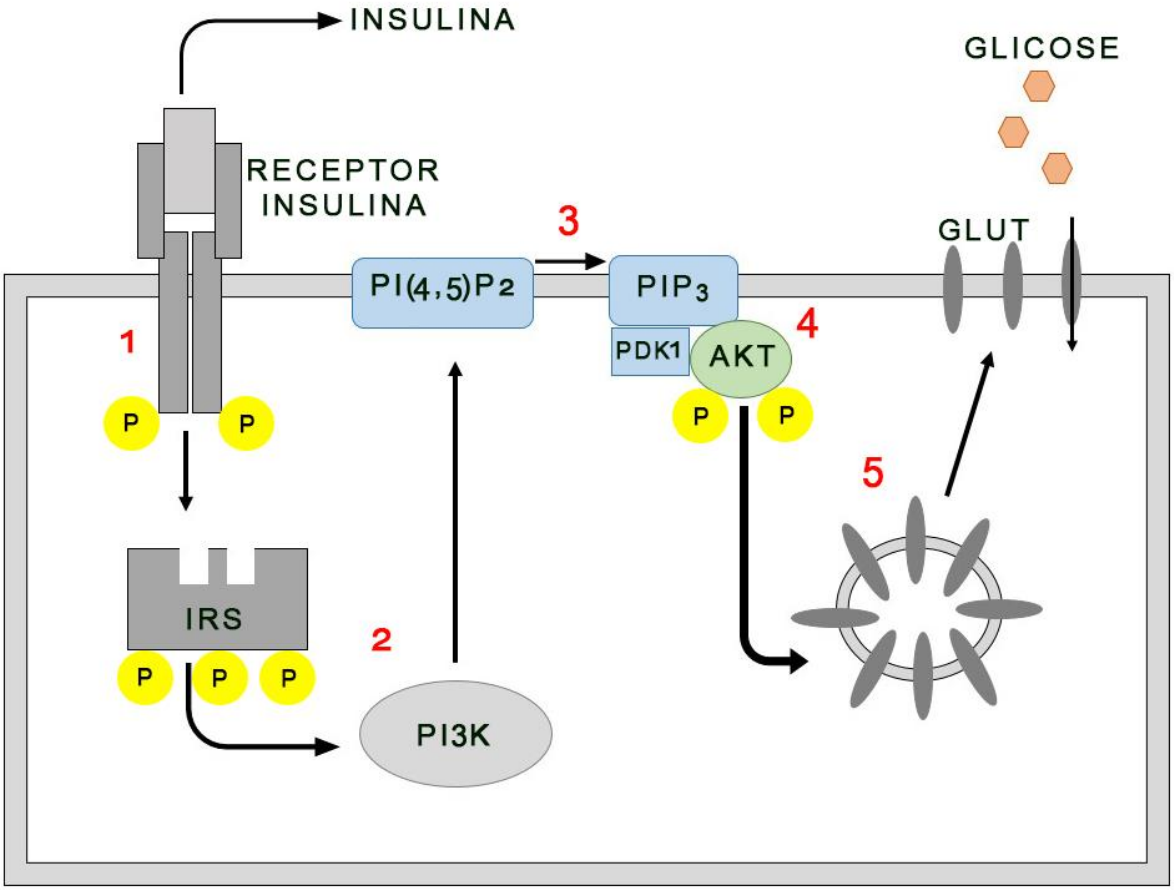

Figura 4. Representação esquemática da cascata de eventos de fosforilação/desfosforilação para translocação de GLUT em uma célula hipotética. - **1.** Insulina se liga ao receptor que se autofosforila em resíduos de tirosina. **2.** Receptor de insulina ativado fosforila seu substrato (o IRS) e recruta PI3K (*Phosphatidylinositol-3-kinase*). **3.** Na membrana plasmática, PI3K converte $PI(4,5)P_2$ (*Phosphatidylinositol-4,5-bisphophate*) em PIP_3 (*Phosphatidylinositol-3,4,5-trisphophate*). **4.** O aumento de PIP_3 direciona PDK1 (*Phosphatidylinositol dependent protein kinase-1*) e Akt (*Protein kinase B*) para a membrana plasmática, onde PDK1 fosforila Akt. **5.** Akt ativado recruta outros mensageiros intracelulares que sinalizam a translocação de vesículas contendo GLUT para a membrana plasmática. A falha no acoplamento da sinalização intracelular pode acontecer já durante a ligação da insulina com seu receptor. (Esquema modificado a partir de (Lin & Sun, 2010)).

Além da predisposição genética, fatores ambientais como estilo de vida sedentário e dieta rica em lipídios e carboidratos contribuem para desordens metabólicas que levam ao desenvolvimento do diabetes (Olokoba *et al*., 2012; Forbes & Cooper, 2013). A obesidade, resultante do desequilíbrio entre a ingestão de calorias e o gasto energético, parece ser um dos principais fatores de risco para o desencadeamento da resistência periférica à insulina (Mao *et al.*, 2013; Y Lee, 2013).

A obesidade é caracterizada por resposta inflamatória sistêmica na qual o tecido adiposo unilocular é responsável por liberar diversos mediadores inflamatórios que podem afetar a ação da insulina, como o TNF-α que está superexpresso em modelos de obesidade (Wellen & Hotamisligil, 2005). A exposição ao TNF-α ou a níveis elevados de ácidos graxos livres, de forma indireta, estimula a fosforilação de resíduos de serina no receptor de insulina (IR), o que reduz a autofosforilação de tirosina levando a uma falha na resposta à insulina (Lin & Sun, 2010; Tripathy & Chavez, 2010).

Estudos clínicos e experimentais sugerem o envolvimento do intestino na evolução dos dois tipos de diabetes (Tremaroli & Bäckhed, 2012). Neu *et al.*, (2005), utilizando animais BioBreeding Propensos (BBDP - capazes de desenvolver de *diabetes mellitus* tipo 1), e animais BioBreeding Resistentes (BBDR), observaram aumento da permeabilidade intestinal associado com alterações estruturais da junção de oclusão no epitélio intestinal nos animais propensos (BBDP). Relataram, ainda, aumento no número de células caliciformes no trato gastrointestinal desses animais, sugerindo a presença de uma resposta inflamatória local. Contribuindo com esses dados experimentais, Bosi *et al.*, (2006), por meio da análise da excreção urinária em pacientes em diferentes estágios do curso do *diabetes mellitus* tipo 1, observaram aumento progressivo da excreção de lactulose, acompanhada do aumento da concentração da circulação de zonulina nesses pacientes. Tais resultados, em conjunto, sugerem que a integridade da barreira paracelular intestinal constitui num possível fator de importância na patogênese do *diabetes mellitus* tipo l.

Quanto à DMT2, tem sido demonstrado que a exposição à uma dieta rica em lipídios altera a microflora intestinal, favorecendo a colonização do intestino por bactérias gram-negativas, cujas endotoxinas liberadas parecem contribuir com o processo inflamatório de baixo grau associado com um quadro de resistência à insulina (Cani *et al.*, 2008, 2012; Amar *et al.*, 2011). As bactérias que compõem a microflora intestinal desempenham um importante

papel para o organismo que as hospedam, pois podem influenciar processos metabólicos como a extração de energia a partir dos alimentos, além de ser um fator ambiental que pode contribuir para o quadro de obesidade e doenças associadas, como o *diabetes mellitus* tipo 2 (Tremaroli & Bäckhed, 2012).

Ley *et al.*, (2005) reportaram que a microbiota de camundongos obesos *ob/ob* contém maior proporção de bactérias Firmicutes e menor proporção de Bacterioides em comparação a camundongos magros após administração de dieta rica em carboidratos. Larsen *et al.*, (2010) também observaram uma alteração significativa na composição da microbiota de pacientes com DMT2 em comparação com indivíduos saudáveis. Os estudos de Cani *et al.*, (2008) comprovaram que a obesidade em camundongos *ob/ob* favorece o aumento de bactérias gram-negativas da microbiota, associado com aumento na permeabilidade intestinal e endotoxemia, caracterizada por aumento do nível plasmático de lipopolissacarídeos (LPS), que induzem a produção de citocinas pró-inflamatórias levando ao agravamento do quadro resistência periférica à insulina.

Portanto, a hipótese vigente, que tenta explicar o envolvimento da microbiota intestinal na patogênese das duas formas de diabetes, preconiza que a alteração na composição e funcionalidade dessa microbiota, devido, pelo menos em parte, a uma dieta rica em lipídios e pobre em fibras, está associada com comprometimento da barreira intestinal. Isto, por sua vez, ocasionaria a entrada sistêmica de bactérias e seus produtos, além de alérgenos alimentares, resultando em hipersensibilidade do sistema imune no caso do *diabetes mellitus* tipo 1, ou um quadro de endotoxemia e inflamação sistêmica de baixo grau, contribuindo para a resistência periférica à insulina no *diabetes mellitus* tipo 2 (Neu *et al.*, 2005; De Kort *et al*., 2011; Everard & Cani, 2013; Scheithauer *et al.*, 2016; Sabatino *et al.*, 2017; Spiljar *et al*., 2017).

Trabalhos recentes do nosso grupo corroboram o papel da barreira paracelular intestinal mediada pela JO na patogênese da DMT2, embora desafiem alguns aspectos dessa hipótese vigente que tenta explicar o eixo microbiota-barreira intestinal-inflamação-diabetes (Fukui, 2016). Demonstramos, pela primeira vez, que camundongos pré-diabéticos, alimentados com dieta hiperlipídica, apresentam alterações na estrutura da JO do epitélio intestinal, que foram mais evidentes no intestino proximal (duodeno e jejuno) que no distal (íleo e cólon) (que concentra grande parte da microbiota intestinal) (Oliveira *et al.*, 2019;

Nascimento, 2019). Esse comprometimento da barreira intestinal paracelular foi associado a um aumento da permeabilidade intestinal a moléculas de baixo peso molecular, que ocorreu antes do estabelecimento da endotoxemia e na ausência de alterações na concentração de zonulina e de aparente inflamação intestinal (Nascimento, 2019). Corroborando os resultados obtidos no modelo *in vivo*, o conteúdo luminal do intestino delgado induziu alterações mais severas na estrutura e função de barreira paracelular da linhagem intestinal Caco-2 quando comparado ao conteúdo luminal isolado do intestino grosso (Oliveira *et al*., 2019).

1.3 BUTIRATO DE SÓDIO: PAPEL METABÓLICO E INTESTINAL

O aumento da incidência de disfunções metabólicas como obesidade e diabetes estão diretamente associadas a uma mudança no estilo de vida que acarreta alteração da microbiota intestinal. Por esse motivo, muito tem se falado sobre alimentação funcional ou pré- e pós-bióticos afim de regular a microbiota intestinal e, por consequência, manter a concentração de seus metabólitos, os ácidos graxos de cadeia curta, que desempenham importantes funções para a homeostase do hospedeiro como descrito a seguir (Canani *et al*., 2012; Sohail *et al.*, 2017).

O butirato, assim como o acetato e o propionato, são ácidos graxos de cadeia curta (AGCCs), produzidos no lúmen intestinal (mais precisamente no cólon) pela microbiota intestinal. Esses ácidos graxos são produzidos a partir da fermentação de carboidratos não digeríveis (fibras) e proteínas, sendo que o primeiro caso é mais frequente, ocorrendo predominantemente no cólon proximal e o segundo, menos frequente, acontece principalmente no cólon distal (Hamer *et al.*, 2008; Khan & Jena, 2016; Miao *et al.*, 2016; Mollica *et al.*, 2017). O butirato é um importate AGCC porque além de ser uma fonte energética para os enterócitos da região do cólon (colonócitos), ainda possui efeitos regulatórios no transporte transepitelial de íons, por meio da estimulação de absorção de NaCl e da inibição da secreção de Cl^-, contribuindo para o balanço de eletrólitos na região do cólon (Canani *et al.*, 2011).

Os AGCCs podem se apresentar de três formas diferentes, sendo elas: forma protonada dos AGCCs, forma não-dissociada (que é lipossolúvel) e forma iônica dissociada (que corresponde a 90% dos AGCCs no cólon). Vários são os mecanismos de captação e absorção dos AGCCS, tais como a difusão, que ocorre na forma protonada, transporte livre

pela membrana celular, no caso da forma não-dissociada, ou troca iônica, no caso da forma iônica dissociada. Essas moléculas ainda podem atravessar a membrana da célula através de agentes transportadores como transportador MCT1 (*monocarboxylate transporter 1* –MCT1), dependente do gradiente de H+ e o SMCT1 (*sodium-dependent monocarboxylate transporter*), dependente de sódio. No caso do butirato de sódio, a maioria é absorvida e metabolizada pelo próprio epitélio do cólon. (Hadjiagapiou *et al.*, 2000; Hamer *et al.*, 2008; Gill & Dudeja, 2011).

Além de serem utilizados pelos colonócitos, os AGCC atuam como ativadores de vias de sinalização (crescimento e morte celular) através dos receptores acoplados à proteína G (GPR ou FFAR – *free fat acid receptor*). Tang *et al.*, (2011) reportaram a ausência do receptor GPR43 em células cancerígenas do cólon e que a restauração da expressão desse receptor em linhagens de células HCT8 (adenocarcinoma colônico humano) acrescido de tratamento com AGCC, em especial o butirato, aumentou a apoptose dessas células, ou seja, o receptor GPR43 pode ser considerado como um supressor de tumor no cólon mediado pelo AGCC.

Estudos realizados em modelos animais e em crianças com diarreia aguda, causada por *V. cholerae* ou sem causa conhecida (associadas às condições de má nutrição, má absorção e falta de crescimento), comprovam que a adição de precursores do butirato na reidratação oral proporcionam uma redução no volume das fezes e uma reidratação mais rápida (Rabbani *et al.*, 1999, 2001; Canani *et al.*, 2004). Além disso, o estudo de Wang *et al.*, (2012) mostrou que o butirato promove também melhora na função de barreira epitelial em ensaios *in vitro* com a linhagem de células intestinais cdx2-IEC. Por meio de análise de resistência elétrica transepitelial (TEER) e de análises de biologia molecular e expressão gênica, esse estudo mostrou que o tratamento com butirato de sódio melhorou a função de barreira *in vitro* devido a um aumento de transcrição da proteína claudina-1.

O efeito do butirato sobre o metabolismo tem sido estudado, porém sua ação ainda é pouco compreendida. Gao *et al.*, (2009) observaram que o butirato, administrado por meio de suplementação alimentar a 5% na DHL, contribuiu para o restabelecimento da sensibilidade à insulina de camundongos C57BL/6. Os autores sugeriram que o mecanismo de ação do butirato sobre a melhora na sensibilidade à insulina está relacionada com o aumento do gasto energético, da função mitocondrial e aumento na expressão gênica e proteica do receptor PPAR-α (Receptores-α ativados por proliferadores de peroxissomas). Trabalho prévio do

nosso grupo também confirmou o efeito benéfico do butirato sobre a obesidade e alterações metabólicas induzidas por dieta hiperlipidica em camundongos (Matheus, 2016).

O butirato também tem efeito sobre o tecido adiposo através dos receptores GPR43 e GPR41 modulando a inflamação. Em co-cultura de adipócitos 3T3-L1 diferenciados e macrófagos RAW264.7, esse ácido graxo inibiu a atividade de NF-κB dos macrófagos, bem como suprimiu a atividade de lipase nos adipócitos, o que atenuou de forma significativa a produção de TNF-α, MCP-1 e IL-6 (Ohira *et al.*, 2013).

É conhecida a ação do butirato de sódio sobre a estrutura e a função da cromatina por meio da inibição da enzima histona deacetilase (HDA) (enzima com função de retirar o grupo acetil dos resíduos de lisina das histonas), sendo, desta forma, um regulador epigenético (Kruh, 1982; Khan & Jena, 2014; Miao *et al.*, 2016; Patnala *et al.*, 2017). A regulação epigenética do butirato de sódio tem por consequência hiperacetilação das histonas (principalmente H3 e H4). Tem sido demonstrado que o butirato de sódio tem efeito sobre a regulação do crescimento celular via ativação/inativação de genes relacionados à proliferação celular (Kumar *et al.*, 2007). Devido a esta propriedade, o butirato de sódio desempenha papel na proliferação celular, além de atuar no metabolismo energético (Canani *et al*., 2012; Mátis *et al.*, 2015).

1.4 OBJETIVOS E ESTRATÉGIAS EXPERIMENTAIS

A presente Tese de Doutorado tem como objetivo geral estudar a ação anti-diabetogênica do butirato de sódio sobre as disfunções metabólicas e teciduais, bem como o efeito protetor sobre a barreira epitelial intestinal mediada pelas junções de oclusão (JO) em modelos *in vivo* e *in vitro* de DMT2.

Como objetivos específicos, essa Tese visou:

a) investigar o efeito protetor do butirato sobre as alterações metabólicas características da pré-diabetes induzida pela exposição do animal à dieta hiperlipidica (DHL) por 60 dias. Para tal, foram analisados vários parâmetros, a saber: a massa corporal, o metabolismo basal, a adiposidade, o acúmulo ectópico de gordura (no figado e pâncreas), a lipidemia, a glicemia (em jejum e pós-prandial), a insulinemia (jejum e pós-prandial), a secreção estática de insulina, e a resposta ao teste de tolerância à insulina (ITT) e à glicose (GTT).

b) avaliar a ação do butirato de sódio sobre o metabolismo basal medindo o gasto energético, o consumo de oxigênio *in vivo* e *in vitro* utilizando-se modelo de linhagem celular de tecido adiposo marrom.

c) verificar o efeito do butirato sobre as possíveis alterações funcionais e estruturais da barreira intestinal mediada pela JO por meio da análise da permeabilidade paracelular a marcadores extracelulares e da expressão gênica, distribuição e conteúdo celular de proteínas juncionais (como claudinas, ocludina e ZO-1) em animais pré-diabéticos. Em paralelo, avaliamos, sob essas condições experimentais, as concentrações plasmáticas/séricas e teciduais de zonulina, LPS e TNF-α, que são marcadores de quebra da barreira epitelial intestinal, endotoxemia e inflamação, respectivamente. .

d) analisar o efeito *in vitro* da exposição ao conteúdo intestinal coletado de animais dos diferentes grupos experimentais sobre a função de barreira epitelial paracelular em monocamadas celulares da linhagem intestinal Caco-2.

CAPÍTULO 2

2. MATERIAL E MÉTODOS

2.1 PROTOCOLOS EXPERIMENTAIS

O fluxograma abaixo representa as etapas desenvolvidas no decorrer desta Tese.

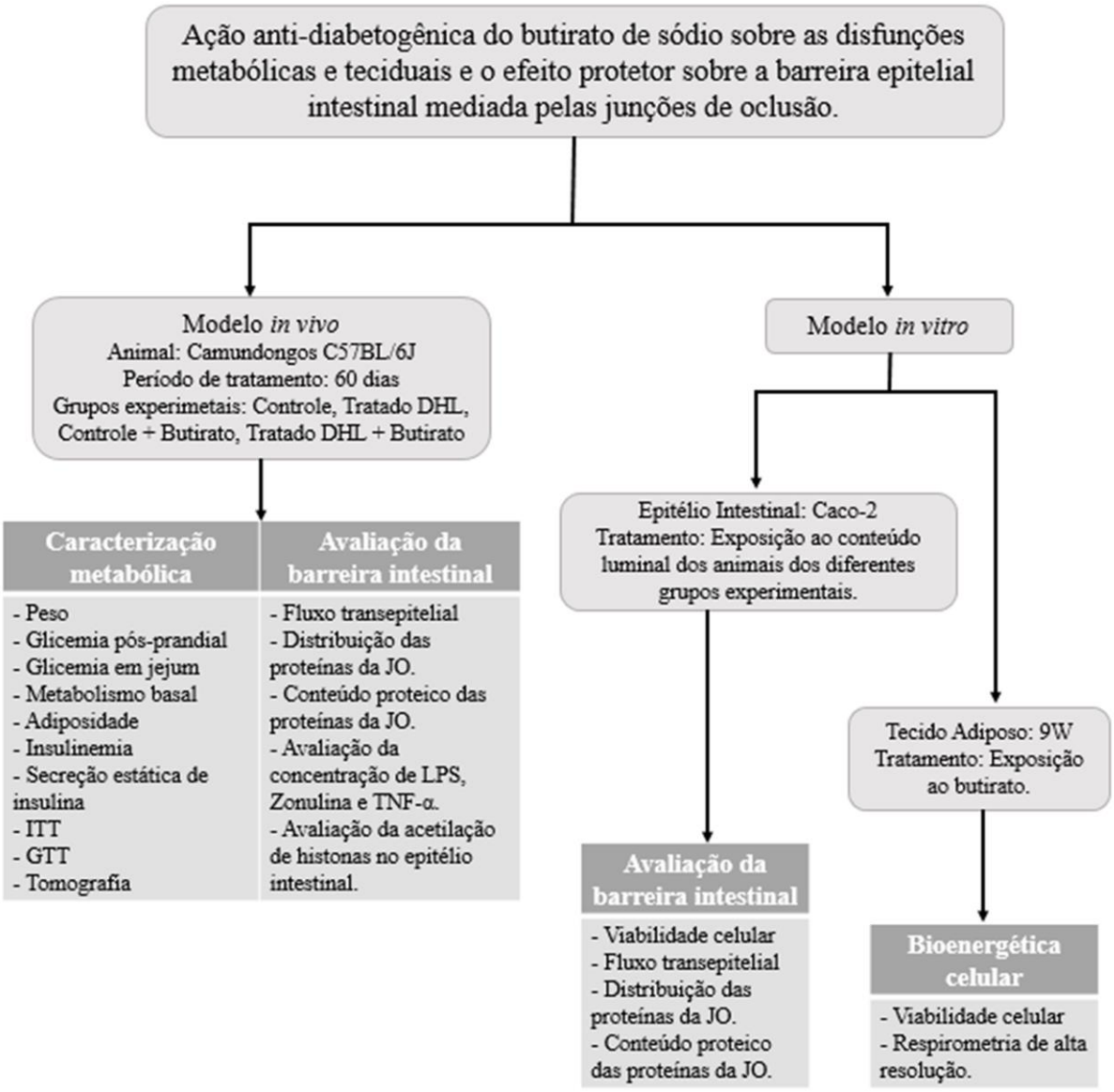

2.2 *IN VIVO*

2.2.1 Animais e Dietas

Foram utilizados camundongos machos da linhagem C57BL6J/Unib com idade de 4 a 5 meses, provenientes do Centro de Bioterismo da UNICAMP (Campinas, SP). Os animais foram distribuídos em quatro grupos experimentais: controle (C), controle + butirato de sódio (CB), dieta hiperlipidica (D) e dieta hiperlipídica + butirato de sódio (DB), n=36 animais/grupo, sendo que, sempre que possível, o mesmo animal foi utilizado em diferentes procedimentos experimentais.

Os camundongos do grupo C foram alimentados com ração NUVILAB CR1 Irradiada (Quimtia) com baixo teor de lipídios (4,5% em peso - Tabela I), que foi previamente triturada. Os camundongos do grupo D foram alimentados com uma ração em pó preparada, no laboratório, com alto teor de lipídios (21% em peso - Tabela I). Os animais do grupo CB foram alimentados com ração triturada NUVILAB CR1 Irradiada (Quimtia), porém suplementada com 5% de butirato de sódio (w/w; 303410 Sigma). A mistura foi preparada manualmente, em uma vasilha, com movimentos variados, em todos os sentidos por 5 minutos. Os animais do grupo DB receberam ração hiperlipídica, que, após seu preparo, recebeu suplementação com 5% de butirato de sódio (w/w; 303410 Sigma) sendo misturado manualmente com movimentos variados, em todos os sentidos por 5 minutos.

Durante o período de 60 dias, os animais foram mantidos em microisoladores acondicionados em racks ventiladas, com no máximo 03 indivíduos por microisolador. Os camundongos tiveram livre acesso ao alimento e à água (filtrada) e foram mantidos em ambiente com temperatura controlada (25°C) com ciclo claro-escuro de 12h durante todo o período de adaptação e experimentação. As diferentes rações eram trocadas diariamente, sempre no mesmo intervalo de horário, em potes de vidro contendo aproximadamente 7g de ração por animal. Os experimentos deste projeto foram aprovados pela Comissão de Ética no Uso de Animais (CEUA – IB – UNICAMP) da Instituição, sob o protocolo nº: 4185-1.

Este protocolo é padrão para os 3 artigos resultantes dessa Tese.

Tabela I. Composição das rações utilizadas.

Componentes	Ração Nuvilab	Dieta hiperlipídica
Proteínas	22,0	20,0
Carboidratos	53,0	50,0
Lipídeos	4,5	21,0
Outros*	20,5	8,0
Kcal/g	2,9	4,7

*Fibras, vitaminas e minerais

2.2.2. Avaliação metabólica dos animais

Todos os animais dos diferentes grupos experimentais (n=36 animais/grupo) foram pesados com o auxílio de uma balança eletrônica de precisão (10002N, Metra) no início e no final do período experimental, ou seja, nos dias 0 e 60º, respectivamente e os valores foram expressos como a porcentagem de ganho de massa corporal em relação à massa corporal inicial. A glicemia pós-prandial (em camundongos alimentados) também foi medida no início e término do período experimental com auxílio de glicosímetro (Accu-Chek® Active – Roche), no entanto, os valores exibidos (mg/dL) foram os obtidos no final do experimento (após 60d) como parâmetro de avaliação do estado glicêmico dos animais após experimentação. Os valores de glicemia pós-prandial (n=36 animais/grupo) inicial foram utilizados para a distribuição dos animais nos diferentes grupos experimentais, agrupando-os de tal forma que a média de glicemia fosse similar entre os grupos. A glicemia em jejum (mg/dL) (18h de jejum) foi medida no ato da eutanásia, que foi realizada em câmara saturada de CO_2 (num fluxo máximo de 20% volume da câmara/min) (n=13 animais/grupo).

Com o intuito de otimizar a utilização de animais e evitar que os mesmos fossem submetidos por períodos múltiplos de jejum, utilizamos o mesmo grupo de camundongos para avaliar a glicemia em jejum e fazer a coleta de fragmentos do intestino. O período de jejum prolongado de 18h foi necessário para o total esvaziamento do conteúdo intestinal e posterior colheita do material biológico (fragmentos de intestino) para imunoistoquímica e Western Blot. A glicemia, tanto em jejum quanto pós-prandial, foram determinadas com auxílio de um glicosímetro (Accu-Chek® Active - Roche) em amostras de sangue retiradas a partir da cauda

dos animais (no caso da glicemia pós-prandial) ou dos vasos cervicais após eutanásia seguida de decaptação decapitação (no caso da glicemia em jejum).

O ITT foi realizado através de injeção intraperitoneal de insulina (0,50 U/kg de peso corporal de insulina humana, Biohulin®R, Biobrás) em animais após jejum de 6h (Pappan *et al.*, 2005). Amostra de sangue foi coletada da cauda dos animais no tempo 0, logo após administração de insulina, e as medidas nas amostras subsequentes foram realizadas nos tempos 10, 15, 30 e 60 minutos com auxílio de um glicosímetro (Accu-Chek® Active - Roche). Os valores de ITT foram expressos como área sobre a curva (AUC) (n=6 animais/grupo).

O GTT foi realizado via gavagem (1,5g/kg de glicose diluída em 4,8ml/kg de água filtrada) em animais com 12h de jejum. Amostras de sangue foram coletadas da cauda dos animais no tempo 0, logo após administração de glicose, e também nos tempos subsequentes, 15, 30, 60 e 90 minutos; a medida da concentração de glicose nas amostras de sangue foi determinada com auxílio de um glicosímetro (Accu-Chek® Active - Roche). Os valores de GTT foram expressos como área sobre a curva (AUC) (n=10 animais/grupo).

Para determinação da insulinemia, foram coletadas amostras de sangue dos vasos cervicais, no momento da eutanásia, após decapitação, seguida de centrifugação das amostras de sangue à 12000 rpm (G=8.049,4 – raio do rotor = 5cm) por 10 minutos a 4°C para separação do plasma. A determinação da concentração de insulina nas amostras foi realizada utilizando um kit ELISA comercial (Ultra Sensitive Mouse Insulin - Crystal Chem Inc., USA) (n=5 animais/grupo).

2.2.3 Material biológico

Sempre com o intuito de otimizar a utilização do menor número de animais para a realização da pesquisa, o sangue coletado pelos vasos cervicais (após eutanásia seguida de decaptação) foi utilizado para obtenção de soro ou plasma e os órgãos de interesse (intestino, fígado, pâncreas, tecido adiposo retroperitoneal e pélvico e o tecido adiposo marrom) foram retirados após laparotomia. O tecido adiposo branco (retroperitoneal e epididimal) e marrom interescapular foram pesados com o auxílio de uma balança analítica (SA 210, Scientech, Curitiba, Brasil). Os intestinos delgado e grosso foram preparados para as técnicas de imunofluorescência indireta (vide seção 2.2.12) (n=6 animais/grupo), *Western Blot* (vide seção 2.2.13) (n=4-6 animais/grupo) ou também congelados em nitrogênio líquido e armazenados em biofreezer a -80°C para posterior dosagem de zonulina, LPS e TNF-α (vide

seção 2.2.8) (n=6 animais/grupo). Por fim o fígado, o pâncreas e o tecido adiposo marrom seguiam protocolo padrão de inclusão em Paraplast (n=5 animais/grupo). Os cortes histológicos do fígado e o tecido adiposo marrom foram corados por Hematoxilina e Eosina (vide seção 2.2.4) e as secções de pâncreas processados para imunoistoquímica para insulina (vide seção 2.2.5).

2.2.4 Histologia

Fragmentos de fígado e de tecido adiposo marrom interescapular foram lavados em PBS e fixados em solução de paraformaldeído 4% por 24h em temperatura ambiente (TA). Após este período, os fragmentos foram lavados 4 vezes por 10 minutos em água destilada e mantidos em álcool 70% até o processo de inclusão. Todos os diferentes tipos de tecidos passaram por protocolo padrão de diafanização e inclusão em Paraplast® (P3558, Sigma). Secções histológicas (4 μm espessura) foram obtidas com navalhas descartáveis em micrótomo (Leica RM 2145 – Germany). Os cortes foram corados por Hematoxilina por 3 minutos e, posteriormente, lavados com água por 5 minutos. Após lavagem, os cortes foram corados com Eosina por 1 minuto e lavados com água destilada. As lâminas foram montadas e a fotodocumentação foi feita por câmera digital acoplada a um microscópio de luz (Nikon Eclipse E-400 - Nikon, Tóquio, Japão – NIS Elements). Este foi o protocolo padrão de inclusão e coloração por afinidade ácido/base dos corantes empregados para obtenção das imagens de micrografia analisadas e apresentadas nos Capítulos 3 e 4. Em seguida, temos a descrição dos diferentes métodos de morfometria utilizados.

Para análise morfométrica de esteatose hepática, foram coletadas de forma randômica, imagens a partir de três secções histológicas por amostras de fígado (n=5 camundongos/grupo). A estimativa morfométrica da esteatose hepática foi realizada por um sistema de contagem de pontos, descrita por (Catta-Preta *et al.*, 2011), com modificações. Utilizando as imagens de micrografia obtidas em alta ampliação (lente objetiva 100x) e um sistema de teste de 88 pontos utilizando o plug-in Grid do free software Image J (http://rsbweb.nih.gov/ij/download.html), a densidade de volume da esteatose hepática, expressa em porcentagem, foi estimada como a razão dos pontos que atingem as vesículas de gordura em comparação ao número total de pontos.

Para análise da alteração morfólogica do tecido adiposo marrom interescapular (iBAT), as imagens foram capturadas com auxílio de câmera digital acoplada a um microscópio óptico

(Nikon Eclipse E-400 - Nikon, Tóquio, Japão - NIS Elements). Foram capturadas 10 imagens de forma aleatória de duas seções diferentes de cada animal (n=5 camundongos/grupo). A morfometria foi realizada com auxílio do programa Image J (http://rsbweb.nih.gov/ij/), cuja base de análise é feita a partir de dados expressos como porcentagem em relação a área total da imagem. A relação é fornecida ao transformar a imagem capturada em imagem binária, na qual o lipídeo assume a cor branca enquanto a matriz assume coloração preta. Após isso as cores são invertidas e os pixels pretos, que agora representam os lipídeos, são contabilizados e exibidos em percentual do total da imagem.

2.2.5 Imunoistoquimica para insulina no pâncreas

Os pâncreas foram fixados em solução de paraformaldeído 4% e, posteriormente, seccionados em 5 fragmentos (1, correspondendo à cabeça e 5 à região da cauda) e processados pela embebição em parafina (Histosec pastilhas, Merck). Foram obtidas secções semi-seriadas de 5µm (com espaçamento de 100µm entre cortes). As lâminas selecionadas foram processadas por imunoperoxidase para insulina (Oliveira *et al.*, 2015).

Os cortes de pâncreas foram desparafinizados, reidratados e lavados com TBS (Trisma base 0,01 M, NaCl 0,15 M). Em seguida, foi feito o bloqueio da peroxidase endógena com uma solução de 0,3% de peróxido de hidrogênio (em metanol) por 30 min seguido de incubação com 5% de leite em pó desnatado em solução de TTBS (TBS/0,1% Tween 20) por 1h. Posteriormente, os cortes foram incubados com anticorpo anti-insulina (Cat# A0564, Dako, diluição 1:50) por 12 horas a 4ºC. Após lavagem com TBS, as secções foram incubadas com anticorpo secundário conjugado com peroxidase (*Horseradish Peroxidase*, HRP, Sigma, diluição 1:1500), por 1 hora e 30 min à TA. A revelação do complexo antígeno-anticorpo foi feita com solução de diaminobenzidina a 10% (DAB) (Sigma) e 0,2% de H_2O_2 (Merck) em TBS. Em seguida, os cortes foram lavados em água destilada e contra-corados com solução aquosa de Hematoxilina de Erlich. Para análise morfométrica do pâncreas, foi medido o volume total de células-beta em relação ao pâncreas total (Volume relativo VR células beta/pâncreas) utilizando método estereológico descrito anteriormente com pequenas modificações (Oliveira *et al.*, 2015). Seis cortes histológicos processados por imunoperoxidase para insulina foram analisados por pâncreas (dois cortes de cada bloco, 1, 3 e 5). Todos foram fotografados com objetiva panorâmica com o auxílio de uma câmera digital (Nikon FDX-35) acoplada a um microscópio de luz (Nikon Elipse E800), e as imagens

capturadas por um sistema de análise de imagens (Image Pro Plus for Windows). A medida do volume relativo das células-beta (imunomarcadas para insulina) foi realizada utilizando o software livre ImageJ. Para tanto, a somatória das áreas dos perfis das ilhotas imunomarcadas para insulina foi dividida pela respectiva área da secção histológica do pâncreas, multiplicando-se por 100.

Os mesmos cortes histológicos processados por imunoperoxidase foram utilizadas para avaliação da deposição de tecido adiposo intrapancreático. A avaliação morfométrica foi realizada atribuindo um valor de acordo com um sistema de *scores* com valores que variavam de 0 a 3 (Tabela II), que representam a quantidade relativa de tecido adiposo intralobular presente. O grau de adiposidade do pâncreas foi determinado calculando-se o valor médio de alteração segundo essa classificação por grupo experimental**.**

Tabela II. Grau de adiposidade do pâncreas.

SCORE	GRAU DE ADIPOSIDADE
0	Sem presença de tecido adiposo
1	Presença de 1-3 adipócitos
2	Presença de 4-6 adipócitos
3	Presença de 7 ou mais adipócitos

2.2.6 Avaliação do padrão de citoarquitetura das ilhotas pancreáticas

Para avaliação de possíveis alterações na citoarquitetura das ilhotas pancreáticas, os cortes histológicos de pâncreas foram submetidos à reação de imunoflorescência para dupla marcação de insulina e glucagon (Oliveira *et al.*, 2015). Os cortes de pâncreas foram incubados com o anticorpo primário anti-glucagon (Cat# A0565, Dako, EUA; diluição 1:75) em 3% de leite desnatado em TBS (Trisma base 0,01 M, NaCl 0,15 M) por 3h em temperatura ambiente (TA). Após lavagem, os cortes foram incubados por 12h a 4°C com o anticorpo secundário específico conjugado com fluoresceína (Sigma, diluição 1:125 em 1% de leite desnatado em TBS). Os cortes foram lavados novamente e incubados por 3h à TA com o anticorpo primário anti- insulina (Cat# A0564, Dako, EUA, diluição 1:75 em TBS com 3% de leite desnatado). Após nova lavagem, os cortes foram incubados com o anticorpo secundário específico conjugado com rodamina (Sigma, diluição 1:100 em 1% de leite desnatado em

TBS) por 2h à TA. Por fim, as lâminas foram montadas em meio de montagem (Vectashield, Vector Laboratories, Burlingame, CA, USA) para observação em microscópio de varredura confocal a laser (LSM510, Zeiss, Alemanha).

2.2.7 Secreção estática de insulina

Para a análise de secreção estática de insulina, as ilhotas pancreáticas foram isoladas por meio de digestão por colagenase do pâncreas (n=5 animais/grupo). Através de canulação do ducto pancreático, foi realizada a injeção de 3mL da solução de colagenase tipo V (EC 3.4.24.3, Sigma, St. Louis, MO, USA) (1,7 mg/mL em solução de Hank's, pH 7,4; composição do Hank's: NaCl 136mM, KCl 5,4mM, $CaCl_2.2H_2O$ 1,26mM, $MgSO_4.7H_2O$ 0,81mM, KH_2PO_4 0,44mM, Na_2HPO_4 0,34mM, NaHCO3 4,2Mm, suplementada com 5,6 mM de glicose e 1 mg/mL de albumina). Em seguida, o pâncreas foi retirado e incubado a 37ºC por 11 minutos nessa solução. Foram realizadas três lavagens com solução tampão de Hank's, seguidas de centrifugação, para a remoção da colagenase e dos fragmentos digeridos do pâncreas exócrino. As ilhotas foram coletadas individualmente sob lupa com o auxílio de uma micropipeta.

Após o procedimento de isolamento, grupos de cinco ilhotas de tamanho semelhante foram pré-incubados em placas de 24 poços com 0,5mL de solução tampão de Krebs (139 mM Na^+, 5 mM K^+, 1 mM Ca_2^+, 1mM Mg_2^+, 123,6 mM Cl^-, 24 mM HCO_3^-) suplementada com 3 mg/mL de albumina bovina (Sigma) e 5,6 mM de glicose, em banho-maria a 37°C durante 30 minutos. Após a aspiração cuidadosa do tampão, as ilhotas foram divididas em dois grupos, as que incubadas com Krebs suplementado com 2,8 mM de glicose (concentração basal) e as incubadas com a solução tampão suplementada com 16,7 mM. Após incubação por 1h a 37°C, alíquotas de 500µL do sobrenadante foram retiradas e armazenadas a – 20ºC até a determinação da concentração de insulina, expressa em ng/mL.ilhota, utilizando o kit ELISA Rat/Mouse Insulin ELISA Kit (Cat # EZRMI-13 K, Millipore, EUA).

2.2.8 Avaliação bioquímica no plasma/soro e tecidos

Para obter o plasma (n=6-10 animais/grupo), as amostras de sangue foram coletadas em heparina e centrifugadas por 15 minutos a 3000 rpm (G = 503,1 – rotor = 5 cm) em centrífuga refrigerada (2-4°C) (Hettich, Alemanha). Para a obteção de soro (n=6-10 animais/grupo), as amostras de sangue permaneceram à TA por 1-2 horas para a formação de coágulos, depois foram centrifugadas por 15 minutos a 3000 rpm (G = 503,1 – rotor = 5 cm) em centrífuga

refrigerada (2-4°C). Amostras de sangue foram também obtidas para análise de hematologia/hematócrito e parâmetros bioquímicos (tais como amilase, ALT, AST e creatinina) realizada por laboratório veterinário especializado (VetPat, R. Cel. Manuel de Morais, 146 - Jardim Brasil, Campinas - SP, 13073-022).

A lipidemia que incluiu a determinação da concentração sérica de triglicérides, colesterol total, e das frações LDL e HDL, foi medida em amostras de soro por meio dos kits comerciais de ELISA (Enzymatic Colestat AA liquid, LDL Cholesterol Reactive Precipitant, HDL Cholesterol Reactive Precipitant e HDL Cholesterol Reactive Precipitant e TG Color GPO/PAP AA, Weiner Lab., St. Ingbert-Alemanha) (n=8-15 animais/grupo).

As concentrações de LPS, em amostras de soro ou de lisado intestinal (n=8 animais/grupo, foram determinadas utilizando o kit Limulus Ameboyte Lysate (LAL) QCL-1000 ™ (Lonza, Basel-SW) (Jayashree *et al.*, 2014), que tem como princípio o método cromogênico de ponto final. Este método utiliza a reação de endotoxina do lisado de amebócitos circulantes do caranguejo ferradura (Limulus polyphemus) para ativar uma enzima que, por sua vez, libera p-nitroanilina (pNA) a partir de um substrato sintético, produzindo uma cor amarela. Em uma placa de 96 wells, as amostras de soro e homogeneizados de fragmentos intestinais juntamente com o reagente LAL foram incubados a 37°C por 10 minutos. Em seguida, foi adicionado o substrato cromogênico e incubado a 37°C por mais 6 minutos. Por fim, foi adicionado a solução de parada e a medição da absorbância foi realizada no comprimento de onda 405nm com o auxílio de um leitor de microplacas (Power Wave XS2, Biotek Inc., Winooski-US). Conforme recomendado pela ficha técnica todos os acessórios e reagentes sem endotoxina foram adquiridos pelo mesmo fabribante do kit (Lonza, Basel-SW)).

A concentração de zonulina em amostras de plasma ou de lisado intestinal (n=8 animais/grupo) foi medida usando o Elisa Mouse Zonulin (MBS748504-MyBioSource) que se baseia no método de imunoensaio enzimático competitivo. As amostras foram incubadas juntamente com o conjugado ZON-HRP em placa pré-revestida por uma hora à TA. Após o período de incubação, os poços foram lavados cinco vezes com solução de lavagem fornecida pelo kit e, em seguida, incubados com o substrato para a enzima HRP por 20 minutos à TA. Finalmente, foi adicionada a solução de parada fornecida pelo kit. A medida da absorbância foi realizada a 450 nm em um leitor de microplacas (Power Wave XS2, Biotek Inc., Winooski-US).

A concentração de TNF-α foi medida em amostras de plasma/soro ou de lisado intestinal (n=8 animais/grupo) com auxílio do kit ELISA MAX™ Deluxe Set Mouse TNF-α (Cat. No. 430904, BioLegend®) que se baseia no método de imunoensaio enzimático sanduíche, ou seja, que se utiliza de um anticorpo de captação e um de detecção. No dia anterior ao ensaio, a microplaca de 96 wells foi tratada com o anticorpo de captação *overnight*. No dia do ensaio, a placa foi lavada (solução de PBS-pH 7,4 + 0,05% Tween-20) e bloqueada com *Assay Diluent A* por 1h à TA, com agitação. Em seguida, a placa foi lavada, as amostras foram pipetadas e incubadas por 2h à TA, com agitação. Após incubação, a placa foi lavada e incubada com o anticorpo de detecção por 1h à TA, com agitação. Após esse período, a placa foi lavada e incubada com o substrato Avidin-HRP por 30 minutos à TA com agitação. Após lavagem, procedeu-se a incubação com o substrato por 15 minutos à TA, no escuro e sem agitação. Por fim, foi adicionada a solução de parada (solução ácida H_2SO_4 2N) e a medida da absorbância foi realizada a 450 nm em um leitor de microplacas (Power Wave XS2, Biotek Inc., Winooski-US).

Os valores da concentração plasmática ou sérica foram expressos em: EU/mLpara LPS, ng/mL para zonulina e pg/mL para TNF-α. Para os segmentos intestinais, os valores foram expressos a partir da relação entre as concentrações obtidas e a respectiva concentração total de proteína (µg/mL), previamente medida em uma alíquota dos respectivos homogenatos com o reagente de Bradford (Protein Assay Dye Reagent Concentrate, cat. # 500-0006, Bio-Rad, Hércules-EUA) a 596 nm em leitor de microplacas (Power Wave XS2, Biotek Inc., Winooski-US).

2.2.9 Permeabilidade intestinal

A permeabilidade intestinal foi avaliada utilizando dois marcadores extracelulares com peso molecular distinto. No artigo constante no Capítulo 3, foi utilizado o Dextran marcado com isotiocianato de fluoresceína, com peso molecuclar de 4-kDa (FITC-Dextran, cat number 46944-500mg-F; Sigma, USA). No artigo que integra o Capítulo 5, foi utilizado o Lucifer Yellow (LY CH lithium salt, Invitrogen, cat number L453; MW 457.25 Da). O protocolo empregado foi o descrito por previamente (Cani *et al.*, 2008), com modificaçãoes. Para ambos os marcadores, os animais permaneceram em jejum por 6 horas e, após este período, receberam, via gavagem, uma solução de FITC-Dextran, na dose de 600mg/kg, diluído em PBS (0,01M pH 7,4), e volume de 4,8 mL/kg peso (n=5 animais/grupo). Para o marcador LY, após o jejum, um grupo distinto de animais (n=11 animais/grupo) foram anestesiados (com 80

mg/kg cetamina hidrocloridrica e 10 mg/kg xilazina hidroclorídrica, através de injeção intraperitoneal) e, então, receberam por gavagem a solução de LY na concentração de 100μM, soro estéril, num volume de 7mL/kg peso. Após 1h de realizada a gavagem com as respectivas soluções, os animais foram eutanasiados e o sangue coletado dos vasos cervicais (após eutanásia e decapitação do animal). As amostras de sangue foram centrifugadas à velocidade de 12000 rpm (G=8.049,6 – raio do rotor = 5cm) por 10 minutos a 4°C para para separação do plasma. Em seguida, cada amostra do plasma (50 μL) diluída em PSB (50 μL) foi pipetado em placa de 96 wells e a leitura feita com um leitor de microplaca Fluorskan Ascent (Thermo Scientific, USA), no comprimento de onda: 458nm de excitação e 535nm de emissão para ambos os marcadores. Os valores da permeabilidade intestinal ao LY e FITC-Dextran foram expressos como valor de absorbância plasmática do marcador subtraindo o valor em branco (valor de absorbância plasmática de um animal que não recebeu o marcador por gavagem).

2.2.10 Tomografia Computadorizada

A técnica de tomografia computadorizada (TC), que faz uso da propriedade dos materiais biológicos de absorverem radiação (Raio X) de forma diferenciada, foi utilizada para avaliar a massa relativa de tecidos adiposo unilocular (ou branco) e muscular. O aparelho utilizado foi o microtomógrafo modelo 1178 (SkyScan®, Bruker, Massachusetts, EUA). O animal foi anestesiado (com 80 mg/kg cetamina hidrocloridrica e 10 mg/kg xilazina hidroclorídrica, através de injeção intraperitoneal) e cuidadosamente posicionado na câmara de raio-x, sob os parâmetros 44 kV; 150 μA; 6.6 W. Após verificação do melhor posicionamento do animal (seja para a aquisição da imagem ou para o possível bem-estar do animal) foi acionado o comando para que o equipamento começasse a aquisição de imagens ao longo de uma rotação de 360º com espaços de angulação bastante precisos, totalizando a obtenção de mil imagens por animal (n=11 animais/grupo). Feito o escaneamento dos camundongos, foi possível ter a imagem 3D de cada animal, a partir de software de reconstrução (N.Recon®, SkyScan®). Com o auxílio do programa DataViewer®, foi possível a visualização prévia dos eixos coronal, tranversal e sagital para avaliar a boa da captura das imagens, ou seja, se não houve falha ou movimentação do animal gerando imprecisão. Os cálculos foram realizados utilizando o software CTAN®. Este software “binariza” a imagem resultando em uma imagem em preto e branco. A partir dessa imagem em preto e branco, é possível distinguir pixels de uma escala de 0 a 255 onde cada intervalo corresponde a um

determinado tecido. Vale ressaltar que para volume do tecido adiposo, foi necessário desenhar e indicar ao software a região do pulmão que possui uma densidade similar do tecido em estudo. Da mesma forma, foi delimitado e indicado ao software, a região ocupada por todo intestino delgado (músculo liso) para a obtenção do volume do músculo estriado esquelético que era nosso foco de estudo. Os valores de massa gorda e massa magra relativos foram expressos como porcentagem do volume total de tecido adiposo e músculo esquelético total, respectivamente, em relação ao volume corporal total.

2.2.11 Gasto energético

O gasto energético basal foi medido com auxílio de um sistema de câmara metabólica (Oxylet - Pan Lab / Havard Apparatus, Espanha). Após 3h de adaptação, os camundongos foram monitorados e os dados registrados por um período de 48h. A atividade motora basal foi registrada por 24 horas, utilizando um sistema de gaiolas acoplado ao equipamento que conta cada movimento (Physiocage - Pan Lab / Havard Apparatus, Espanha). Para ambos os procedimentos, os camundongos dos diferentes grupos experimentais foram alojados individualmente em um ciclo claro e escuro de 12 horas a 24ºC, com livre acesso a água e alimentos. Os valores foram expressos como média dos valores obtidos durantes os períodos claro e escuro (n=5-12 animais/grupo).

2.2.12 Imunoistoquímica para proteínas de junção (Cld-1, -2, -3 e ZO-1) e para histonas 3 e 4 acetiladas

Para avaliar a influência do butirato de sódio sobre as proteínas da junção de oclusão (Cld-1, -2, -3 e ZO-1) e sobre a acetilação das histonas 3 e 4, foi utilizada a técnica de imunofluorescência indireta (Oliveira *et al.*, 2019). Fragmentos do intestino delgado (jejuno e íleo) e do cólon foram coletados, lavados em PBS e congelados em meio Tissue-Tek® a -70°C com n-hexano resfriado com N_2 liquido. Os cortes obtidos foram obtidos por criotomia (secções com 5 μm de espessura) e, posteriormente, fixados em acetona a -20ºC por três minutos e mantidos em biofreezer -80°C até o momento da reação.

Para a reação de imunofluorescência, os cortes foram lavados em PBS (0,01M, pH 7,4), e submetidos à solução bloqueadora (BSA 5% + 0,1% Tween 20, em PBS) por 1h. Após este período, os cortes foram incubados *overnight* a 4°C, com solução BSA 3% (diluída em PBS) acrescida de anticorpo primário (Tabela III). Após lavagem com PBS, os cortes foram incubados por 2h com anticorpo secundário específico conjugado com FITC (F0382 Sigma;

diluição 1:100) e DAPI para marcação nuclear (D9542 Sigma; diluição 1:1000) diluídos em solução BSA 1% + PBS. Em seguida, os cortes foram lavados em PBS, montados em meio de montagem ProLong® (Invitrogen P36930) e fotodocumentados com auxílio de microscópio de fluorescência (Observer.Z1; Zeiss – AxioCam, MRC, USA ou Microscópio Confocal Invertido Zeiss LSM510, Carl Zeiss AG, Germany).

Para a obtenção das imagens da imunfluorência tanto das proteínas de junção quanto das histonas, foi seguido o seguinte protocolo: na mesma sessão de microscopia e mantendo como padrão os parâmetros estabelecidos para obtenção das imagens do grupo controle (C), como tempo de exposição e potência da luz, foram capturadas todas as imagens de todos os demais grupos experimentais (D, CB e DB), garantindo desta forma maior confiabilidade na comparação de grau de fluorescência entre os grupos. Ao todo, foram fotografadas 5 imagens do epitélio de revestimento intestinal de 5 secções histológicas diferentes, obtidas de cada segmento intestinal (jejuno, íleo e cólon) por animal (n=5) dos 4 diferentes grupos experimentais.

Para avaliar o grau de fluorescência das proteínas de junção, com auxílio do programa Image J (http://rsbweb.nih.gov/ij/) foram marcados 50 pontos em diferentes regiões de contato intercelular no epitélio de cada imagem, totalizando aproximadamente 1250 pontos/grupo. Para avaliar o grau de fluorescência das diferentes histonas, também com auxílio do programa Image J, foram delimitadas 5 regiões contendo apenas núcleos de células epiteliais intestinais de cada imagem e foi medido o grau de fluorescência por área delimitada. Os valores foram expressos como razão entre a intensidade de fluorescência e a área selecionada.

Tabela III. Anticorpos para imunofluorescência

ANTICORPOS PRIMÁRIOS		
Anti Rabbit – Claudin-1	Abcam ab15098	1:50
Anti Rabbit – Claudin-2	Abcam ab53032	1:30
Anti Rabbit – Claudin-3	Invitrogen 1700	1:50
Anti Rabbit – ZO-1	Invitrogen 7300	1:50
Anti Acetyl Histone H3 (lys 9 e lys 14)	Invitrogen PA5-16194	1:50
Anti Acetyl Histone H4 (lys5,8,12,16)	Invitrogen PA5-32029	1:50
ANTICORPO SECUNDÁRIO		
Goat anti-Rabbit FITC	Sigma F0382	1:75

2.2.13 Western Blot

Raspados da mucosa intestinal do intestino delgado (jejuno e íleo) e do cólon foram lavados em PBS e lisados, com o auxílio de um sonicador, em coquetel anti-protease (composição: 10 mM imidazol pH 7,4; 4 mM EDTA; 1 mM EGTA; 200 μM DTT; 0,5 μg/mL pepstatina; 200 KIU/mL aprotinina; 200 μM fenilmetilsufonilfluoreto; 2,5 μg/mL leupeptina e 30 μg/mL inibidor de tripsina). A quantificação da concentração de proteínas totais nos homogeneizados foi feita por meio do método de Bradford utilizando o reagente da Bio-Rad (Protein Assay Dye Reagent Concentrate - Hercules, CA - USA). Após a obtenção das concentrações de proteína total de cada amostra, foram pipetados os volumes necessários de cada homogeneizado para obtenção de uma concentração de 45-50μg/μL de proteína total. As amostras foram incubadas por 1h a 37°C com 30% em volume de tampão de amostra Laemmli (1 mol fosfato de sódio/ L (pH 7,8), 10% de SDS, 2% de β-mercaptoetanol, 50% de glicerol e 0,1% de azul de bromofenol – 5x concentrado) (Carvalho *et al.*, 2010) e, posteriormente, aplicadas em gel de acrilamida a 12% (para Claudinas -1, -2 e -3, e ocludina) e a 6,5% (ZO-1) (Peixoto & Collares-Buzato, 2005). As amostras proteicas foram separadas por meio de eletroforese e transferidas para uma membrana de nitrocellulose (Bio-Rad). A membrana obtida foi corada com solução Ponceau (Sigma) para confirmação da adequada transferência das proteínas. Para detecção das proteínas de interesse, as membranas foram bloqueadas por 4 horas à TA com Solução Basal (0,01M Trisma Base, 0,15 M NaCl, 0,05% de Tween 20, pH 7,4) suplementada com 5% leite em pó desnatado (Molico). Em seguida, as membranas foram incubadas *overnight* a 4°C com anticorpo primário (Tabela IV) diluido em Solução Basal (SB) contendo 3% leite em pó desnatado. Após lavagens com SB, as membranas foram incubadas com o anticorpo secundário específico conjugado com HRP (Sigma) diluído (1:500) em SB contendo 1% de leite em pó desnatado, por 2h à TA. A detecção das bandas foi feita com a utilização de kit de quimioluminescência Super Signal (Thermo Fisher Scientific - USA) e sua imagem capturada por fotodocumentador Gene Genome (Syngene Bio Imaging, UK) e software Gene Genome 5 (Genesys, UK). O tamanho relativo das bandas foi quantificado por densitometria óptica utilizando o programa Image J (http://rsbweb.nih.gov/ij/). Como controle interno da quantidade de proteínas aplicada no gel, foi realizado *reblotting* com anticorpo anti-beta-actina (Tabela IV). Os valores da densitometria óptica foram expressos como razão entre o valor da banda da proteína de interesse pelo valor da banda de beta-actina (controle interno) (5-8 membranas/proteína).

Tabela IV. Anticorpos para *Western Blot In Vivo*.

ANTICORPO PRIMÁRIO		
Anti Rabbit – Claudin-1	Abcam ab15098	1:300
Anti Rabbit – Claudin-2	Abcam ab53032	1:300
Anti Rabbit – Claudin-3	Invitrogen 1700	1:400
Anti Rabbit – Occludin	Abcam ab31721	1:300
Anti Rabbit – ZO-1	Invitrogen 7300	1:300
Anti Rabbit – Beta actin	Uniscience 4970S	1:600
ANTICORPO SECUNDÁRIO		
Goat anti-Rabbit HRP	Sigma A4914	1:600

2.2.14 PCR quantitativo absoluto (RT-qPCR) em homogeneizados de tecido adiposo marrom e hipotálamo

Fragmentos de tecido adiposo marrom e hipotálamo (50 a 100 mg de tecido) foram homogeneizados em 1mL de Trizol e incubados por 5 min à TA e, posteriormente, armazenados em -80°C até a extração do RNA. Para a extração de RNA total, foi adicionado o volume de 300 µL de clorofórmio gelado às amostras e homogeneizado vigorosamente durante 15 s e incubado por 2-3 minutos à TA. Em seguida, as amostras foram centrifugadas a 12000 rpm (G = 8.049,6 – rotor = 5 cm) por 15 min, à 2-8ºC. A fase aquosa resultante de centrifugação foi transferida para outro tubo no qual foi adicionado 500 µL de álcool isopropílico gelado. Após 10 min de incubação em TA, o material foi novamente centrifugado a 12000 rpm (G = 8.049,6 – rotor = 5 cm) por 10 min à 2-8ºC. O sobrenadante foi descartado, o pellet lavado em 1 mL de etanol 75% gelado (preparado com água DEPC – água milliq filtrada no fluxo) e centrifugado a 7500 rpm (G = 3.144,4 – rotor = 5 cm) por 10 min a 2-8ºC, esta dinâmica foi repetida por mais uma vez e, por fim, o pellet foi ressuspendido em 40µL de água DEPC. A concentração do RNA total foi medida com o auxílio de um Nanodrop ND-1000 UV-Vis (Nanodrop Technologies, Wilmington, USA), a partir da absorbância no comprimento de ondas de 260 nm. Foi realizado o cálculo da razão 260/280 nm (razão entre RNA/DNA, ou seja, indica o quanto a amostra está contaminada com DNA).

A síntese de cDNA foi realizada com auxílio do kit High Capacity cDNA reverse transcription Kit (#4368814, Applied Biosystems^{TM}, Foster City, CA, USA). A partir da

quantificação da concentração de RNA total, foram calculados os volumes necessários de cada amostra para obtenção de uma concentração de 2µg de RNA total, aos quais foram complementados com água pra 10µL. Foi adicionado o volume de 10 µL do mix (RT Buffer 10x, dNTPMix 25x -100mM), RT Random Primers 10x, MultiScribe Reverse Transcriptase - 50U/µL, Nuclease-free water). As amostras foram colocadas, então, em termociclador com os seguintes ciclos: 25°C por 10 minutos, 37°C por 1 hora e 85°C por 5 segundos.

As amplificações por RT-qPCR foram realizadas em duplicatas. Às amostras, foram adicionados os reagentes padronizados para PCR em tempo real (SYBR® Green PCR Master Mix, Applied Biosystems) adicionado os conjuntos de *primers (Foward e Reverse)* (Tabela V*)* e H_2O DEPC. Quantidades absolutas de mRNAs de interesse foram normalizadas pelo gene de controle Hypoxanthine-guanine phosphoribosyltransferase (HPRT), usando o método 2-ΔΔCt (Soares *et al.*, 2019).

Tabela V. Primers específicos utilizados

Gene	Sequência do primer 5'- 3'
POMC	Forward: GGCTTGCAAACTCGACCTC Reverse: TGACCCATGACGTACTTCCG
CART	Forward: ACCTTTGCTGGGTGCCCGTG Reverse: TGCAACGCTTCGATCAGCTCC
NPY	Forward: TACTCCGCTCTGCGACACTA Reverse: TCTTCAAGCCTTGTTCTGGG
AgRP	Forward: GAGTTCCCAGGTCTAAGTCTGAATG Reverse: ATCTAGCACCTCCGCCAAAG
UCP-1	Forward: CTGCCAGGACAGTACCCAAG Reverse: TCAGCTGTTCAAAGCACACA
HPRT	Forward: TCAGTCAACGGGGGACATAAA Reverse: GGGGCTGTACTGCTTAACCAG

2.3 IN VITRO

2.3.1 Animais e dietas

Os animais, utilizados para a aquisição do conteúdo luminal do intestino delgado, foram manipulados seguindo o protocolo descrito anteriormente para os experimentos *in vivo*, otimizando, assim, a utilização de animais, sendo que o Comitê de Ética em Experimentação Animal Institucional aprovou todos os experimentos desse projeto (CEUA/UNICAMP; Protocolo: 4185-1).

2.3.2 Cultura de linhagem celular Caco-2

Células da linhagem Caco-2 (adenocarcinoma de cólon humano) foram cultivadas em frascos estéreis (Nest Biotech Co. Ltd, China) em meio DMEM com alta glicose (*Dulbecco's Modified Eagle Medium* - DMEM). O meio foi suplementado com 10% de soro fetal bovino, 2% de aminoácidos não essenciais, 1% de L-glutamina e 60 mg/L de gentamicina (Cultilab, Campinas, São Paulo) e mantidas em incubadora umidificada a 37°C, com 5% de CO_2 (Incusafe Sanyo MCO-17A, Sanyo Electric Ltd., Japão). O meio foi trocado pelo menos três vezes por semana e o repique das células foi realizado por digestão parcial com tripsina/EDTA (Solução Tripsina (2.500g/L)/EDTA (250mg/L) 10-15 minutos). Para os experimentos, as células foram semeadas em suportes contendo membrana permeável de 12 ou 30 mm de diâmetro (Millicell, Merck Millipore, German) previamente revestidos com solução de colágeno extraída das caudas de ratos Wistar (Hauschka and Konigsberg, 1966). As células foram semeadas em uma densidade de $1{,}5x10^4$ células/cm². Após a total confluência das células (aproximadamente 10 a 11 dias), as monocamadas foram expostas de ambos os lados (apical + basal) ao conteúdo luminal do intestino delgado de camundongos dos diferentes grupos experimentais.

2.3.3 Exposição ao conteúdo luminal intestinal de camundongos

Para obtenção do conteúdo luminal ao qual as células foram expostas, camundongos dos diferentes grupos experimentais (C, D, CB e DB) foram eutanasiados em câmara saturada de CO_2 e o intestino delgado removido sob condições estéreis (dentro do fluxo laminar). A utilização do intestino delgado para a obtenção do conteúdo luminal a ser empregada no estudo *in vitro* foi fundamentada em trabalho prévio de nosso grupo de pesquisa (Oliveira, Canuto and Collares-Buzato, 2019). Neste trabalho constatamos que o conteúdo luminal do

intestino delgado induziu um comprometimento mais significativo da integridade da barreira epitelial *in vitro* em relação ao conteúdo intestinal do intestino grosso.

O conteúdo luminal foi obtido, injetando-se, com o auxílio de uma seringa estéril, 15 mL de tampão estéril de Krebs-bicarbonato (concentração em mM: NaCl 115, KCl 5, $MgCl_2$ 1, $CaCl_2$ 1, $NaHCO_3$ 10, HEPES 15; glucose 100; 100 mg/dL de glicose; pH = 7.4 equilibrado com CO_2) no segmento isolado do intestino delgado. A solução obtida por lavagem do conteúdo luminal intestinal foi centrifugada em tubos Falcon a 2100 x g por 90 segundos, o sobrenadante foi coletado e e diluído na proporção 1:5 em Krebs-bicarbonato estéril. Essa diluição do conteúdo intestinal do intestino delgado foi necessária para eliminar/diminuir o efeito citotóxico sobre as células, como observado e descrito anteriormente (Oliveira *et al*, 2019). As monocamadas celulares foram expostas em ambas as superfícies (apical e basolateral) ao conteúdo intestinal por um período de 6 horas. Posteriormente, foram avaliados os seguintes parâmetros de integridade da barreira epitelial paracelular: viabilidade celular, resistência elétrica transepitelial (Rt) e fluxo transepitelial (Ft) ao marcador Lucifer Yellow. Os métodos adotados para avaliação desses parâmetros estão descritos a seguir.

2.3.4 Viabilidade celular

A viabilidade celular foi avaliada pelo teste de absorção do corante vermelho neutro (Neutral Red). Para isso, células Caco-2 foram cultivadas em microplaca de 96 poços tratada com colágeno (densidade $7{,}5x10^4$ células/poço). Após atingirem confluência, as monocamadas foram expostas ao conteúdo luminal intestinal por 6h (12-21 monocamadas/grupo). Em seguida, as monocamadas foram incubadas com vermelho neutro (40μg/mL em solução Krebs-bicarbonato) por 3h a 37°C. Posteriormente, as células foram lavadas 3 vezes com de solução contendo paraformaldeído (4%) e cloreto de cálcio (1%). Em seguida, foi adicionado, em cada poço, um volume de 200uL de solução contendo etanol (50%) e ácido acético glacial (1%). Finalmente, foi feita a leitura da absorbância em leitor de microplaca (PowerWave XS2) com comprimento de onda 570nm e a viabilidade celular foi expressa em porcentagem em relação à média da absorbância das monocamadas expostas à solução Krebs-bicarbonato (grupo controle, considerado como 100% de viabilidade).

2.3.5 Resistência elétrica transepitelial (Rt) e fluxo paracelular (Ft)

A medição da Rt foi realizada com o auxílio de dois eletrodos Ag/AgCl 'chopstick' acoplados a um voltímetro combinado e a uma fonte de corrente constante (EVOM, World Precision Instruments, Reino Unido) em monocamadas de Caco-2 confluentes cultivadas em suportes Millicell de 12mm (n=4/grupo). A medida de Rt foi observada a cada hora durante o intervalo de 6 horas após a exposição ao conteúdo luminal intestinal. A Rt final foi calculada da seguinte forma: a resistência do suporte da membrana vazia (sem células) foi subtraída do valor da Rt do suporte com as células e depois multiplicada pela área da membrana (1,13 cm^2) para obter o valor final da Rt ($\Omega \cdot cm^2$) . Os dados da Rt foram expressos como uma porcentagem do valor médio inicial (às 0h, antes da exposição ao conteúdo luminal).

O marcador de quebra de barreira utilizado para avaliar o fluxo transepitelial foi o Lucifer Yellow (LY) (MW 457,25 Da) (Mongelli-Sabino *et al*., 2017; Oliveira *et al*., 2019). Para este propósito, as monocamadas celulares cultivadas em suportes de cultura permeáveis de 30 mm foram transferidas para uma nova placa contendo a suspensão do conteúdo luminal intestinal ou solução de Krebs, onde foi adicionado o marcador LY (100 μM) (meio basal) (n=6-8 monocamadas/grupo).. Na superfície apical, a mesma solução basal foi adicionada, mas sem o marcador. Após o período de incubação (6h), foram coletadas amostras das soluções apical e basolateral. As amostras foram lidas em triplicatas (0,2 mL) em uma placa de 96 poços e a leitura foi realizada com o auxílio de um um leitor de microplacas Synergy H1 (Biotek Instruments, EUA) a 428 nm (comprimento de onda de excitação) e 535 nm (comprimento de onda de emissão). O fluxo transepitelial (Ft) de Lucifer Yellow tomado como um índice de permeabilidade paracelular, foi calculado da seguinte forma: Ft = Fluorescência apical x 100 / Fluorescência apical + Fluorescência basal.

2.3.6 Imunoistoquímica para proteínas juncionais

As monocamadas das células Caco-2 cultivadas nos suportes permeáveis de 12 mm (n=3-4 monocamadas/grupo) foram fixadas e mantidas em metanol a -20°C até a reação de imunofluorescência indireta. Após lavagem com solução salina tamponada com fosfato (PBS - 0,05M, pH = 7,4), as monocamadas foram bloqueadas com soro fetal bovino (SFB) a 3% em PBS por 30 min à temperatura ambiente (TA) e depois incubadas com anticorpos primários anti-Claudina-1 (Abcam ab15098, 1:30) e ZO-1 (Invitrogen 7300, 1:50) diluídos em PBS suplementado com 3% SFB, *overnight* a 4°C. Os anticorpos anti-Ocludina e Claudinas 2 e 3 (cat number e diluições Tabela III) não mostraram imunoreatividade em células Caco-2 pelo

nosso método de imunofluorescência e suas variações. Subsequentemente, as monocamadas foram incubadas por 1 h com o anticorpo secundário específico conjugado com FITC (Sigma-F0382, 1:75) e DAPI (D9542-Sigma, diluição 1:1000 em PBS mais 3% de FBS) à temperatura ambiente. As monocamadas foram lavadas cinco vezes com PBS, montadas com (ProLong® Gold Antifade Mountant (Invitrogen P36930) e analisadas na mesma sessão microscópica, usando os mesmos parâmetros de iluminação/contraste para comparar a fluorescência entre os grupos tratado e controle (Observer. Z1; Zeiss - AxioCam, MRC).

2.3.7 Western Blot

Para a técnica *Western Blot*, as monocamadas Caco-2 foram raspadas dos suportes permeáveis de 30 mm utilizando-se um scraper em solução de PBS. O material coletado foi centrifugado a 1500 rpm (G = 125,77 – rotor = 5 cm) por 3 minutos a 4ºC, o sobrenadante descartado e o sedimento celular foi ressuspenso em 20 ml de coquetel antiprotease (composição: 10 mM imidazol pH 7,4; EDTA 4 mM; EGTA 1 mM; EGTA 1 mM; EGT 200 μM; DTT 200 μM; 0,5 μg/ml de peptostatina A; 200 KUI/ml de aprotinina; fluoreto de fenilmetanossulfonil 200 μM; 2 μg/mL de leupeptina e 30 μg/mL inibidores de tripsina) e sonicados. Uma quantidade igual de proteína (20 μg) foi misturada com o tampão de amostra Laemmli (30% do volume da alíquota) e fracionada por eletroforese em géis de poliacrilamida a 6,5% ou 12%, transferida eletroforeticamente para membranas de nitrocelulose (Bio-Rad) e corada com a solução Ponceau S (Sigma) para verificar a eficiência da transferência de membrana. As membranas foram bloqueadas em SB com 5% de leite desnatado e depois incubadas *overnight* a 4 °C com o anticorpo primário (Tabela VI) diluído na mesma SB, contendo 3% de leite em pó desnatado, seguido de incubação com anticorpo secundário específico conjugado com peroxidase (HRP) (A4914-Sigma) (diluição 1:600 em solução basal contendo 1% de leite em pó desnatado) por 2 horas à TA. As bandas imunorreativas foram detectadas usando um kit de quimioluminescência (Super Signal, Thermo Fisher Scientific, EUA) e fotografadas por um sistema de captura de imagem (Genome Gene, Syngene Bio Imaging, Reino Unido). O tamanho relativo das bandas imunorreativas foi quantificado por densitometria usando o software ImageJ. As mesmas membranas foram reincubadas com anticorpo anti-beta-actina (Tabela VI), usado como controle interno. Finalmente, os valores densitométricos ópticos foram expressos como uma razão da densitometria da proteína de interesse e beta-actina (controle interno) (n=4 membranas/grupo).

Tabela VI. Anticorpos para Western Blotting *In Vitro*.

ANTICORPO PRIMÁRIO

Anti Rabbit – Claudin-1	Abcam ab15098	1:300
Anti Rabbit – Claudin-3	Invitrogen 1700	1:500
Anti Rabbit – Occludin	Abcam ab31721	1:500
Anti Rabbit – ZO-1	Invitrogen 7300	1:300
Anti Rabbit – Beta actin	Uniscience 4970S	1:700

2.3.8 Cultura de linhagem celular de fibroblastos e diferenciação em adipócitos

Nesse estudo, foram utilizadas células precursoras de adipócitos, imortalizadas, isoladas de tecido adiposo subcutâneo (células 9W) para se avaliar o efeito do butirato na bioenergética celular (Mori *et al.*, 2012). As células 9W foram cultivadas em placas de 90 x 15 mm em DMEM com alta concentração de glicose suplementada com soro fetal bovino a 10% (Gibco) e 1% de estreptomicina e penicilina (Gibco) e mantidas em uma incubadora a 37 ° C com 5% de CO_2 e 70 % de umidade. Ao atingir 70-80% de confluência, as células foram lavadas com tampão fosfato-salino (pH 7,4), destacadas das placas com 0,25% de tripsina-EDTA (Gibco), centrifugadas (1200 rpm por 5 minutos), ressuspensas em DMEM suplementado e semeadas (5 x 10^3 células) em placa de 24 wells. Após confluência, as células indiferenciadas foram usadas para os experimentos. Para a diferenciação celular, após a semeadura em placa de 24 wells, foi adicionado meio adipogênico contendo Insulina 20 nM (Sigma-Aldrich), 2 mg/mL de Dexametasona (Sigma-Aldrich), 500 µM 3-isobutil-1-metilxantina (Sigma-Aldrich), 1 µg/mL de rosiglitazona (Sigma-Aldrich), 1 nM 3,3 ', 5-Triiodo-L-Tironina (Sigma-Aldrich) e 125 µM de Indometacino (Sigma -Aldrich). Após 8 dias de diferenciação, as células foram usadas para os experimentos.

2.3.9 Viabilidade celular

Células 9W não diferenciadas e diferenciadas foram tratadas com 0,5 mM de butirato de sódio (Sigma-Aldrich) por 24 horas. Posteriormente, as células tratadas com butirato foram lavadas com PBS e incubadas com DMEM High Glucose mais 0,5 mg / mL de brometo de tiazolil azul-tetrazólio (Sigma-Aldrich) por 1h (células diferenciadas) ou 4h (células indiferenciadas). Após a incubação, o meio foi aspirado, os poços foram lavados com PBS.

Foram adicionados 100 µL de DMSO (Synth, Brasil) por poço e as placas foram incubadas por 30 minutos a 37 ° C. A absorvância foi medida a 570 nm usando um leitor de microplacas (PowerWave XS2).

2.3.10 Consumo de oxigênio

A bioenergética celular das células 9W (indiferenciada e diferenciada) foi medida por respirometria de alta resolução (OroborosOxygraph-O2K, Oroboros Instruments, Innsbruck, Áustria) a 37 ° C em Krebs-Ringer pH 7,4 (NaCl 130 mM, KCl 4,7 mM, 1,24 mM MgSO4, CaCl2 2,5 mM, HEPES 10 mM, NaH2PO4 2,5 mM, BSA a 2%). As células foram tratadas por 6 ou 24 horas com 0,5 mM de butirato de sódio diluído em DMEM com alta glicose. Essa concentração relativamente baixa de butirato foi escolhida com base nas seguintes premissas: 1) está dentro da faixa de concentração fisiológica (Caminhotto *et al.*, 2019) e 2) não possui citotoxicidade aparente além de exibir efeitos biológicos em diferentes tipos de células *in vitro* (Singh *et al*., 1997; Kaiko *et al.*, 2016; Kespohl *et al.*, 2017; Liu *et al.*, 2020). Células com uma densidade de 8 x 10^5 (diferenciada) ou 1,5 x 10^6 (não diferenciada) foram adicionadas às câmaras de oxígrafo para obter fluxos de consumo de oxigênio de acordo com um protocolo publicado anteriormente (Doerrier *et al.*, 2018). Com o objetivo de obter consumo de oxigênio dependente de ATP e vazamento de prótons, foi adicionada às câmaras oligomicina (2µg/mL). Posteriormente, desacopladores mitocondriais foram tritiados (0,05 µM por adição) - CCCP (carbonilciaeto de m-clorofenil-hidrazona) ou FCCP (cianeto de carbonil-4- (trifluorometoxi) fenil-hidrazona - para atingir a respiração máxima. Finalmente, foi adicionada antimicina A (2,5 µM) para registros de valores de respiração não mitocondrial. Os resultados foram expressos como Fluxo de O_2 por célula [pmol / (s * 10^6 células)].

CAPITULO 3

Butyrate-induced inhibition of insulin resistance is associated with reduction in hepatic steatosis and improvement of beta-cell secretion and intestinal barrier function in prediabetic mice*.

* Artigo publicado no periódico:
Experimental Biology and Medicine
Vol 242, Issue 12, pp. 1214 – 1226, 2017
https://doi.org/10.1177/1535370217708188

INTRODUCTION

Diabetes mellitus is a disorder that affects the metabolism of carbohydrates (particularly glucose) as well as of lipids and proteins, as result of either a deficiency in insulin secretion or reduced sensitivity of tissues to this hormone (American Diabetes Association, 2014). There are two forms of diabetes, type 1 (T1DM) and type 2 diabetes mellitus (T2DM), that have distinct pathogenesis. T1DM is an autoimmune disease that results from a combination of genetic susceptibility, immune dysregulation and exposure to certain environmental factors (such as viral infection, dietary substances, etc.), leading to beta cell death and, as consequence, in deficiency of insulin production (Canivell & Gomis, 2014; Thomas & Philipson, 2015). T2DM has a more complex etiology/pathogenesis and a higher incidence/prevalence in the world population nowadays. It is established that physical inactivity and obesity are important contributors to the onset of this disease, although there may be genetic and environmental predisposing factors associated with T2DM (Tripathy & Chavez, 2010; Olokoba *et al*., 2012).

Insulin resistance is one of the first sign of T2DM, being characterized by a general decrease in cell sensitivity to insulin, that lead to hyperglycemia due to reduced glucose uptake (mainly in muscle and adipose tissue) or increased glucose output (such as in the liver) (Björnholm & Zierath, 2005; Wilcox, 2005; Lee & Lee, 2014). Although it is not completely known which factors trigger the insulin resistance, high levels of circulating fatty acids and adipose tissue-derived pro-inflammatory cytokines certainly contribute to this condition (Lin *et al.*, 2005; Olokoba *et al*., 2012; Forbes & Cooper, 2013; Lee & Lee, 2014). In addition, it has been recently proposed that microbiota-derived lipopolysaccharides, crossing a leaky

intestinal epithelia, may also play a role in the long term development of insulin resistance in T2DM (De Kort *et al*., 2011; Amar *et al.*, 2011; Cani *et al.*, 2012; Ghaisas *et al*., 2015).

In order to compensate the permanent state of insulin resistance, pancreatic beta cells is capable of an adaptive response that involves changes in their secretory function and mass in the endocrine pancreas (Rhodes, 2005; Sone & Kagawa, 2005; Prentki & Nolan, 2006; Collares-buzato, 2015). At initial stages, beta cells increase insulin biosynthesis and release but, subsequently, due to the continuous resistance of biological tissues to insulin, beta cell mass expands to promote further increase in secretion of this hormone necessary for the maintenance of normoglycemia (Sone & Kagawa, 2005; Prentki & Nolan, 2006; Collares-buzato, 2015; Oliveira *et al.*, 2015). In advanced stages, the constant demand for insulin hypersecretion in association with long-term exposition to hyperglycemia/dyslipidemia and a chronic inflammatory state within the pancreatic islet milieu result in secretory impairment and then beta-cell death by apoptosis, reducing its mass in the pancreas (Gómez-Dumm *et al*., 1990; Rhodes, 2005; Sone & Kagawa, 2005; Prentki & Nolan, 2006; Tripathy & Chavez, 2010; Oliveira *et al.*, 2014). As consequence, replacement therapy with insulin is needed to recover glucose homeostasis.

In addition to hormone replacement treatment of T2DM, alternative therapies have been proposed, particularly at the early stages of this disease, in order to control obesity and altered metabolism of carbohydrates, leading to reversal of the prediabetic state. These therapies involve regular physical exercise and special diets and the intake of prebiotic and probiotic in view of the recent discovery of a possible association between microbiota and the development of diabetes (Matsuzaki *et al.*, 1997; Meddings *et al.*, 1999; Neu *et al.*, 2005; Bosi *et al.*, 2006; Cani *et al.*, 2007; Al-Salami *et al.*, 2008; Cani *et al.*, 2008, 2012).

Butyrate is a short-chain fatty acid (SCFA) produced by the intestinal microbiota through the fermentation of non-absorbable carbohydrates and proteins (e.g., fibers). It has been demonstrated that butyrate has beneficial effects on intestinal mucosa, displaying anti-inflammatory, anti-oxidant and anti-carcinogenic actions (Inan *et al.*, 2000; Hamer *et al.*, 2008; Li *et al*., 2013; Chang *et al.*, 2014; Wang *et al.*, 2015). *In vitro* conditions, butyrate induces an increase in tight junction (TJ)-mediated epithelial barrier function by increasing the expression of the TJ-associated claudin-1 in intestinal cell line (Wang *et al.*, 2012). Regarding its systemic effect, there has been recently suggested an anti-diabetogenic effect of

this SCFA (Gao *et al.*, 2009; Canani *et al.*, 2011; Dudakovic *et al.*, 2013; Li *et al*., 2013; Khan & Jena, 2014, 2016) in animal models of T1DM and T2DM, which was related to its action as histone deacetylase (HDAC) inhibitor. Nevertheless, to the best of our knowledge, there is no study looking at the relationship between the effect of butyrate on the T2DM-associated metabolic, hepatic and pancreatic alterations and its action on TJ-mediated intestinal epithelial barrier. Therefore, the aim of the present work was to investigate the effect of diet supplementation with sodium butyrate on metabolic parameters, adiposity, hepatic and pancreatic lipid accumulation, beta cell function/mass as well as on the structure and function of the intestinal epithelial barrier of obese and prediabetic mice.

MATERIALS AND METHODS

Animals and Diets

Male C57BL/6JUnib mice (aged 4-5 months) were obtained from the breeding colonies of the Multidisciplinary Center for Biological Investigation on Laboratory Animal Science (CEMIB) of the University of Campinas (UNICAMP, Brazil). The animals were divided into four experimental groups: control (C), control + butyrate (CB), high-fat diet (HF) and high-fat diet + butyrate (HFB). Sodium butyrate (cat number 303410, Sigma) was incorporated into the regular and HF diets at concentration of 5% (w/w) as previously described (Gao *et al.*, 2009). The C group received a standard rodent diet (in powder) (containing 4.5% lipids, 53 % carbohydrates, and 23 % proteins; w/w). The CB group received the standard diet mixed with 5% of sodium butyrate (w/w). Animals from the HF group received a prepared high-fat diet (in powder) (containing 21 % lipids, 50 % carbohydrates, and 20 % proteins; w/w) while the HFB group received the same high-fat diet but mixed with 5% of sodium butyrate (w/w). The lipid composition of the HF diet was mainly lard (20g/100g diet), but also contained soy oil (1mL/100g diet). The different animal groups had free access to food and water and were kept in a controlled temperature environment (25 °C) and 12h light-dark cycle during the entire experimental period (60 days). All the experiments in this project were approved by the Institutional Committee for Ethics in Animal Experimentation of the University of Campinas (CEUA/UNICAMP; under Protocol: 3439-1).

Weight gain and metabolic evaluation

The following parameters were evaluated in mice from all experimental groups: the weight gain, the visceral (retroperitoneal and epididymal) fat accumulation, the fast and fed glycemia, the fast insulinemia and response to the insulin tolerance test (ITT, expressed as area values under curve (AUC)). These procedures were performed as previously described (Carvalho *et al.*, 2012; Oliveira *et al.*, 2015; Falcão *et al.*, 2016) and at the same period during the day (9am-11am). The blood glucose concentration was measured using an Accu-Chek Advantage II glucometer (Roche Diagnostic, Switzerland). Insulin plasma concentration was determined using a commercial ELISA kit (Rat/Mouse Insulin ELISA Kit, Cat# EZRMI-13K, Millipore, USA).

Static insulin secretion

Pancreatic islets were isolated from pancreas by collagenase digestion (Carvalho *et al.*, 2012). Groups of five islets of similar size were collected and preincubated in 24-wells plates with 0.5 mL Krebs solution supplemented with 3mg.mL^{-1} bovine albumin (Sigma) and 5.6mM glucose for 30 min at 37 °C (Carvalho *et al.*, 2012; Falcão *et al.*, 2016). After this period, islet pools were incubated for 60 min at 37 °C in Krebs solution supplemented with 2.8mM or 16.7mM glucose (Falcão *et al.*, 2016). After incubation, the supernatants were collected, stored at -20°C until determination of insulin concentration, expressed as ng.mL^{-1}.islet^{-1} using the ELISA kit (Rat/Mouse Insulin ELISA Kit, Cat# EZRMI-13K, Millipore, USA).

Pancreas and liver histology and morphometry

Pancreas fragments were fixed, embedded in Paraplast® (P3558, Sigma), and routinely processed for Hematoxylin-Eosin (HE) staining or for immunoperoxidase detection of insulin (Falcão *et al.*, 2016). To determine the **relative volume of pancreatic beta cells per pancreas**, a morphometric analysis was performed as previously described (Falcão *et al.*, 2016). Briefly, six histological sections from each animal (2 sections per pancreas region, i.e. head, body and tail) were photographed using a digital camera coupled to a conventional inverted microscope (Nikon Eclipse E-400 - Nikon, Japan). The relative volume of beta cells in the pancreas (as an estimate of beta cell mass) was determined by the sum of all insulin immunostained-islet areas divided by the respective pancreas section area using the software ImageJ (http://rsbweb.nih.gov/ij/download.html).

For the analysis of islet cytoarchitecture (i.e. the typical arrangement of beta- and non beta-cells within the islet) (Kim *et al.*, 2009), the pancreas sections were processed for dual immunofluorescence for insulin (using the anti-insulin, cat number A0564, Dako, USA) and glucagon (using the anti-glucagon, cat number A0565, Dako, USA) using a standard protocol (Oliveira *et al.*, 2015; Falcão *et al.*, 2016) and observed by confocal laser microscopy (LSM 510-Zeiss, Germany).

For the evaluation of adipocyte infiltration within the pancreas, we have used the same histological sections processed previously for HE staining and insulin immunoperoxidase (totalizing 120 pancreas sections/animal; 10 animals/group). Each pancreas section was scored according to the amount of intralobular fat tissue as follows: score 0, absence of intralobular adipose tissue; score 1, low fat accumulation (presence of 1 to 3 adipocytes within pancreas parenchyma section); score 2, moderate fat accumulation (presence of 4 to 6 adipocytes within pancreas parenchyma section); score 3, high fat accumulation (presence of more than 7 adipocytes within pancreas parenchyma section). The degree of fat accumulation within the pancreas parenchyma was determined by calculating the score mean value for each experimental group according to this classification.

For the analysis of liver steatosis, liver fragments were fixed, embedded in Paraplast® (P3558, Sigma), and routinely processed for HE staining. Digital images (five per liver section) were acquired randomly from three 5μm-thick sections per liver specimes using a digital camera coupled to a conventional microscope (Nikon Eclipse E-400 - Nikon, Japan). The morphometric estimation of liver steatosis was performed by a point-counting system, as previously described with some modifications (Catta-Preta *et al.*, 2011), using digital images obtained at high magnification (100x objective lens) and a test system of 88 points employing the Grid pluging of Image J. The sum of points hitting fat droplets within the hepatocyte was divided by the total points and expressed as percentage, that was taken as an index of liver steatosis degree.

Immunolabelling and immunoblotting of Claudin-1 in intestine fragments

The localization and distribution of the tight junctional protein claudin 1 in intestinal epithelia were determined by indirect immunofluorescence in cryosections of intestine fragments. For that, fragments of jejunum, ileum and colon, obtained from 12h-fasted mice, were frozen in *n*-hexane with liquid nitrogen and the cryosections obtained were

permeabilized and fixed with acetone at -20°C for 3 min. For the immunofluorescence reaction, intestine cryosections were incubated with a blocking solution (phosphate-buffered saline (0.01 mM PBS, pH 7.4) containing 5% bovine serum albumin (BSA) plus 0.1% Tween 20) for 1 h and, then, incubated overnight at 4 °C with the anti-claudin 1 primary antibody (Abcam; cat number ab15098; diluted 1:50 in PBS plus 3% BSA). After washing with PBS, the intestine sections were incubated with FITC-conjugated specific secondary antibody (Sigma) (dilution 1:100 in PBS plus 1% BSA solution) and DAPI (D 9542 Sigma) (dilution 1:1000) for 2h at room temperature (RT). All sections were mounted in a commercial antifading agent (Vectashield, Vector Laboratories, Burlingame, CA) and photographed by a digital camera coupled to a inverted fluorescence microscope (Observer.Z1; Zeiss – AxioCam, MRC, USA). Digital images of the intestine sections from all experimental groups were obtained and compared during the same session using identical microscope parameters (gain and time exposure). To determine the junctional content of claudin-1 in epithelia from the different intestine segments, five images of intestinal epithelium were captured from each cryosection from animals of all experimental groups. Then, the integrated densities of 50 points per image, placed at the intercellular region of enterocytes (immunolabelled for claudin-1), were measured in all captured images using the free software ImageJ (given a total of 1250 points sampled per experimental group).

Fragments of jejunum, ileum and colon, where the serosal layer was removed, were sonicated in an antiprotease cocktail (10 mM imidazole, pH 7.4, 4 mM EDTA, 1 mM EGTA, 0.5 $\mu g.mL^{-1}$ pepstatin A, 200 $KIU.mL^{-1}$ aprotinin, 2.5 $\mu g.mL^{-1}$ leupeptin, 30 $\mu g.mL^{-1}$ trypsin inhibitor, 200 µM DL-dithiothreitol, DTT, and 200 µM phenylmethylsulfonylfluoride (PMSF); Sigma) and processed for Western Blotting, using a standard protocol (Carvalho *et al.*, 2012; Oliveira *et al.*, 2014). Briefly, homogenate aliquots (containing 50µg of total protein) were applied on 12% polyacrylamide gels and proteins were fractionated by electrophoresis and electrophoretically transferred into nitrocellulose membranes (Bio-Rad). After staining with Ponceau solution (Sigma) to check the efficiency of sample loading and transfer, membranes were blocked for 4 h at RT with a buffer solution (0.01M Trisma Base, 0.15M NaCl, 0.05% Tween 20; pH 7.4) containing 5% skimmed milk powder and then incubated overnight at 4 °C with primary antibody anti-claudin-1 (Abcam; cat number ab15098; dilution 1:150 in basal solution containing 3% skimmed milk powder). After washing with basal solution, the membranes were incubated with specific secondary antibody

conjugated with HRP (Sigma) (dilution 1:500 in basal solution containing 1% skimmed milk powder) for 2h at RT. Immunoreactive bands were detected using an enhanced chemiluminescence kit (Super Signal, Thermo Fisher Scientific, USA) and an imaging system (Genome Gene, Syngene Bio Imaging, UK). The relative size of the immunoreactive bands was quantified by densitometry using the ImageJ software. After stripping, the membranes were reincubated with anti-beta-actin antibody, used as internal control. Optical densitometric values were expressed as ratio of the claudin-1 and beta-actin signals.

Intestinal permeability to FITC-Dextran

Intestinal permeability was assessed by using fluorescein isothiocyanate-conjugated Dextran (FITC-Dextran, 4 kDa, (cat number 46944, Sigma, USA)) as a paracellular tracer (Cani *et al.*, 2008). Animals were fasted for 6 h, and after this period, received by gavage FITC-Dextran (FITC-Dextran) solution at a dose of 600mg.kg^{-1} and volume of 4.8 ml.kg^{-1} (diluted in PBS (0.01M pH7.4)). After 1h, the animals were euthanized in CO_2 chamber; blood samples were collected from the cervical veins (after decapitation) and centrifuged at a speed of 8000*g* for 10 min at 4°C to separate the plasma. Then, plasma aliquots were diluted in equal volume of PBS (pH 7.4), added into 96 wells plate and read by a fluorescence microplate reader (Fluorskan Ascent; Thermo Scientific, USA) at the excitation wavelength of 485nm and the emission wavelength of 535 nm. The values of intestinal permeability to FITC-Dextran were expressed as Absorbance absolute values of the marker within the animal plasma.

Statistical analysis

The Two-way ANOVA was used to assess the interaction between the two treatments, exposure to butyrate and high-fat diet, followed by the Bonferroni post-test. To determine the degree of statistical significance between control (C or CB) and treated (HF or HFB) groups, it was employed the Student's t test. All statistical analyses were performed using the GraphPad *Prism* Software version 5.00 (GraphPad Software, USA). Results are expressed as means + SE (Standard Error), and the significance level was set at $P<0.05$.

RESULTS

The exposure to high-fat diet (HF group) for 60 days induced a significant increase in body weight gain (of 35.8%) ($P<0.001$) (Fig. 1a) and in visceral adipose tissue deposition (of 6.3 fold) ($P<0.0001$) (Fig. 1b) as compared to control (C) group. HF diet also induced

metabolic disturbances that included, marked peripheral insulin resistance ($P<0.05$) (Fig. 1c, 1d), significant fast ($P<0.0001$) and fed ($P<0.0001$) hyperglycemia (Fig. 1e, 1f) as well as fast hyperinsulinemia ($P<0.05$) (Fig. 1g). Interestingly, diet supplementation with 5% sodium butyrate (HFB group) significantly reduced the adiposity and all metabolic alterations induced by HF diet. Butyrate treatment blocked completely the development of insulin resistance and hyperinsulinemia states induced by HF diet (Figure 1 d, g). Mice from HFB group displayed a significant decrease of 50.5% in body weight gain, 27.7% in adipose tissue accumulation, and 19.7% and 15.9% in fast and fed hyperglycemia, respectively, as compared to those from HF group (Figure 1). In addition, butyrate *per se* (CB group) has no adverse effects on the parameters evaluated as compared to the control group (Figure 1).

In order to confirm that the protective effect of sodium butyrate on the parameters studied was not result of differences in diet ingestion, we have monitored the daily food consumption in all experimental groups throughout the experimental procedure. The food intake values expressed in kcal confirm that there was no significant difference in kcal intake between HF and HFB groups (Figure 1h). In addition, the food consumption in grams was similar among the different treatments (C 6.04±0.16g HF 6.35±0.08g; CB 5.19±0.18g; HFB 6.05±0.09g (n=18)).

It is well known that insulin resistance state in T2DM can result in structural adaptations of the endocrine pancreas and functional defects in the insulin-secreting pancreatic beta cells (Lin *et al.*, 2005; Sone & Kagawa, 2005; Prentki & Nolan, 2006; Collares-buzato, 2015; Oliveira *et al.*, 2015). To investigate whether supplementation with sodium butyrate has also an effect on insulin secretion, batches of isolated pancreatic islets from mice of all experimental groups were in vitro exposed to 2.8mM or 16.7 mM glucose for 60 min (Figure 2). At basal condition (2.8mM glucose), islets isolated from mice of the HF group showed a significant increase in basal insulin release as compared to control group (Fig. 2a), which is in agreement with our previous data (Carvalho *et al.*, 2012; Oliveira *et al.*, 2014). Interestingly, this increased basal secretion was not observed in islets from mice receiving diet supplementation with butyrate (HFB group) (Fig. 2a). At stimulated condition (when exposed to 16.7mM glucose), the release of insulin by islets isolated from HF-fed mice group was similar to that by control islets (Fig. 2b). Comparatively, islets from mice receiving supplementation with butyrate (CB and HFB groups) displayed a tendency of an increase, although not statistically significant, in insulin secretion at supraliminar concentration of

glucose (16.7 mM) (Fig. 2b). This change resulted in a significantly higher (P=0.012) fold increase in glucose-induced insulin secretion in HFB islets (56.5±18.8 (10) fold as compared to basal secretion) than HF islets (10.5±3.4 (13) fold as compared to basal secretion), which, in turn, displayed a significant lower (P=0.02) secretory response to glucose as compared to control (C) islets (32.4±7.9 (14) fold as compared to basal secretion).

In accordance with our previous data (Carvalho *et al.*, 2012; Oliveira *et al.*, 2014, 2015), 60d exposure to HF diet induced a compensatory beta cell mass expansion as revealed by the significant increase in relative volume of beta cells in relation to total pancreas (Fig. 3b, e,) as compared to controls (Figure 3a, e). This was accompanied by no changes in islet cytoarchitecture, characterized by a core of insulin-secreting beta cells surrounded by a peripheral mantle of glucagon-secreting alpha cells in HF mice, which was verified in all other experimental groups (C, CB, HFB) (Fig. 3f-i). Interestingly, the compensatory beta cell mass expansion was not observed in the groups that received supplementation with sodium butyrate (HFB and CB) (Fig. 3 c,d,e).

Considering the protective effect of sodium butyrate against the HF diet-induced adiposity and disturbance of the beta cell insulin secretion, we also evaluated the degree of lipid accumulation in the liver and adipocyte infiltration in the pancreas in all experimental groups studied (Figure 4). As compared to C group, exposure to HF diet induces a significant accumulation of fat in liver (21.3% of total liver volume), which was characterized by the presence of large- and medium-sized lipid droplets within hepatocytes cytoplasm (macrovesicular steatosis). Supplementation with sodium butyrate resulted in a significant reduction in hepatic steatosis (11.3% of total liver volume) (Fig. 4 e) (P<0.0001), where hepatocytes of HFB mice displayed mainly a single small-sized lipid droplet or multiple lipid vesicles of very small size in their cytoplasm (Fig. 4 d). No signals of hepatic lipid accumulation were observed in the control groups, receiving or not butyrate (C and CB) (Fig. 4a, c). In addition, adipocyte infiltration was observed in the pancreas of animals exposed to HF diet (Fig 4 g,j) as compared to the C group (Fig. 4 f,j). In HF diet-fed mice that received diet supplementation with sodium butyrate, there was a significant decrease in intrapancreatic deposition of adipose tissue (Fig. 4 i, j) as well as reduction in adipocyte size as compared to pancreas from HF group (Fig. 4g,j). In contrast, the amount of intrapancreatic adipose tissue was negligible in the control groups (C and CB) (Fig. 4 f,h,j).

Considering the protective effect of butyrate on the metabolic parameters studied, as well as on the reduction of the accumulation of lipids within organs directly related to the insulin body response, we evaluated whether there was a concomitant effect of butyrate on the intestinal epithelial barrier. The evaluation of the intestinal epithelial barrier by claudin-1 immunodectection in intestinal cryosections showed a significant decrease in the intercelular content of this TJ-associated protein in enterocytes of HF-fed mice, in all studied intestinal segments (jejunum (reduction of 26.4%) (Figure 5c,e), ileum (of 25.6%) (Figure 5c,e) and colon (of 19.4%) (Figure 6 c,e)) as compared to that observed in the C group, suggesting an impairment of the structure of the intestinal epithelial barrier after HF diet treatment. Supplementation with sodium butyrate reversed this alteration by inducing a significant increase in the degree of junctional content of claudin-1 within intestinal epithelia (jejunum (increase of 46.4%) (Figure 5 d,e), ileum (34.3%) (Figure 5 d,e) and colon (66.1%) (Figure 6 d,e) in comparison with that observed in the HF group. Besides the increased intercellular content, we consistently observed a higher labelling for claudin-1 at enterocyte cytoplasm of intestine fragments from mice treated with butyrate, which suggested increased protein expression. However, the immunoblotting analyses showed no significant change in total protein content of claudin 1 in intestinal fragment homogenates among the differents experimental groups. Nevertheless, we observed a tendency of a decrease in claudin-1 protein content in HF group as compared to C group as well as a tendency of increase in claudin-1 protein content in the groups receiving supplementation with sodium butyrate (Figures 5 and 6). A possible explanation for the apparent discrepancy between the immunofluorescence and immunoblotting data is that, in the case of immunofluorescence, measurements of claudin 1 junctional content were made exclusively at the region of the epithelium, that highly express this protein, while the evaluation of the total cell content by Western Blot was done in homogenates of intestinal fragments that contain not only the epithelium, but other tissues (particularly the connective layer of the lamina propria and submucosa) that make up the intestinal wall. The presence of these tissues, where the expression of TJ proteins is low or non-existent, may interfere with the sensitivity of the immunoblotting method to detect subtle differences in the expression of these proteins in the epithelium, as probably happened in our experiments.

Taken into account the marked increase in claudin-1 immunodetection seen in intestinal epithelial cryosections of butyrate-treated mice in comparison with controls, we

performed a functional analysis of the intestinal epithelial barrier using the FITC-Dextran (FITC-DX) permeability test. This analysis revealed that CB (Abs DX-FITC 0.61±0.15(6)) and HFB mice (Abs DX-FITC 0.47±0.13(6)) showed a significant decrease in intestinal absorption of the paracellular marker compared to control (C) group (Abs DX-FITC 2.1±0.55(6) ($P<0.05$), which was in agreement with the immunofluorescence data.

DISCUSSION

Type 2 diabetes (T2DM) associated with obesity is reaching worldwide epidemic proportions (Tripathy & Chavez, 2010; Olokoba *et al*., 2012; American Diabetes Association, 2014). Therefore, there are an increasing interest in understanding thoroughly the T2DM pathogenesis in order to find new strategies of treatment and prevention of this disorder. The central feature of the T2DM is the development of a body resistance to insulin that is characterized by a reduction in tissue response/sensitivity (particularly of muscle, adipose and hepatic tissues) to this hormone and, as consequence, a chronic state of hyperglycemia develops (Björnholm & Zierath, 2005; Wilcox, 2005; Lee & Lee, 2014; Castro *et al.*, 2015). It has been recently suggested that consumption of a lipid-enriched diet results in disruption of the intestinal epithelial barrier, allowing the passage of noxious agents leading, in turn, to a systemic inflammatory response that could be a primary cause of the peripheral insulin resistance(Matsuzaki *et al.*, 1997; Meddings *et al.*, 1999; Neu *et al.*, 2005; Bosi *et al.*, 2006; Cani *et al.*, 2007; Al-Salami *et al.*, 2008; Cani *et al.*, 2008, 2012). Recent works have focused on changes in microbiota and in luminal content composition as a result of high-fat diet consumption and its relation to intestinal barrier disruption, local/systemic immune response and/or insulin resistance state in T1DM and T2DM diabetes (Larsen *et al.*, 2010; Suzuki & Hara, 2010; Cani *et al.*, 2012; Johnson *et al.*, 2015). These studies have opened a new perspective of investigation aiming at the use of probiotics, prebiotics and postbiotics (such as, short-chain fatty acids (SCFA)) as adjunctive therapy of diabetes (Matsuzaki *et al.*, 1997; Al-Salami *et al.*, 2008; Canani *et al.*, 2011; Li *et al*., 2013; Henagan *et al.*, 2015; Wang *et al.*, 2015). Some studies have demonstrated that sodium butyrate, a SCFA, has beneficial effects on animal models of T1DM and T2DM (Gao *et al.*, 2009; Li *et al*., 2013; Khan & Jena, 2014). In the present work, we demonstrated that butyrate alleviates the metabolic impairments induced by high-fat diet administration in mice, by inhibiting the development of an insulin resistance state, which was associated with improvement of

insulin-secreting function of beta cells and strengthening of the tight junction-mediated intestinal epithelial barrier.

Confirming our previous works (Carvalho *et al.*, 2012; Oliveira *et al.*, 2014, 2015), we described herein that the exposure to a diet with high content of lipids (21% w/w, corresponding to 45% of fat in calories) for only 60d induced, in C57 mice, obesity and prediabetes, which were characterized by a significant body adiposity, marked insulin resistance associated with moderate hyperglycemia and significant hyperinsulinemia. The treatment with sodium butyrate prevented all these HF diet-induced alterations, which can not be attributed to differences in food intake since diet consumption in calories was similar between the HF and HFB groups. Gao and co-workers, employing a comparable animal model of T2DM (mice fed a HF diet containing 58% of fat in calories for up to 16 weeks), have shown similar results with butyrate. They suggested that the anti-obesity effect of butyrate is a result of an increase in body energy expenditure, induction of mitochondria function and fatty acid oxidation, which were mediated by the activation of PGC-1α in brown adipose and skeletal muscle tissues (Gao *et al.*, 2009). However, their study lacked the control groups (receiving a regular chow diet with or without supplementation with butyrate) which made it difficult to establish the effectiveness of the butyrate treatment in reaching control values regarding the parameters evaluated in HF diet-fed mice, as well as it did not investigate the metabolic effects of this SCFA *per se.* This was overcome in our study that interestingly showed that diet supplementation with butyrate completely blocked the development of the insulin resistance state in these HF diet-fed mice, that displayed a sensitivity to insulin similar to control values, as revealed by ITT analysis. In addition, butyrate treatment significantly reduced the body weight gain (in 50%), the visceral adipose tissue accumulation (in 28%) and hyperglycemia at fast (in 16%) and fed (in 20%) conditions after HF diet exposure when compared to the group that did not received this SCFA (HF group). However, in contrast to the response to ITT, the adiposity and glycemia of animals from HFB group did not reach control levels after butyrate. In addition, we showed that butyrate treatment *per se* did not affect markedly body weight and metabolic parameters in mice fed a regular diet, indicating that this SCFA acts mainly when animal metabolism is challenged by a modified diet.

One of the consequences of consumption of high-fat diet is the development of a fatty liver, condition known as hepatic steatosis (Yki-Järvinen, 2015). Hepatic steatosis is closely

related to obesity, insulin resistance state, and T2DM, and, although it is reversible, can aggravate the metabolic disturbances associated with these disorders or evolved to a more serious condition known as non-alcoholic steatohepatitis (NASH) (Byrne *et al.*, 2009; Yki-Järvinen, 2015; Willebrords *et al.*, 2016). In our study, we investigated whether butyrate could revert a possible hepatic steatosis in our animal model. Firstly, we showed that 60d exposure to HF diet resulted in the appearance of lipid-containing hepatocytes representing approximately 21% of total liver volume, as revealed by morphometric analysis, which typically characterize a hepatic steatosis state (clinically defined as the accumulation of lipids in at least 5% of hepatocytes) (Willebrords *et al.*, 2016). Interestingly, the diet supplementation with butyrate reduced significantly the hepatic steatosis in HF diet-fed mice by decreasing not only the number of hepatocytes affected (to only 11% of total liver volume) but also the size and frequency of cytoplasmic lipid droplets. In agreement with our data, Khan & Jena have recently showed that butyrate decreased the fat accumulation in the liver in streptozotocin-induced diabetic rats fed a HF diet, although they did not analyze these data morphometrically but only qualitatively. It has been proposed that the accumulation of triglycerides (TG)-based lipid droplets within hepatocyte cytosol is result of one or a combination of the following mechanisms: 1) increased uptake of free fatty acids (FFAs) from high-fat food and of those released by adipocytes at IR condition (where lypolysis is upregulated); 2) increased *de novo* synthesis of FFAs in the liver from glucose or acetate by IR; 3) decreased hepatic mitochondrial β-oxidation of FFAs; and 4) decreased clearance of TG by VLDL particles from the liver (Byrne *et al.*, 2009; Yki-Järvinen, 2015; Willebrords *et al.*, 2016). Therefore, the inhibitory effect of butyrate on high fat diet-induced hepatic steatosis reported by us may reside from the fact that at least three of these mechanisms (identified as 1, 2 and 3) could be potentially reversed by this SCFA treatment as result of its beneficial action on glycemia homeostasis, peripheral insulin sensitivity, FFA oxidation and mitochondrial function as documented herein and by others (Gao *et al.*, 2009).

It is well known that the pancreatic beta cell plays a central role in the T2DM pathogenesis, displaying adaptive response in order to compensate the resistance of peripheral tissues to insulin (Lin *et al.*, 2005; Sone & Kagawa, 2005; Tripathy & Chavez, 2010; Collares-buzato, 2015; Oliveira *et al.*, 2015) . For that, beta cells initially enhances the biosynthesis and release of this hormone followed by an increment of beta-cell mass by hypertrophy and/or hyperplasia. When the beta cells fail to maintain the normoglycemia,

T2DM is triggered, resulting in insulin secretory impairment and then beta-cell death by apoptosis at advanced stages, which leads to an irreversible body dependence on exogenous insulin. In our animal model of prediabetes, we observed an increased release of insulin at basal glucose concentration (2.8mM) by pancreatic islets isolated from HF diet-fed mice as compared to controls, which agrees with our previous works (Carvalho *et al.*, 2012; Oliveira *et al.*, 2014). Increased basal insulin secretion is one of the features of the early phase of T2DM in human (Weyer *et al.*, 2000; Dankner *et al.*, 2009) and rodents (Kato *et al.*, 1996; Asghar *et al.*, 2006) and it has been associated with an aggravation of the insulin resistance state and glycemia dysregulation. Interestingly, we demonstrated that butyrate diet supplementation prevented this condition in HFB islets, which displayed a basal insulin release level similar to control islets (C and CB groups). In addition, we observed a tendency of an increase in stimulated insulin secretion (at 16.7mM glucose) in CB and HFB islets. As a consequence, butyrate treatment led to a significant improvement of the glucose-induced secretory response of beta cells, assessed as fold stimulation at 16.7mM over that at 2.8mM glucose exposure; i.e. HFB islets displayed a 56-fold increase in contrast with the 10-fold increase in glucose-stimulated insulin secretion observed in HF islets. To the best of our knowledge, this is the first study reporting a positive effect of this SCFA on insulin secretion in isolated islets. However, the mechanism involved in this phenomenon is still unknown as also is our knowledge very limited on the cellular processes underlying the changes in basal insulin secretion during T2DM. Nagaraj and co-workers (Nagaraj *et al.*, 2016) have recently proposed that the reduced presence of cholesterol-enriched membrane rafts in beta cells, that well known determine the spatial organization of the exocytosis-related SNARE proteins and K^+ and Ca^{2+} channels, could contribute to the elevated basal insulin secretion seen in type 2 diabetes. Interestingly, they also showed that prolonged high-glucose exposure (up to 72h) decreased membrane rafts in a beta cell lineage in culture, suggesting that hyperglycemia could be involved in the phenomenon (Nagaraj *et al.*, 2016). Therefore, the general protective action of butyrate on glucose homeostasis after HF diet challenge may explain, at least partially, the effect of this SCFA on insulin secretion at cellular level. Additionally, Pinnick and co-workers have suggested that changes in fatty acid milieu of the islet, as result of adipocyte infiltration in pancreatic exocrine tissue associated with high-fat feeding in mice and with type 2 diabetes in humans, can be deleterious to islet secretory function. Taken this into consideration, the fact that butyrate-treated mice displayed significant lower adipose

tissue infiltration within pancreas parenchyma after HF diet exposure, as compared to HF mice, may be another contributing factor.

Our prediabetic mice also displayed a significant beta cell mass expansion, which was not accompanied by changes in islet cytoarchitecture, as compared to control animals. The increase of beta cell mass and basal insulin secretion observed in our HF diet-fed mice corroborates the data showing a significant hyperinsulinemia at fast condition in these animals. In previous works, we have shown that the increased beta cell mass resulted from beta cell hypertrophy as well as from self-replication of this cell type, as revealed by Ki67 immunodetection (a marker of cell proliferation) (Oliveira *et al.*, 2014, 2015). In addition, Oliveira and co-workers showed that there is a direct correlation between the degree of beta cell mass expansion and the level of hyperglycemia (mainly at fed state), and insulin resistance in HF diet-fed mice, where the former parameter displayed a higher correlation index (r=0.929) than the latter as assessed by ITT (r=0.817). In the present study, we reported that butyrate treatment significantly reduced the HF diet-induced increase in beta cell mass, which is in line with our findings showing a marked inhibitory effect of this SCFA on postprandial hyperglycemia and insulin resistance state (that was completely blocked).

Besides the endocrine pancreas, the intestinal tract and the associated microbiota have been considered as a pivotal organ for the onset and evolution of both T1DM and T2DM (Bosi *et al.*, 2006; Sapone *et al.*, 2006; Cani *et al.*, 2007; 2008; Valladares *et al.*, 2010). Based on clinical and experimental evidences, the current hypothesis postulates that a dysruption of the intestinal epithelial barrier induced by a modified microbiota or altered luminal content would lead to an increased intestinal permeability to antigens from dietary, viral or bacterial origin, that in turn could activate autoimmune reactions against insulin-producing beta cells (in T1DM) and/or elicit secretion of pro-inflammatory cytokines, locally and systemically, leading to insulin resistance (in T2DM) (Groschwitz & Hogan, 2009; Suzuki & Hara, 2010; De Kort *et al*., 2011; Fasano, 2011). Given our current knowledge, one may assume that reinforcing the intestinal barrier can offer and open new therapeutic horizons in the treatment of these two types of diabetes. Taken all into consideration, we went to investigate the effect of butyrate supplementation on intestinal barrier function in our animal model of T2DM, focusing on the structure and function of the intestinal TJ, an essential element of this barrier (Groschwitz & Hogan, 2009; Furuse, 2010; Krug *et al*., 2014; Van Itallie & Anderson, 2014).

Exposure to high-fat diet for 60d induced a significant decrease in the junctional content of claudin-1, a constitutive protein of intestinal TJ (Van Itallie & Anderson, 2014), and a tendency of reduction in total protein content of this protein in the epithelium of intestinal segments (jejunum, ileum and colon), as revealed by immunohistochemistry and Western Blot, respectively. The decrease of the junctional content claudin 1 in the intestinal epithelium observed in our prediabetic mice may be a result of the internalization of this protein from the TJ site to cytoplasm for degradation, which certainly leads to disruption of TJ function. Similar changes in molecular structure of TJ associated with increased epithelial permeability to paracellular markers have been reported in vitro system using colonic cell lines exposed to Escherichia coli bST toxin (Mukiza & Dubreuil, 2013) or to pro-inflammatory cytokines IFN-γ and TNF-α (Cao *et al.*, 2013). To the best of our knowledge, this is the first report showing changes in the molecular arrangement of TJ in animal model of T2DM and is in line with works documenting enhancement of intestinal permeability, as revealed by permeability assays with paracellular markers, in type 2 diabetic rodents and humans (Cani *et al.*, 2007; 2008; Ding *et al.*, 2010; Horton *et al.*, 2014; Johnson *et al.*, 2015). Interestingly, exposure to sodium butyrate induced a strengthening of the intestinal epithelial barrier, as revealed by the statistically significant decrease in intestinal permeability to FITC-dextran in CB and HFB groups compared to C group. In accordance with this data, we found that treatment with butyrate resulted in significant increase in immunostaining (both at intercellular and cytoplasmic region) and a tendency to increase in the protein content of claudin 1 in the intestinal segments studied. This result is in accordance with the inhibitory effect of this SCFA on the metabolic alterations (particularly the insulin resistance state) induced by HF diet feeding and corroborate the hypothesis suggesting a role of the intestinal tract in the T2DM pathogenesis.

Studies investigating the effect of butyrate on the expression of junctional proteins in epithelium are rare, but overall they are in agreement with a positive action of this agent on TJ function. Wang and co-workers (Wang *et al.*, 2015) have observed that sodium butyrate induced increase in gene expression and protein content of claudin 1 in the intestinal epithelial cell line IEC, possibly due to a higher level of interaction between the SP1 transcription factor, and its promoter. Additionally, Huang and co-workers (Huang *et al.*, 2015) reported that the decrease in paracellular intestinal permeability, as measured by lactulose/mannitol assay in urine, is associated with increased expression of occludin in jejunum and colon

segments of newborn pigs after butyrate treatment in combination with antibiotics. The authors suggested that this effect on intestinal function was probably due to anti-inflammatory action of this SCFA, since the TNF-α concentration was lower in the mucosa of animals receiving treatment with butyrate (Huang *et al.*, 2015).

The mechanism of action of sodium butyrate on cellular expression of claudin 1 or other structural proteins of TJ is still unknown; however, it may also be related to its action as inhibitor of the histone deacetylase enzyme. Sodium butyrate causes hyperacetylation of histones by inhibiting histone affinity with DNA and thus increases the exposure of regions for transcription of certain genes (Kumar *et al.*, 2007; Dudakovic *et al.*, 2013). It is known that proteins associated with intercellular junctions such as connexins (the gap junction proteins), and ZO-1 (a TJ-associated protein) may undergo epigenetic regulation under certain experimental conditions (Vinken *et al.*, 2009; Luo *et al.*, 2013). However, future experiments will be necessary to unravel, at the molecular level, how butyrate affects junctional protein expression and/or assembly/disassembly at intestinal TJ in our experimental model of type 2 prediabetes.

In conclusion, our data showed a protective action of butyrate on metabolic, hepatic and pancreatic alterations induced by HF diet in mice. Given the well-known association between obesity and T2DM (Tripathy & Chavez, 2010; Olokoba *et al*., 2012; Lee & Lee, 2014), the improvement of glucose homeostasis and insulin sensitivity in HF-fed mice after butyrate treatment may be related to the inhibitory effect of this SCFA on adiposity as reported herein and to the butyrate-induced increase in energy expenditure as described elsewhere (Gao *et al.*, 2009). In addition, the strengthening of the intestinal epithelial barrier associated with butyrate treatment may play a role in the process. A deeper understanding of the molecular pathways involved in the regulation of intestinal barrier and lipid/carbohydrate metabolism by butyrate will have important clinical implications by potentially opening new horizons in the treatment and prevention of diabetes mellitus and related metabolic disorders, as well as of unrelated intestinal diseases.

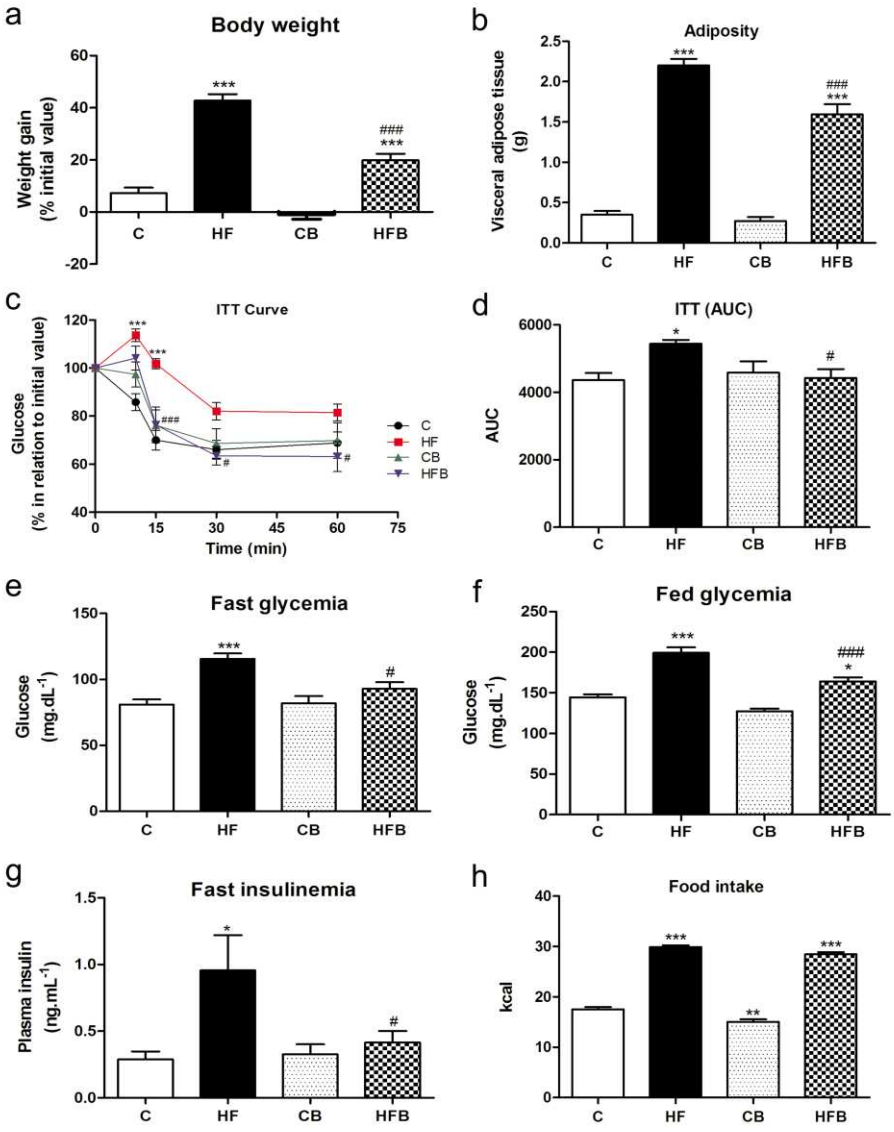

Figure 1. Butyrate treatment significantly reduced the high fat diet-induced obesity and metabolic dysfunctions in mice without changing food intake. As compared to control group, high-fat (HF) diet for 60 days induced a significant increase in weight gain (a), adiposity (b), in peripheral insulin resistance (c, as assessed by the insulin tolerance test (ITT) and expressed as area values under curve (AUC), d), in fast (e) and fed (f) glycemia and in fast insulinemia (g), suggesting the development of prediabetes in these mice. However, dietary supplementation with 5% sodium butyrate (HFB group) showed a protective effect reducing significantly all these metabolic alterations induced by HF diet, without changing the food intake expressed as calories (h). Administration of butyrate *per se* (CB) did not significantly affect the parameters evaluated as compared to control group (C). Data are expressed as means + SE of at least three independent experiments (n=14-18 mice per group). Groups: C = control (fed a regular diet alone); HF = High-fat diet alone; CB = Control+butyrate; HFB=High-fat diet+butyrate.*P<0.05, ** P<0.001, *** P <0.0001 compared to C group; # P<0.05, ### P <0.0001 compared to HF group.

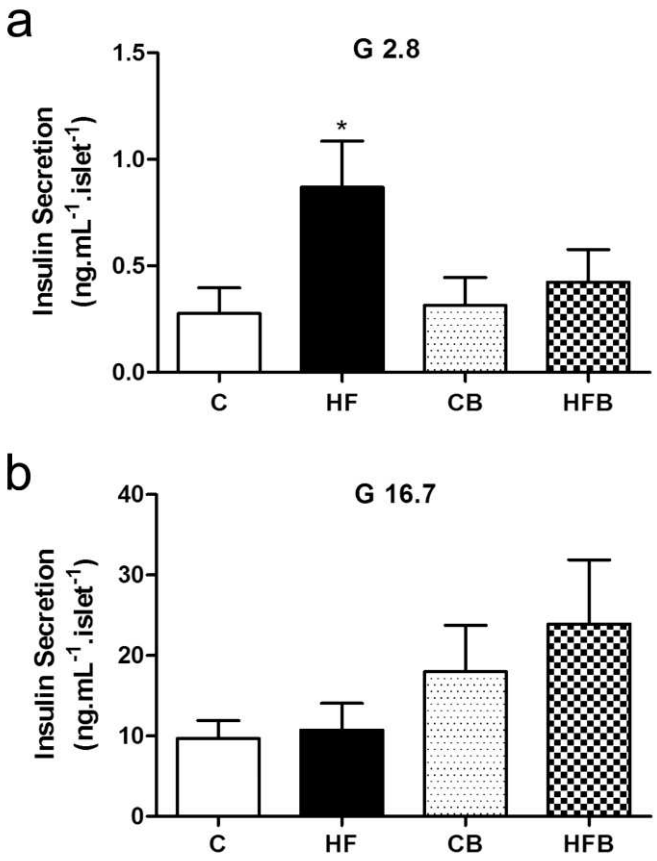

Figure 2. Pancreatic islets from high fat-fed mice show altered insulin secretion that was not observed after treatment with butyrate. Batches of isolated islets from mice of all experimental groups were exposed to 2.8 (a) or 16.7 mM glucose (b) for 60 min. Compared with controls (C), islets from HF-fed mice (HF) showed increased basal insulin secretion (expressed as $ng.mL^{-1}.islet^{-1}$) in the presence of 2.8 mM glucose (G 2.8) but a comparable insulin release when stimulated by 16.7 mM glucose (G 16.7) (b). This increased basal secretion was not observed in HF-fed mice receiving diet supplementation with butyrate (HFB) as compared to its control (CB)(a); but a tendency of an increase in stimulated insulin release (b) was verified in mice with butyrate diet supplementation (CB and HF groups) as compared to those not receiving this SCFA (C and HF groups). Bars represent means + SE of 4 independent experiments (10-14 batches of 5 islets isolated from 4 mice per group). *$P<0.05$ compared to C.

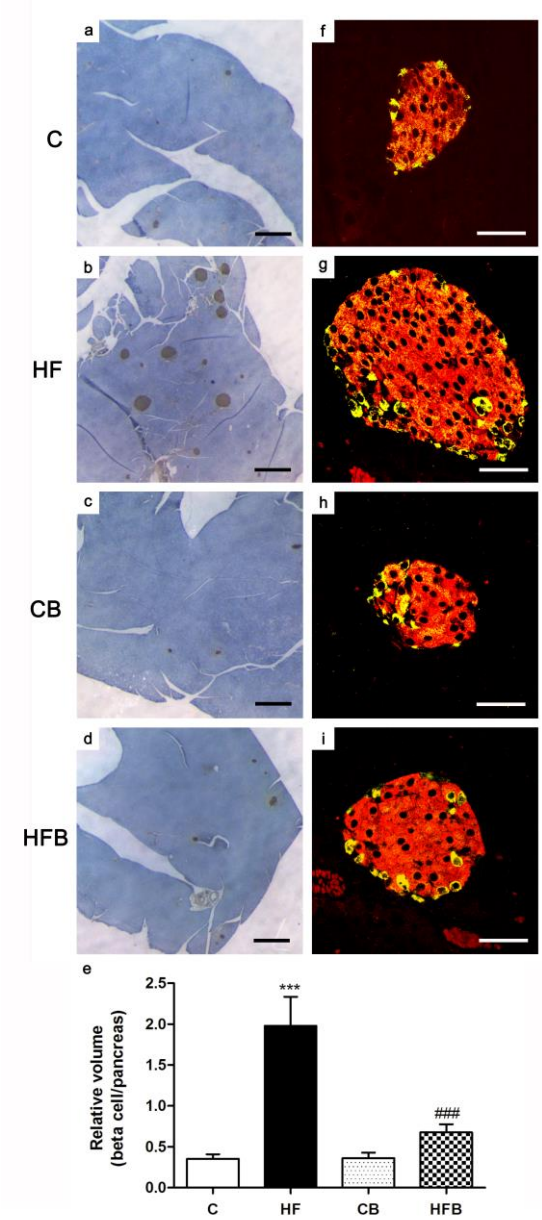

Figure 3: The compensatory beta cell mass expansion induced by high-fat diet in mice was not observed after butyrate administration. Photomicrographs of pancreatic islets processed for insulin immunoperoxidase (a-d) (brown) or for double immunofluorescence to detect insulin (red) and glucagon (yellow)(f-i). Note the increase in number and size of insulin-labelled islets (b,g), with no change in the islet cytoarchitecture (g), in high-fat diet-fed mice (HF) in comparison with control group (C) (a,f). This increase in relative volume of insulin-producing beta cells induced by HF diet was not observed after butyrate treatment (HFB)(d,i) as compared to its control (CB) (c,h); this result was confirmed quantitatively as shown in e. Bars in graph e represents means + SE of 6 mice per group. Images were obtained by light (a-d) or confocal laser microscopy (f-i). Scale bars, 500µm in a-d; 50µm in f-i. *** P <0.0001 compared to C group; ### P <0.0001 compared to HF group.

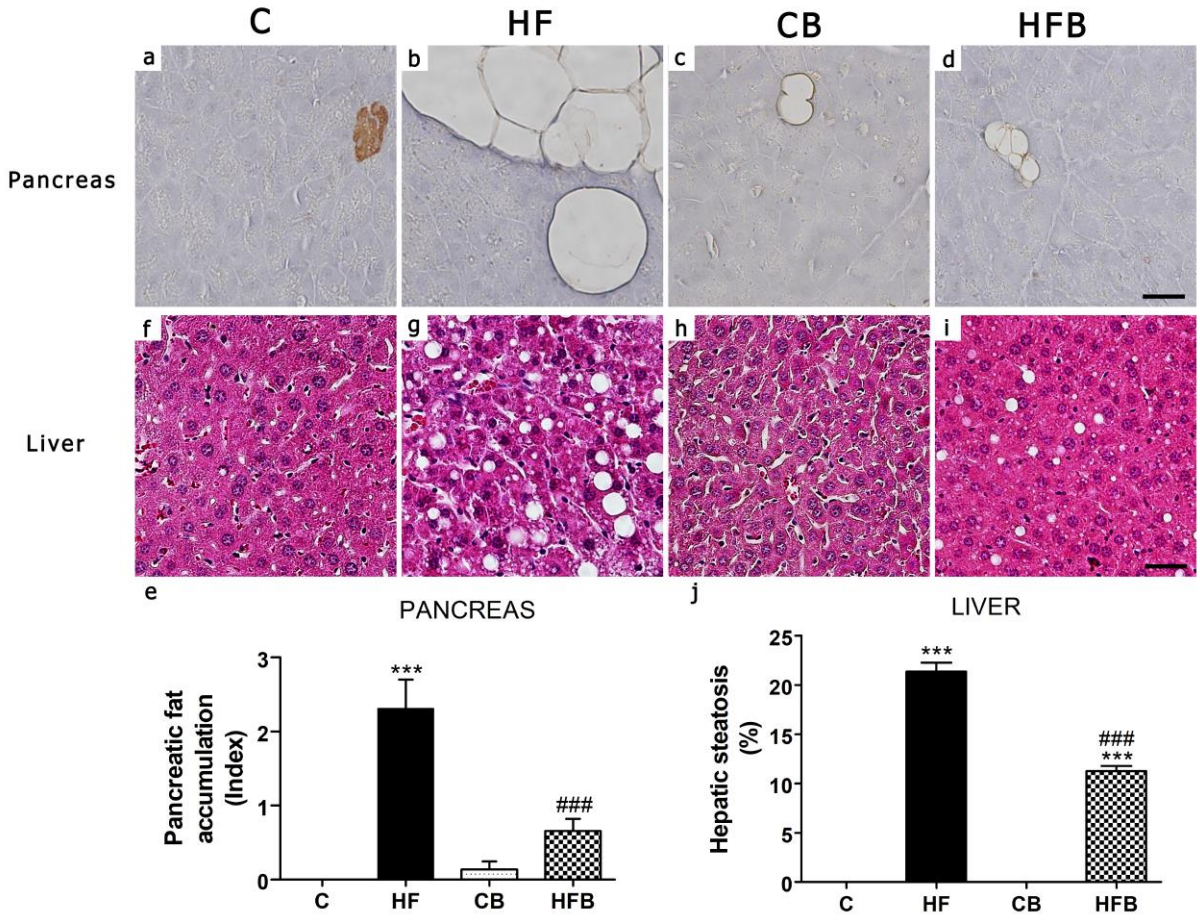

Figure 4. Diet supplementation with butyrate inhibited hepatic steatosis and pancreatic fat accumulation induced by high-fat diet in mice. Photomicrographs of liver (a-d) routinely processed for HE staining and pancreas processed for insulin immunoperoxidase (brown) (f-i). Exposure to high-fat (HF) diet induced liver steatosis (b,e) and pancreatic fat accumulation (g,j) in HF mice as compared to controls (C) (a,f,e,j), that were significantly reduced by administration of butyrate (HFB)(d,i,e,j). No significant changes were observed with butyrate *per* se (CB group) (c,h) in comparison with C group (a,f). Scale bars, 50µm. *** P<0.0001 compared to C group ; ### P <0.0001 compared to HF group.

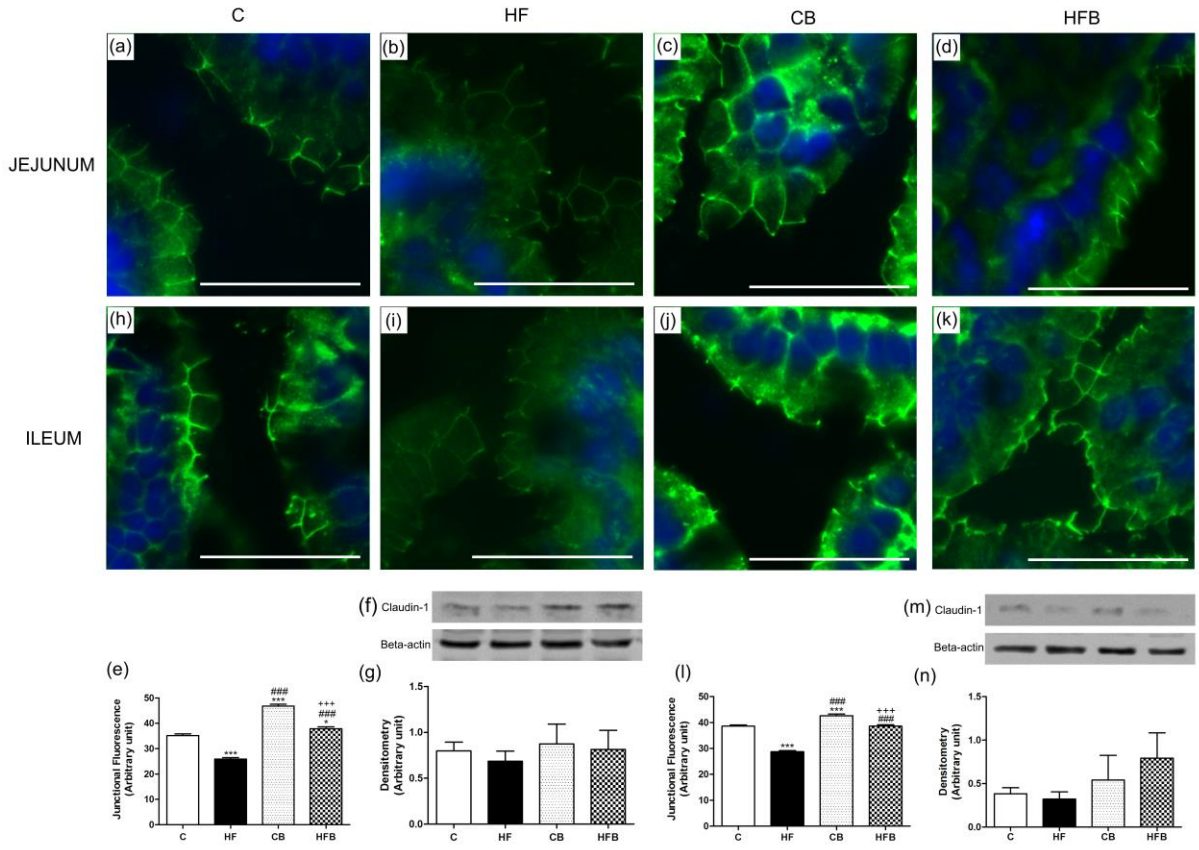

Figure 5: Butyrate, given as dietary supplementation, increased the junctional content of claudin-1, a tight junction-associated protein, in intestinal epithelia of small intestine (jejunum and ileum). The junctional and total cell contents of claudin-1 were evaluated by immunofluorescence in intestinal cryosections (claudin-1 in green; DAPI/nuclei in blue) and by Western Blot in intestine homogenates, respectively. The analysis of the degree of fluorescence at the cell-cell contact showed a significant decrease in the intercelular content of claudin-1 in enterocytes of small intestine from HF diet-fed mice (HF group)(c,e), which was inhibited by the administration of butyrate to treated animals (HFB group) (d,e). The total cell content of this junctional protein displayed no significant changes after HF diet and/or butyrate treatment as revealed by immunoblotting (f,g). Groups: C=control (fed a regular diet alone); HF=High-fat diet alone; CB=Control+butyrate; HFB=High-fat diet+butyrate. Scale bars, 15µm (insets); 50µm (images a-d).*P<0.05, ***P<0.0001 compared to C group; ###P<0.0001 compared to HF group; +++P<0.0001 compared to CB group.

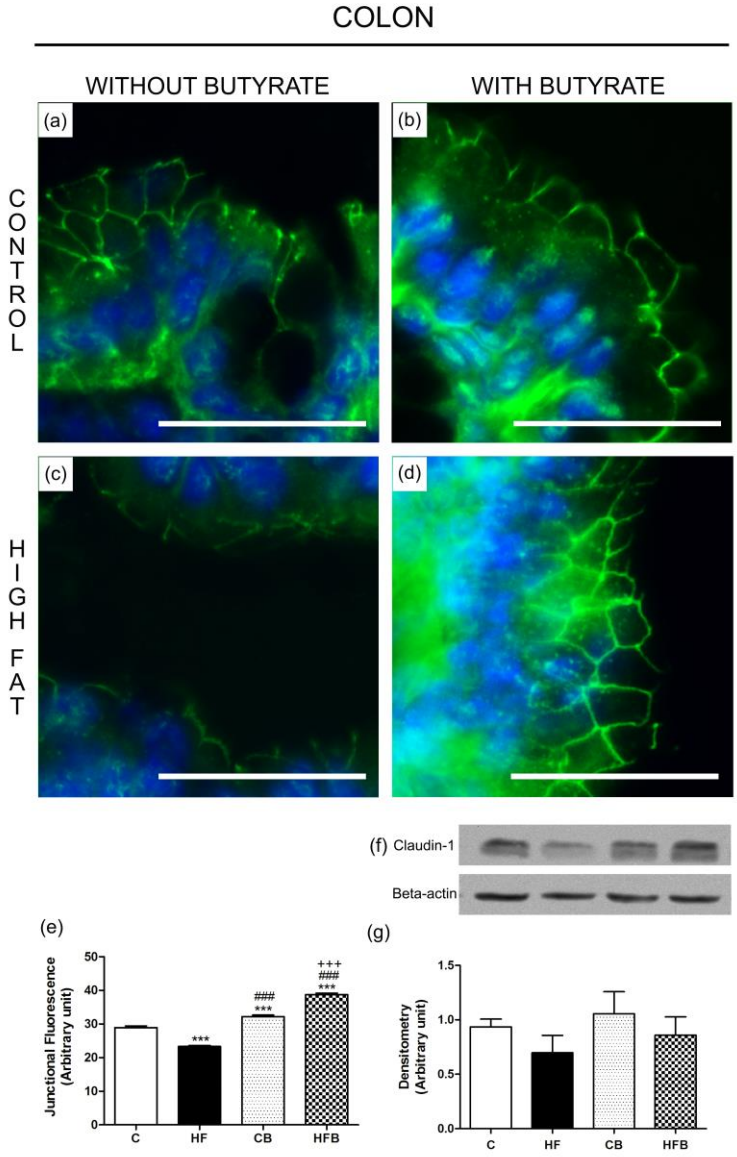

Figure 6: Butyrate inhibited the reduction in junctional content of claudin-1 in enterocytes of large intestine (colon) induced by exposure to high-fat diet in mice. The junctional and total cell contents of claudin-1 were evaluated by immunofluorescence in colon cryosections (claudin-1 in green; DAPI/nuclei in blue) and by Western Blot in colon homogenates, respectively. The analysis of the degree of fluorescence at the cell-cell contact showed a significant decrease in the intercelular content of claudin-1 in enterocytes of colon from HF diet-fed mice (HF group) (c,e) as compared to controls (C group) (a,e); this was inhibited by the administration of butyrate to treated animals (HFB group) (d,e). The total cell content of this junctional protein displayed no significant changes after HF diet and/or butyrate treatment as revealed by immunoblotting (f,g). Groups: C=control (fed a regular diet alone); HF=High-fat diet alone; CB=Control+butyrate; HFB=High-fat diet+butyrate. Scale bars, 15µm (insets); 50µm (images a-d). ***P<0.0001 compared to the C group; ###P<0.0001 compared to HF group; +++P<0.0001 compared to CB group.

CAPÍTULO 4

The beneficial effect of butyrate on BAT and basal energy expenditure in prediabetic mice.

INTRODUCTION

Type 2 diabetes mellitus (T2DM) is a chronic metabolic disorder of complex pathogenesis that be affected by genetic and environmental factors (Olokoba *et al*., 2012; American Diabetes Association, 2020). One of the main clinical signs of T2DM is the peripheral insulin resistance defined as the inability of organs and tissues (particularly the liver, adipose tissue, and muscles) to properly respond to insulin, which increases blood glucose level (Tripathy & Chavez, 2010; Collares-buzato, 2015). At the early stage of T2DM, hyperglycemia can be partially compensated by hypersecretion of insulin and/or hypertrophy and hyperplasia of the pancreatic beta cells (Collares-buzato, 2015; Falcão *et al.*, 2016; Maschio *et al.*, 2016). Later, the reduction of beta-cell mass by apoptosis results in a permanent hyperglycemic state, and, at this stage, the hormonal replacement with exogenous insulin is required to reach a glycemic balance (Montanya, 2014).

A link between the intake of a high-fat diet, obesity, and T2DM is well established (De Kort *et al*., 2011). Besides hyperglycemia, T2DM is often associated with significant alterations in lipid metabolism leading to dyslipidemia (Mooradian, 2009; Shulman, 2014; Tangvarasittichai, 2015) This condition is characterized by high plasma levels of circulating triglycerides, cholesterol and free fatty acids (FFAs). The combination of hyperglycemia and high FFAs has been directly related to the onset and aggravation of the insulin resistance state as well as to the dysfunction of the pancreatic beta-cell during T2DM (Lin *et al.*, 2005; Collares-buzato, 2015). In this respect, the white adipose tissue (WAT) seems to play an important role since it manages the levels of FFAs in the circulatory system by storing them as triacylglycerols (TAG) with the involvement of the nuclear receptor peroxisome proliferator-activated receptor (PPAR-c) (Banerjee *et al.*, 2019). During T2DM, it has been demonstrated that PPAR-c is downregulated, which is associated with adipogenesis and release of cytokines and inflammatory factors by the inflammation WAT (Ye, 2008; Banerjee *et al.*, 2019). The brown adipose tissue (BAT), which is relatively less studied in the context of diabetes, also display functional and morphological alterations during obesity and T2DM (Cypess & Kahn, 2010; Lapa *et al.*, 2017). These changes can result in a process known as

"whitening" of BAT that involves the downregulation of UCP-1 and eventually led to a functional shift from thermogenesis and energy expenditure toward lipid storage (Lapa *et al.*, 2017).

T2DM is one of the most prevalent endocrine-metabolic diseases in the world and has become a global health problem with an estimated over 400 million affected adults (World Health Organization, 2016). Therefore, it has been an increasing interest in alternative therapies of T2DM using nutrients and natural substances that act against the processes that trigger the insulin resistance, such as the excess of circulating glucose and FFAs, the release of cytokines and inflammatory factors by the WAT, and the entrance of substances from an altered microbiota into the circulation through a disrupted intestinal barrier (Kahn *et al*., 2006; Shoelson *et al.*, 2006; De Kort *et al*., 2011).

Sodium butyrate is a short-chain fatty acid (SCFA) produced by the intestinal microbiota (mainly in the colon), from the fermentation of non-digestible carbohydrates. In addition to serving as an energy source for colonocytes, sodium butyrate can affect the transport of ions and molecules across the intestinal mucosa (Rabbani *et al.*, 1999; Canani *et al.*, 2004, 2011). Studies showed that the production of this SCFA is reduced in diabetic individuals (Khan & Jena, 2016). Butyrate can improve metabolism in some pathophysiological states by, in part, promoting an increase in energy expenditure via modulation of mitochondrial function (Gao *et al.*, 2009; Kootte *et al.*, 2012; Khan & Jena, 2016). Previous results from our research group showed that supplementation with sodium butyrate significantly inhibited the insulin resistance and the changes in some parameters of glucose homeostasis, as well as the hepatic steatosis and intestinal barrier dysfunction in prediabetic C57BL6 mice induced by a high-fat diet (Matheus *et al.*, 2017). Nevertheless, studies on the effect of sodium butyrate on lipid metabolism and adipose tissue biology at the early stages of T2DM are still scarce and the direct action of this SCFA on food intake is a point of debate (Gao *et al.*, 2009; Matheus *et al.*, 2017). In order to extend our previous findings (Matheus *et al.*, 2017), this work aimed to evaluate the effect of supplementation with butyrate on dyslipidemia, adipose tissue, and muscle masses, the basal energy expenditure *in vivo* and *in vitro* conditions, as well as on the gene expression of UCP-1 in BAT and orexigenic/anorexigenic genes in the hypothalamus of C57BL6 mice fed a high-fat diet for 60 days.

MATERIAL AND METHODS

Animals, treatments and metabolic/biochemical analyses

Male C57BL/6JUnib mice, aged 16-18 weeks, were obtained from the breeding colonies of the Multidisciplinary Center for Biological Investigation on Laboratory Animal Science (CEMIB) at the University of Campinas (UNICAMP, Brazil). They were maintained in micro isolator cages under controlled conditions of temperature and light-dark cycle of 12h and had free access to food and water during the entire experimental period (60 days). Sodium butyrate (cat number 303410, Sigma) was incorporated into a regular diet or a high-fat (HF) diet at the concentration of 5% (w/w) (Matheus *et al.*, 2017). Mice were divided into four experimental groups (7-8 animals/group): 1) Control group (C), received a standard rodent diet (Nuvilab, Quintia - in powder; containing 4.5% lipids, 53 % carbohydrates, and 23 % proteins; w/w); 2) Control + Butyrate group (CB), received the standard diet mixed with 5% of sodium butyrate (w/w); 3) High-fat group (HF), received a prepared high-fat diet (in powder;containing 21 % lipids, 50 % carbohydrates, and 20 % proteins; w/w); 4) High-fat + Butyrate group (HFB), received the prepared high-fat diet mixed with 5% of sodium butyrate (w/w). The following parameters were evaluated in all animals: the body weight gain, the weight of the retroperitoneal and epididymal white adipose tissue (WAT) and the interscapular brown adipose tissue (iBAT), the fast and fed glycemia and the lipidemia (serum concentration of triglycerides, cholesterol, HDL and LDL) and response to the glucose tolerance test, GTT (via gavage - 1.5g/kg of glucose diluted in 4.8ml/kg of filtered water) in animals with 12h fasting, expressed as area values under the curve (AUC). These procedures were performed as previously described (Carvalho *et al.*, 2012; Oliveira *et al.*, 2015; Falcão *et al.*, 2016) between 9 am to 11 am. The blood glucose concentration was measured using an Accu-Chek Active glucometer (Roche Diagnostic, Switzerland). Lipidemia was measured in serum using commercial ELISA kits (Enzymatic Colestat AA liquid, LDL Cholesterol Reactive Precipitant, HDL Cholesterol Reactive Precipitant, and TG Color GPO/PAP AA, Weiner Lab., St. Ingbert-Germany). All the experiments were approved by the Institutional Committee for Ethics in Animal Experimentation of the University of Campinas (CEUA/UNICAMP; under Protocol: 4185-1).

Evaluation of fat/lean mass ratio, the basal energy expenditure, and locomotor activity

The measurement of the basal energy expenditure was performed using a metabolic chamber system (Oxylet – Panlab/Havard Apparatus, Barcelona, Spain). After 3h of adaptation, the mice were monitored and the data recorded for a period of 48h. The basal locomotor activity was recorded for 24h using a cage system coupled to the equipment that counts each movement (Physiocage - Panlab/Havard Apparatus, Spain). For both procedures, mice from the different experimental groups were housed individually under a light and dark cycle of 12 hours at 24ºC, with free access to water and food (Branco *et al.*, 2019). The computerized microtomography technique was used to evaluate the fat and lean masses per total body mass (Judex *et al.*, 2010; Raposo *et al.*, 2015; Santos *et al.*, 2018). Anesthetized mice (with 80 mg/kg ketamine hydrochloride and 10 mg/kg xylazine hydrochloride, intraperitoneal injection) were placed in the micro-CT scanner (Bruker - Skyscan 1178 - USA). The X-Ray energy parameters were: 44 kV; 150 μA; 6,6 W. One thousand images were obtained along at 360° rotation, followed by the reconstruction of these images to create a 3D image using the program NRecon version 1.6.10.2 (SkyScan, USA) and the Feldkamp algorithm. The region of interest was determined according to differences in tissue radiodensity and processed accordingly in order to measure relative volumes of fat and lean masses.

Histological analysis of BAT

Fragments of the interscapular brown adipose tissue (iBAT) obtained from each experimental group were fixed in a 4% paraformaldehyde (PFA) solution, and then paraffin-embedded, sectioned (4 μm thickness), and processed for Hematoxylin-Eosin (H.E.) staining. A number of 10 images (40x) were randomly captured from two different sections per animal (n=5 mice/group) using an optical microscope (Nikon Eclipse E-400 - Nikon, Tóquio, Japão - NIS Elements) coupled to a digital camera (Olympus U-TV 0.5 C-3, Olympus Corporation, Waltham, US). The quantification of spaces previously occupied by lipids and its relation with total image area was used as an indirect way to measure lipid accumulation. This was determined using the Image J program (http://rsbweb.nih.gov/ij/).

Quantitative real-time PCR

Total RNAs were extracted from the total hypothalamus and fragments of BAT using TRIzol®. The reverse transcription in cDNA was performed using the Superscript II kit (Invitrogen, Carlsbad, CA, USA). Quantitation of mRNAs was performed using the Real-Time PCR System 7500 with the Master Mix SYBR Green PCR (AppliedBiosystems, Carlsbad, CA, USA). Primer sequences used are shown in Table 1 (Table 1). The relative expression of mRNAs of interest were normalized by the control gene Hypoxanthine-guanine phosphoribosyltransferase (HPRT), using the 2-ΔΔCt method (Soares *et al.*, 2019).

Tabela I. Primers.

Gene	Primer 5'- 3'
POMC	Forward: GGCTTGCAAACTCGACCTC Reverse: TGACCCATGACGTACTTCCG
CART	Forward: ACCTTTGCTGGGTGCCCGTG Reverse: TGCAACGCTTCGATCAGCTCC
NPY	Forward: TACTCCGCTCTGCGACACTA Reverse: TCTTCAAGCCTTGTTCTGGG
AgRP	Forward: GAGTTCCCAGGTCTAAGTCTGAATG Reverse: ATCTAGCACCTCCGCCAAAG
UCP-1	Forward: CTGCCAGGACAGTACCCAAG Reverse: TCAGCTGTTCAAAGCACACA
HPRT	Forward: TCAGTCAACGGGGGACATAAA Reverse: GGGGCTGTACTGCTTAACCAG

Abbreviations: C*ocaine- and amphetamine- regulated transcript* (*CART*), *Pro-opiomelanocortin* (*POMC*), *Neuropeptide* (*NPY*), *Agouti-related protein* (*AgRP*), *Uncoupling protein 1* (*UCP-1*), *Hypoxanthine-guanine phosphoribosyltransferase* (*HPRT*).

Cultured 9W adipose cell line

Immortalized adipocyte precursor cells isolated from inguinal subcutaneous adipose tissue - 9W cells - were used in this study to evaluate butyrate effects on cellular bioenergetics (Mori *et al.*, 2012). Briefly, 9W cells were cultured in 90 x 15 mm plates on DMEM High-Glucose supplemented with 10% Fetal Bovine Serum (Gibco) plus and 1% Streptomycin and

Penicillin (Gibco) and kept in an incubator at 37ºC with 5% CO_2 and 70% humidity. When reaching 70-80% of confluence, cells were washed with phosphate-saline buffer (pH 7.4), detached from the plates with 0.25% Trypsin-EDTA (Gibco), centrifuged (1200 rpm for 5 minutes), resuspended in DMEM High-Glucose and seeded (5 x 10^3 cells) in working plate. Then, after confluency, cells were used for experiments (for undifferentiated cells) or induced to differentiate into 9W adipocytes by addition of adipogenic medium containing 20 nM Insulin (Sigma-Aldrich), 2 mg/mL Dexamethasone (Sigma-Aldrich), 500 µM 3-Isobutyl-1-Methylxanthine (Sigma-Aldrich), 1 µg/mL Rosiglitazone (Sigma-Aldrich), 1 nM 3,3',5-Triiodo-L-Tyronine (Sigma-Aldrich) and 125 µM of Indometacyn (Sigma-Aldrich). After 8 days of the differentiation process, cells were used for experiments.

Cell viability – MTT assay

Undifferentiated or differentiated 9W cells were treated with 0.5 mM of sodium butyrate (Sigma-Aldrich) for 24 hours. Subsequently, butyrate-treated cells were washed with PBS and incubated with DMEM High Glucose plus 0.5 mg/mL of Thiazolyl Blue Tetrazolium Bromide (Sigma-Aldrich) for 1h (differentiated cells) or 4h (undifferentiated cells). After incubation, the medium was aspirated, the wells were washed with PBS, 100 µL DMSO (Synth, Brazil) was added per well and plates were incubated for 30 minutes at 37°C The absorbance was measured at 570 nm using a microplate reader (PowerWave XS2).

Cell respiration – Oroboros Assay

Cellular bioenergetics of the 9W cells (undifferentiated and differentiated) was measured by high resolution respirometry (OroborosOxygraph-O2K, Oroboros Instruments, Innsbruck, Austria) at 37 ° C in Krebs-Ringer pH 7.4 (NaCl 130 mM, KCl 4.7 mM, 1.24 mM $MgSO_4$, 2.5 mM $CaCl_2$, 10 mM HEPES, 2.5 mM NaH_2PO_4, 2% BSA). The cells were treated for 6 or 24 hours with 0.5 mM of sodium butyrate diluted in DMEM High-glucose. This relatively low concentration of butyrate was chosen based on the following premises: 1) it is within the physiological concentration range (Caminhotto *et al.*, 2019), and 2) it has no apparent cytotoxicity besides displaying biological effects on different cell types *in vitro* (Singh *et al.*, 1997; Kaiko *et al.*, 2016; Kespohl *et al.*, 2017; Liu *et al.*, 2020). Cells at a density of 8 x 10^5 (differentiated) or 1.5 x 10^6 (undifferentiated) were added to oxygraph chambers to obtain oxygen consumption fluxes according to a previously published protocol (Doerrier *et al.*, 2018) Briefly, oligomycin (2 µg/mL) was added into the chambers aiming to

obtain ATP-dependent and proton leak oxygen consumption. Afterward, mitochondrial uncouplers were tritiated (0.05 µM per addition) – CCCP (Carbonylcianeto m-chlorophenylhydrazone) or FCCP (Carbonyl cyanide-4-(trifluoromethoxy) phenylhydrazone – to reach maximal respiration. Finally, antimycin A (2.5 µM) was added to for non-mitochondrial respiration values records. The results were expressed as O_2 Flow per cells [pmol/(s*10^6 cells)].

Statistical analysis

To determine the degree of statistical significance among the four experimental groups we have used the One-way ANOVA, followed by the Bonferroni post-test to compare pairs of data. Two-way ANOVA was used to statistically analyze the GTT curve data. The Student's t-test was employed to determine the degree of statistical significance between two experimental groups. Results were expressed as means + SEM (Standard Error of the mean), and the significance level was set at $P < 0.05$. All statistical analyses were performed using GraphPad Prism Version 5.00 for Windows (GraphPad Software, USA).

RESULTS

Exposure to the high-fat diet (HF) for 60 days induced a significant increase in fast glycemia ($P<0.0001$) (Fig. 1a) associated with an intolerance to glucose as assessed by GTT (Fig. 1b-c) ($P<0.001$). HF-fed mice also displayed dyslipidemia characterized by significantly increased plasma levels of triglycerides ($P<0.001$) (Fig. 1d), cholesterol ($P<0.0001$) (Fig. 1e), and LDL fraction (Fig. 1f) but not of HDL fraction (Fig. 1g) as compared to the control group. Sodium butyrate had a marked effect on the fast glycemia and response to GTT, reducing significantly both parameters in the HFB group in relation to the HF group. However, this SCFA seems to display a less protective action on dyslipidemia induced by HF diet intake (Fig. 1 d-f). The effect of butyrate on triglyceride, cholesterol, and LDL levels was not significant in the HFB group. Sodium butyrate *per se* maintained the serum concentration of circulating glucose and lipids identical to the C group. The data obtained by qPCR in the hypothalamus from the groups receiving butyrate supplementation (CB and HFB) showed no significant difference in anorexigenic (*CART, POMC*) and orexigenic (*NPY, AgRP*) markers (Hillebrand *et al*., 2002; Rojczyk *et al*., 2015) when compared to their respective controls (C and HF) (Fig. 1h). This result corroborates previous work showing that butyrate does not affect food intake (Matheus *et al.*, 2017).

As shown in Figure 2, exposure to the HF-diet resulted in a significant increase in total body weight gain (P<0.0001) (Fig. 2a), and the weight of both eWAT (epididymal adipose tissue) (P<0.0001) (Fig. 2b) and rWAT (retroperitoneal adipose tissue) (P<0.0001) (Fig. 2c) as compared to C group. As revealed by microtomography, a significant increase in the relative white adipose tissue mass (WAT - fat mass) (P<0.0001) (Fig. 2d) associated with a significant decrease in skeletal muscle tissue (lean mass) were observed in animals from the HF group in comparison with C group (P<0.0001) (Fig. 2e). Dietary supplementation with 5% sodium butyrate (HFB) significantly reduced the body weight gain (P<0.0001) (Fig. 2a) and the accumulation of rWAT (P<0.001) (Fig. 2c) as well as ameliorated the fat/lean ratio (Fig. 2 d, e, f), but did not change eWAT depot (Fig. 2b) when compared to the HF group). Sodium butyrate *per se* (CB) did not affect these parameters, maintaining the levels of C group (Fig. 2 a-f).

The evaluation of basal energy expenditure (without exercise induction) was performed using a metabolic chamber. The group receiving high-fat diet showed a significant decrease in energy expenditure (P<0.05) (Fig. 3a), in oxygen volume (VO_2) (P<0.05) (Fig. 3b) and respiratory quotient (RQ) (P<0.0001) (Fig. 3c) compared to the control group at night. The group receiving the high-fat diet with supplementation with 5% sodium butyrate (HFB) showed a significant increase in energy expenditure (P<0.001; Student's t-test) (Fig. 3a), in VO_2 (P<0.001) (Fig. 3b) compared to the high-fat diet group, reaching levels similar to the C and CB groups. However, butyrate had no significant effect on the RQ parameter in HFB mice when compared to the HF group (Fig. 3c). The CB group did not show a difference in these parameters (Fig. 3 a-c) compared to the control group (C). As shown in Fig. 3d, sodium butyrate (in CB and HFB groups) did not affect significantly the motor activity in comparison with the groups that did not receive supplementation (C and HF).

In comparison with the control group, the intake of high-fat diet-induced significant changes in brown adipose tissue (BAT), that included BAT "whitening" revealed by the significant increase in intracellular lipid accumulation, as confirmed morphometrically (P<0.0001) (Fig. 4a, b), associated with a significant increase in BAT weight (P<0.0001) (Fig. 4c) and a decrease in the tissue expression of UCP-1 gene (P <0.05) (Fig. 4d). All these BAT alterations were significantly attenuated after diet supplementation with sodium butyrate (Figura 4a-d).

Since sodium butyrate increased the basal metabolism in vivo conditions after HF diet intake (Fig 3), we went to test whether this SCFA would have a direct effect on the

mitochondrial respiration of an adipose cell line, the 9W cells, at undifferentiated (Figure 4e) and differentiated states (Fig. 4 f). As shown in Figure 4 (e, f), the addition of butyrate at low concentration (0.5mM) to the cell media for 6h and 24h did not affect the oxygen consumption by cultured 9W cells in any of the experimental conditions tested, besides showing no cytotoxic effect (viability after 24h exposure to 0.5mM: Control 9W cells 100%; undifferentiated 9W cells 101.2 ± 6.6 (4)%; differentiated 9W cells 95.6 ± 6.6 (4)%).

DISCUSSION

Type 2 diabetes mellitus (T2DM) involves a complex set of metabolic disturbances that include impaired metabolism of carbohydrates and lipids (Wu *et al.*, 2014). The hallmarks of T2DM are hyperglycemia, insulin resistance, and insulin deficiency, and it is increasingly recognized that insulin resistance contributes to the dyslipidemia associated with this type of diabetes (Brinton, 2003; Brunzell & Ayyobi, 2003; Collares-buzato, 2015; Khan & Jena, 2016). Dyslipidemia has been frequently observed in type 2 diabetic patients and is characterized by elevated triglyceride and total cholesterol levels, a high plasma concentration of low-density lipoprotein particles (LDL) but a low high-density lipoprotein cholesterol (HDL) levels (Mooradian, 2009; Vijayaraghavan, 2010; Tangvarasittichai, 2015). These disturbances of the lipid metabolism appear to be an early event in the development of type 2 diabetes, often related to the ingestion of saturated fat-enriched diets and obesity. The association between hyperglycemia and microvascular complications in type 2 diabetes is unequivocal, while dyslipidemia has been correlated more directly with cardiovascular complications and increased risk of renal dysfunction, which are the two main life-threatening comorbidities of diabetes (Vijayaraghavan, 2010). Several lipid-lowering agents are available to target normalization of the entire lipid profile, nevertheless, many patients with type 2 diabetes do not achieve lipid targets even with the use of a combination and high-dose lipid-lowering agents (Vijayaraghavan, 2010).

An important role of the intestinal microbiota for host homeostasis through its metabolites, the short-chain fatty acids (SCFAs), has been proposed (Everard & Cani, 2013; Bron *et al.*, 2017). These SCFAs seem to be involved in several signaling pathways influencing the cell metabolism and, for this reason, they are being studied as a possible alternative for the prevention of metabolic disorders such as obesity and Type 2 Diabetes Mellitus (Zhang *et al.*, 2019). SCFAs act on receptors known as GPR or FFAR that are present in several tissues, including adipose tissue (Xiong *et al.*, 2004). Interestingly, the

formation of SCFAs, particularly butyrate, is significantly reduced after the ingestion of high-fat diets (Jkobsdottira *et al.*, 2013). In this work, we focused on the putative effect of butyrate on the lipidemia, adiposity, and basal metabolism using an animal model of T2DM that has been extensively employed and well-characterized by our research group. In previous studies, we have shown that mice with prediabetes induced by a high-fat diet lead to a series of metabolic disorders leading to changes in the metabolism of carbohydrates and lipids, such as: weight gain, dyslipidemia, impaired response to insulin and glucose and adiposity (Carvalho *et al.*, 2012; Oliveira *et al.*, 2015; Matheus *et al.*, 2017; Maschio *et al.*, 2019; Oliveira *et al*., 2019). The present study corroborates the previous results since these metabolic alterations were also observed in our animals fed the HF diet.

In previous work, we have demonstrated that dietary supplementation with butyrate had a beneficial effect on the glucose homeostasis by reversing the insulin resistance state and significantly reducing both fast and fed hyperglycemia and hyperinsulinemia in HF diet-fed prediabetic mice (Matheus *et al.*, 2017). All these alterations occurred without significant changes in daily food consumption or energy intake suggesting a direct effect of the butyrate on glucose metabolism (Matheus *et al.*, 2017). The present study not only corroborated these data but went further by showing that the HF diet does not affect the hypothalamic expression of anorexigenic and orexigenic genes and that butyrate significantly increases glucose tolerance (as seen in the GTT test) in obese and prediabetic mice.

Regarding the effect of butyrate on dyslipidemia, our prediabetic mice that received this SCFA surprisingly displayed no marked difference in the lipid profile as compared to mice that were fed only the HF diet, although a subtle reduction in the triglycerides, total cholesterol and LDL was observed after butyrate. We also demonstrated that butyrate did not affect the reduction in RQ (Respiratory Quotient) index induced by the HF diet. The RQ is the ratio of carbon dioxide production to oxygen consumption and reflects the relative contribution of fat, carbohydrate, and protein to the fuel oxidation (Issekutz *et al*., 1962). The RQ typically ranges between 0.7 and 1.0 and is an indicator of metabolic fuel or substrate use in tissues. A ratio near 0.7 is indicative of mixed fat use, whereas a ratio of 1.0 indicates the exclusive use of carbohydrates. Our HF diet-treated animals displayed a RQ of 0.85 (in contrast to the RQ of 0.95 in C and CB groups), indicating a preference for fat over carbohydrate oxidation, which was not affected by the butyrate administration. Taken all together, these data suggest that butyrate displays a relatively small effect on circulating lipids in HF diet-fed mice, besides this SCFA does not alter the energy consumption towards fat

metabolism in these animals. This contrasts with the marked protective action of butyrate on glucose homeostasis. Although we do not have a conclusive explanation for this observation, it is plausible to suggest that butyrate does not reduce the intestinal absorption of lipids, and, by doing so, the lipids remain at high levels under chronic HF diet ingestion that cannot be counteracted by the metabolic actions of butyrate. In accordance with this idea, it has been demonstrated that dietary fat digestion and absorption in the gastrointestinal tract is identical between HF diet-fed mice that received butyrate supplementation and those that did not (Gao *et al.*, 2009).

In pioneering work, Gao *et al*. (2009) also demonstrated the beneficial effects of butyrate on metabolic changes induced by the high-fat diet. However, this work was limited since analyzed only two experimental groups: the group that received the hyperlipidemic diet, in association or not with butyrate. Therefore, the metabolic effects were not properly compared with a group that received a standard diet (control) and/or with a group that received this standard diet associated with butyrate supplementation. Our work brings interesting comparisons regarding the difference between the four experimental groups and shows that the supplementation with sodium butyrate significantly ameliorates the metabolic disorders induced by a hyperlipidemic diet, however, it does not reestablish the disorders studied at the level of the control animals. Furthermore, we demonstrated that supplementation with butyrate *per se* (that is, in the absence of the metabolic challenge of the high-fat diet) maintained the metabolic parameters at levels equivalent to the control.

A possible contributing factor to the anti-diabetogenic and anti-obesogenic effects of butyrate is its protective action on brown adipose tissue (BAT). BAT burns energy for thermogenesis (Cypess & Kahn, 2010). BAT activity has been inversely associated with adiposity and indexes of the metabolic disorders suggesting that increasing BAT mass and/or activity may be a target for pharmacologic and nutritional interventions that modulate energy expenditure to treat obesity and T2DM (Cypess & Kahn, 2010). Our studies show that supplementation with butyrate preserves the histological characteristics of brown adipose tissue and, as a consequence, it probably maintains the functionality of this tissue. The change in the appearance of the BAT was also noted at the time of its dissection (data not shown), as evidenced by the greater weight of this tissue in animals that received a high-fat diet without supplementation, and its more "whitish" appearance as compared to the BAT of the animals of the others experimental groups. Other studies have reported an impaired function of this tissue in obese and diabetic animals and the improvement of these dysfunctions after brown

adipose tissue transplantation (Stanford *et al.*, 2013; Lapa *et al.*, 2017). The metabolic activity of brown adipose tissue is also related to the expression of UCP-1, an integral membrane protein located on the inner membrane of mitochondria (Krauss *et al*., 2005; Ricquier, 2017). It was decreased in animals that received a high-fat diet without supplementation compared to animals in the other experimental groups. The decrease in UCP-1 contributes to a lower metabolic activity, which may have even contributed to the lower energy expenditure displayed by these animals, as well as to the increase in the lipid accumulation seen in the BAT. Our results corroborate other studies that show that butyrate decreases the weight of BAT, and induces an increase in the protein content of UCP-1, allowing greater thermogenic capacity to this tissue. (Khan & Jena, 2016; Li *et al.*, 2018).

Given the observed action of butyrate in BAT biology in our prediabetic mice, we investigated whether this SCFA could have a direct effect on an in vitro model of brown adipose cells. For this, we used an adipocyte precursor cell line with a great capacity for thermogenesis, the 9W cells (Mori *et al.*, 2012). However, the effect on energy expenditure observed *in vivo* with sodium butyrate supplementation was not observed *in vitro*, which leads us to believe that this effect is not related to a direct response at the cellular level. It is noteworthy that this work used a concentration of 0.5mM sodium butyrate, which was not toxic for this cell type. It cannot be ruled out, however, the possibility that higher concentrations of butyrate may have more pronounced effects on the energy biology of these cells. Future experiments will be necessary to verify this alternative.

Taken all together, we can conclude that sodium butyrate supplementation significantly ameliorated the body weight gain, the adiposity and fat/lean mass ratio, however, the positive effect on lipid metabolism was not as marked as that seen on carbohydrate metabolism. In addition, this SCFA induced significant increase in the basal metabolism (energy expenditure) of HFB mice as compared to the HF group, without affecting the motor basal activity. Butyrate supplementation preserved the morphological and functional characteristics of brown adipose tissue (BAT) and increased the UCP-1 BAT expression, which may contributed to the increased energy expenditure. However this effect on BAT was not observed *in vitro*, suggesting that a systemic action of butyrate rather than a direct effect on BAT is involved in the phenomenon.

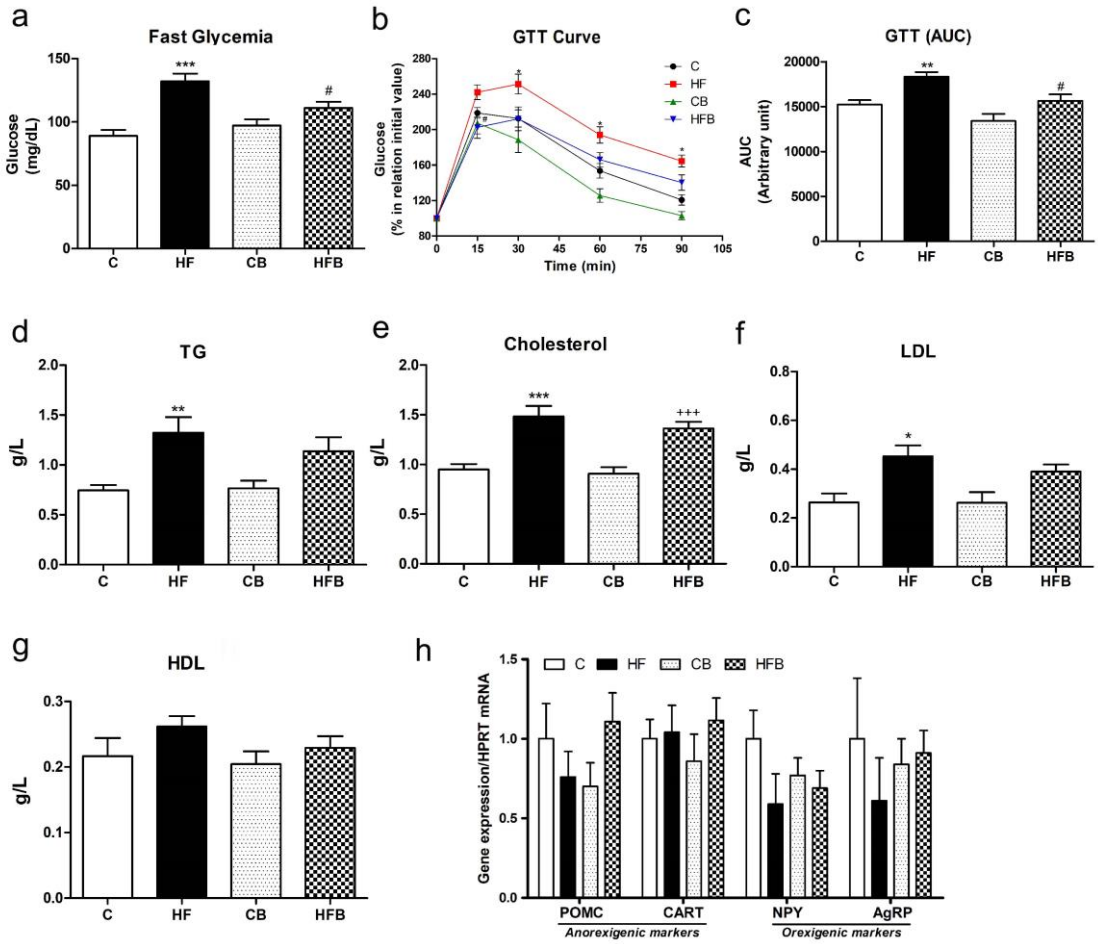

Figure 1. Effect of butyrate on metabolic parameters and hypothalamic expression of orexigenic/anorexigenic genes in mice fed a high-fat diet. In comparison with the control group, the high-fat diet (HF) for 60 days induced a significant intolerance to glucose as assessed by the Glucose Tolerance Test (GTT) curve in **b**, area under curve (AUC) in **c** associated with a significant increase in fast glycemia (**a**), in the level of the triglycerides (TG) (**d**), cholesterol (**e**), and LDL fraction (**f**) but no significant changes in HDL level and gene expression in the hypothalamus related to food intake. Dietary supplementation with 5% sodium butyrate (HFD) presented a protective effect by inhibiting the glucose homeostasis dysfunctions (**a-c**) and dyslipidemia (**d-f**) induced by the HF diet (HF group), but also did not have an effect on orexigenic/anorexigenic gene expression in the hypothalamus (**h**). Butyrate supplementation alone (CB) did not affect the evaluated parameters when compared to the control group (C) (**a-h**). Data are expressed as means ± SEM (n=8-15 mice per group).
Groups: C: control (fed a regular diet alone); HF: high-fat diet alone; CB: Control+butyrate; HFB: high-fat diet+butyrate. *P<0.05, **P<0.001, ***P<0.0001 compared to C group; #P<0.05 compared to HF group; +++P<0.0001 in relation to CB (One-way or two-way ANOVA followed by the Bonferroni's post-test).

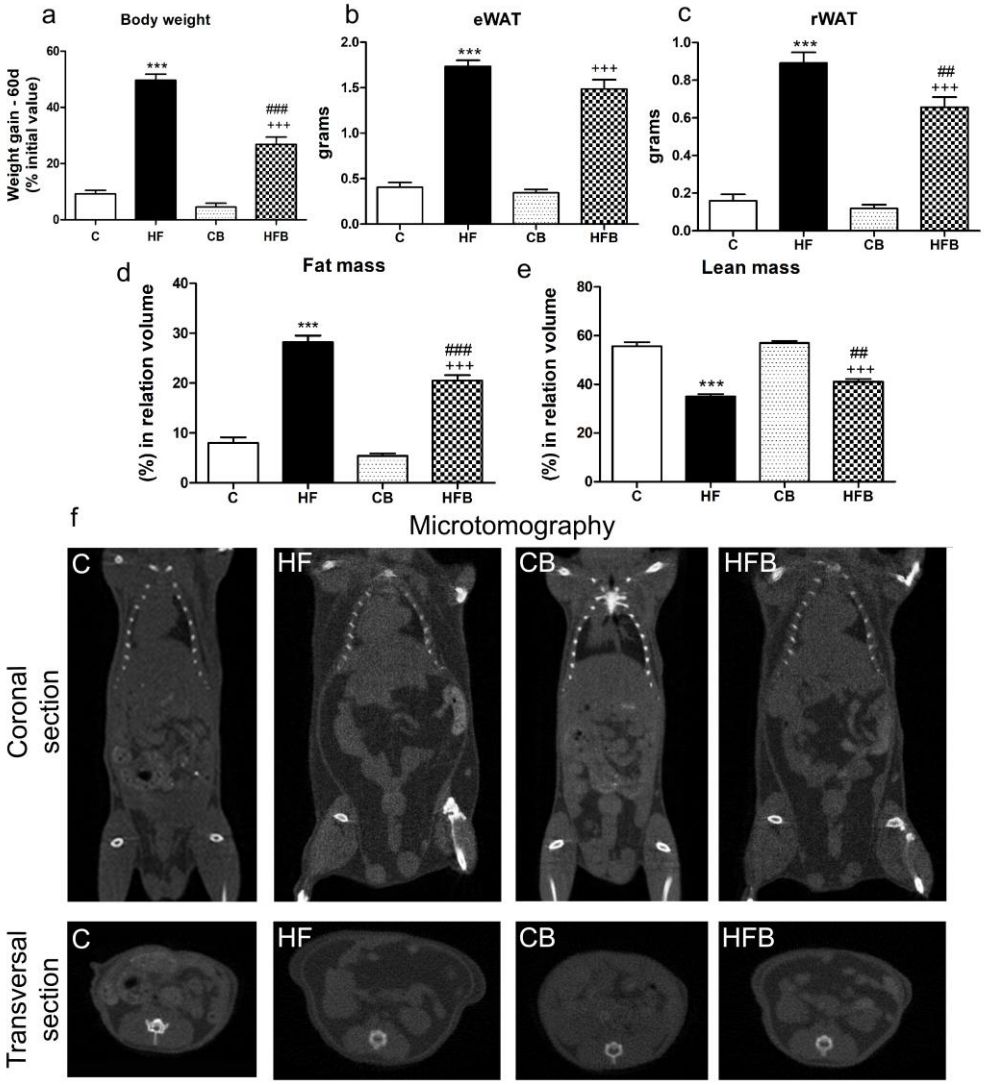

Figure 2: Effect of butyrate on body weight, fat depot, and masses of white adipose and muscle tissues in mice fed a high-fat diet. The fat depot was assessed by the weight of epididymal (eWAT) (**b**) and retroperitoneal white adipose tissue (rWAT) (**c**), expressed as grams. The white adipose tissue (fat) and skeletal tissue (lean) masses were determined by microtomography (**d, e**). In **f**, representative tomography images of mice from each experimental group. The intake of a high-fat diet for 60d induced a significant increase in body weight gain (**a**), epididymal and retroperitoneal fat depot (**b, c**), and fat mass (**d**) associated with a significant decrease in lean mass (**e**). Dietary supplementation with butyrate partially reversed these alterations in the HFB group but did not display effect per se in the CB group. Data are expressed as means ± SEM (n=11-20 mice per group). Groups: C: control (fed a regular diet alone); HF: high-fat diet alone; CB: Control+butyrate; HFB: high-fat diet+butyrate. ***P<0.0001 compared to C group; ##P<0.05, ###P<0.0001 compared to HF group; +++P<0.0001 compared to CB group (One-way ANOVA followed by the Bonferroni's post test).

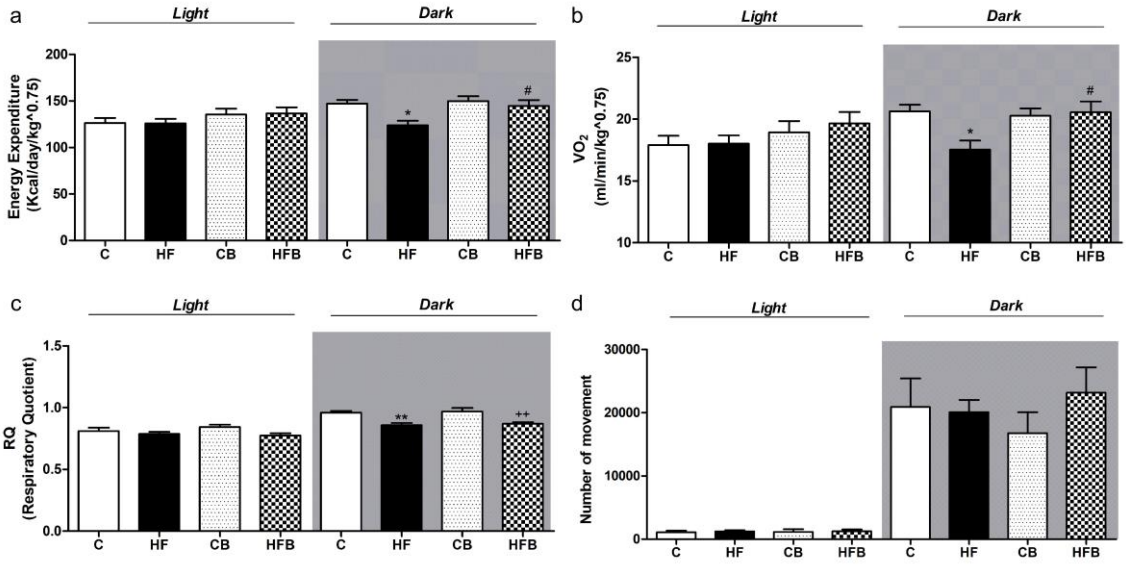

Figure 3. Supplementation with sodium butyrate significantly increased the basal energy expenditure in mice fed a high-fat diet. Compared to the control group, the high-fat diet group showed a significant decrease in energy expenditure (**a**), Oxygen Volume (VO_2) (**b**) and Respiratory Quotient (RQ) (**c**) at the nocturnal period. The diet supplementation with butyrate in the HFB group significantly reversed these changes induced by HF diet (**a, b, c**). The CB group did not show difference in these parameters (**a, b, c**) as compared to the control group (C). No difference in motor activity during day and night was observed among the experimental groups (**d**). Data are expressed as means ± SEM (n=8-11 mice per group).

Groups: C: control (fed a regular diet alone); HF: high-fat diet alone; CB: Control+butyrate; HFB: high-fat diet+butyrate. *P<0.05, **P<0.0001 compared to C group; #P<0.001 compared to HF group (One-way ANOVA followed by the Bonferroni's post-test and Student's t-test).

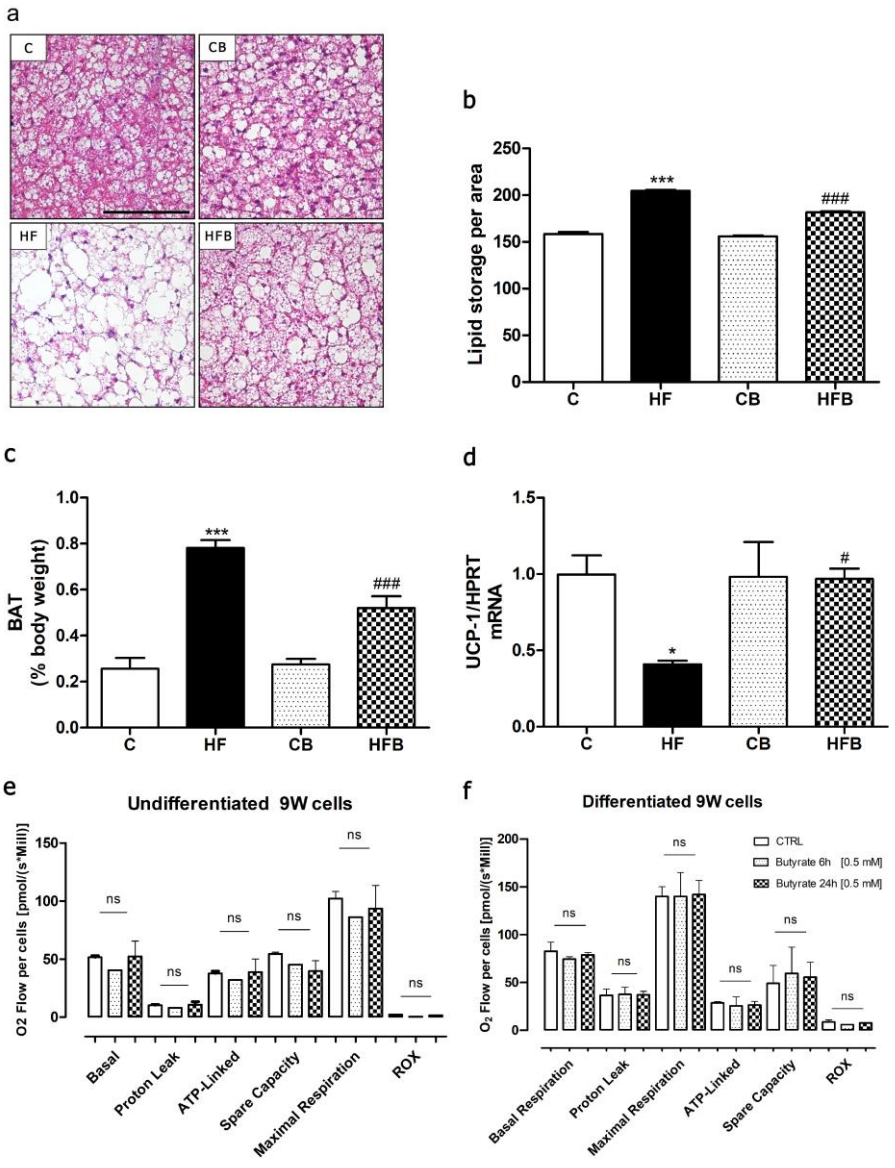

Figure 4: Effect of butyrate on the biology of the brown adipose tissue (BAT) in mice fed a high-fat diet and *in vitro*. Representative photomicrographs of BAT histological sections stained by HE of each experimental group are shown in **a**. Scale bar 50µm. In comparison with the control group, the HF diet induced an increase in the intracellular lipid storage (**a,b**) and weight (**c**) associated with a decrease in UCP-1 expression (**d**), indicative of "whitening" of BAT. All these changes in BAT were significantly inhibited by dietary supplementation with 5% sodium butyrate (HFB group) (**a-d**). The UCP-1 expression was determined in BAT homogenates by qPCR. (**e-f**) *In vitro* experiment, assessing cellular bioenergetics in undifferentiated (**e**) and differentiated (**f**) 9w cells, showed no significant changes after 0.5 mM butyrate exposure. Data are expressed as means ± SEM (n=5-8 mice per group). Groups: C: control (fed a regular diet alone); HF: high-fat diet alone; CB: Control+butyrate; HFB: high-fat diet+butyrate. *P<0.05, ***P<0.0001 in comparison with C group; #P<0.05; ###P<0.0001 in comparison with HF group (One-way ANOVA followed by the Bonferroni's post-test).

CAPITULO 5

Sodium butyrate reinforces the structure and function of the tight junction-mediated intestinal epithelial barrier in prediabetic mice

INTRODUCTION

Diabetes mellitus is one of the most prevalent endocrine-metabolic diseases in the world, being the type 2 diabetes (T2DM) the most frequent form (approximately 90% of the diagnosed cases of diabetes), that is a result of the insensitivity of target tissues to the action of insulin (known as the peripheral insulin resistance) (Chaudhury *et al.*, 2017). Increasing evidence has shown that inflammatory pathways are the principal pathogenetic mediators in the natural course of diabetes under the stimulus of the risk factors such as obesity, sedentarism, and intake of an unhealthy diet (reviewed by (Tsalamandris *et al.*, 2019). Obesity and its associated conditions, including metabolic syndrome, hypertension, and dyslipidemia, are positively associated with high systemic concentrations of inflammatory biomarkers (i.e. TNF-alpha, IL-1, IL-6, IL-10), which are predictive of insulin resistance and the incidence of T2DM (Tsalamandris *et al.*, 2019). In addition, recent studies have suggested an involvement of intestinal microbiota and dysfunction of the intestinal epithelial barrier in the pathogenesis of obesity-associated T2DM (Neu *et al.*, 2005; De Kort *et al*., 2011; Everard & Cani, 2013; Scheithauer *et al.*, 2016; Sabatino *et al.*, 2017; Spiljar *et al*., 2017). According to this hypothesis, changes in the intestinal microbiota can lead to an increase in the proportion of Gram-negative bacteria associated with intestinal barrier impairment, favoring the chronic absorption of lipopolysaccharides (LPS) and other toxins, and, consequently, the induction of metabolic endotoxemia that aggravates the peripheral insulin resistance (Geurts *et al.*, 2014; Gomes *et al*., 2017).

Butyrate is a short-chain fatty acid (SCFA), produced by the intestinal microbiota through the fermentation of nondigestible carbohydrates (fibers) (Khan & Jena, 2016; Miao *et al.*, 2016; Mollica *et al.*, 2017). Studies have demonstrated that this organic acid partially reversed obesity and metabolic changes induced by a high-fat diet in mice (Gao *et al.*, 2009; Matheus *et al.*, 2017). Butyrate has also shown a beneficial effect on gastrointestinal function (Rabbani *et al.*, 2001) and, under in vitro conditions, induces reinforcement of the epithelial barrier associated with an increase in the gene expression of proteins of the tight junction (TJ) (Wang *et al.*, 2012). As previosly showed, we have also observed that diet supplementation

with butyrate significantly inhibited the decrease in claudin 1 junctional content in intestinal epithelia of prediabetic mice (Matheus *et al.*, 2017) (Chapter 3 of this Ph.D. Thesis).

It has been suggested that part of the cellular effects of butyrate results of its action as an epigenetic regulator through inhibition of the histone deacetylase (Kruh, 1982; Khan & Jena, 2014; Miao *et al.*, 2016; Patnala *et al.*, 2017). It has been demonstrated, for instance, that the regulation of cell growth mediated by this SCFA occurs via activation or inactivation of genes related to cell proliferation (Kumar *et al.*, 2007).

The objective of this work was to further investigate the protective effect of sodium butyrate on the intestinal epithelial barrier mediated by tight junction (TJ) *in vitro* and *in vivo* model of T2DM, taking into account its characteristic as epigenetic and inflammation regulator. As an animal model, we have used mice fed a high-fat diet for 60d (Carvalho *et al.*, 2012; Oliveira *et al.*, 2015; Falcão *et al.*, 2016). As an *in vitro* model of the epithelial intestinal barrier, we employed the human colorectal adenocarcinoma cell line Caco-2, which is vastly employed *in vitro* intestinal toxicology studies since it displays many physiological and morphological features of mature enterocytes (Oliveira *et al*., 2019). The function and structure of the intestinal epithelial barrier, in both models, were assessed by measuring the paracellular flux with the marker Lucifer Yellow (LY), and by analyzing the distribution and cell content of other proteins associated to TJ (namely, claudins 2 and 3, occludin and ZO-1) by immunofluorescence and immunoblotting. The degree of acetylation of histones H3 and H4 in cryosections of the intestinal epithelium was also measured, as well as the plasma/serum and intestinal concentrations of LPS, TNF-α, and zonulin a known endogenous modulator of the TJ-associated the intestinal barrier (Cani *et al.*, 2008; Fasano, 2012; Jayashree *et al.*, 2014). Finally, given the possible therapeutic use of butyrate as an adjunct in the treatment of metabolic and intestinal diseases, we have also investigated the effect of butyrate on hematological and biochemical parameters in the animals of the different experimental groups.

MATERIALS AND METHODS

Animals

Male C57BL/6JUnib mice, aged 16 weeks, were obtained from the breeding colonies of the Multidisciplinary Center for Biological Investigation on Laboratory Animal Science (CEMIB) at the University of Campinas (UNICAMP, Brazil). The animals were maintained

under controlled conditions of temperature and light-dark cycle of 12h and had free access to food and water until the moment of experimentation. All the experiments in this project were approved by the Institutional Committee for Ethics in Animal Experimentation of the University of Campinas (CEUA/UNICAMP; under Protocol: 4185-1).

Diets

The animals were divided into four experimental groups as follows: control (C), control + butyrate (CB), high-fat diet (HF), and high-fat diet + butyrate (HFB). Sodium butyrate (cat number 303410, Sigma) was incorporated into the regular and HF diets at a concentration of 5% (w/w) as previously described (Matheus *et al.*, 2017) (see Chapter 2 of this Ph.D. Thesis). The C group received a standard rodent diet (in powder) (containing 4.5% lipids, 53 % carbohydrates, and 23 % proteins; w/w). The CB group received the standard diet mixed with 5% of sodium butyrate (w/w). Animals from the HF group received a prepared high-fat diet (in powder) (containing 21 % lipids, 50 % carbohydrates, and 20 % proteins; w/w) while the HFB group received the same high-fat diet but mixed with 5% of sodium butyrate (w/w). The lipid composition of the HF diet was mainly lard (20g/100g diet), but also contained soy oil (1mL/100g diet).

Weight gain, glycemia and intestinal permeability with Lucifer Yellow evaluation

The following parameters were evaluated in mice from all experimental groups: the body weight gain, the fed glycemia, and the intestinal permeability. The blood glucose concentration was measured, between 9 am to 11 am, using an Accu-Chek Advantage II glucometer (Roche Diagnostic, Switzerland). The intestinal permeability was assessed using Lucifer Yellow (LY CH lithium salt, Invitrogen, cat.# L453; MW 457.25 Da) as a paracellular tracer (Nascimento, 2019). After a 6-hour fast, the animals were anesthetized (with 80 mg/kg ketamine hydrochloride and 10 mg/kg xylazine hydrochloride, via intraperitoneal injection) and received by gavage LY solution (concentration of 100 μM in sterile saline, volume 7mL/kg body weight). After 1h of the solution administration, they were euthanized and the blood sample obtained was centrifuged at a speed of 12000 rpm (G = 8.049,6 - rotor radius = 5cm) for 10 minutes at 4 ° C for separation of the plasma. In a 96-well microplate, 50 μL of the plasma samples were added to 50 μL of PBS (1: 1 dilution). The reading was performed using a Fluorskan Ascent microplate reader (Thermo Scientific, USA), at a wavelength: 458nm excitation and 535nm emission. The values were expressed as LY plasma absorbance

value by subtracting the blank value (plasma absorbance value of an animal that did not receive the marker by gavage).

Immunolabelling of Claudins -2, -3, and ZO-1 in intestine sections

The localization of the tight junctional proteins (claudins -2, -3 and ZO-1) at the intestinal epithelia was determined by indirect immunofluorescence. For that, fragments of jejunum, ileum, and colon, obtained from 12h-fasted mice, were frozen in *n*-hexane with liquid nitrogen, and the cryosections obtained were permeabilized and fixed with acetone at -20°C for 3 min. For the immunofluorescence reaction, intestine cryosections were blocked with 5% bovine serum albumin (BSA) solution in PBS containing 0.1% Tween 20 for 1h. Then, intestine cryosections were incubated overnight at 4° C with the primary antibody (Table I; diluted in 3% BSA solution). After washing with PBS, the intestine sections were incubated with a FITC-conjugated specific secondary antibody (Sigma) (dilution 1:75 in BSA 1%) and DAPI (cat number D9542, Sigma) (dilution 1:1000) for 2h at room temperature (RT). All sections were mounted on coverslips with a commercial antifading agent (ProLong® Gold Antifade Mountant,Invitrogen P36930) and photographed using a digital camera coupled to an inverted fluorescence microscope (Observer: Z1; Zeiss – AxioCam, MRC, USA; or Leica DM5500 B, or Zeiss 510). Digital images of the intestine sections from all experimental groups were obtained and compared during the same session using identical microscope parameters (gain and time exposure). To determine the junctional content of each TJ protein, five images of intestinal epithelium were captured from each cryosection from animals from all experimental groups. Then, the integrated densities of 50 points per image, placed at the cell-cell contact region of enterocytes, were measured in all captured images using the free software ImageJ (given a total of 1250 points sampled per experimental group).

Table I. Antibody dilutions for Immunofluorescence

PRIMARY ANTIBODY	
Anti Rabbit – Claudin -2 (Abcam ab53032)	1:30
Anti Rabbit– Claudin -3 (Invitrogen 1700)	1:50
Anti Rabbit– ZO-1 (Invitrogen 7300)	1:50
SECONDARY ANTIBODY	
Goat anti-Rabbit FITC (Sigma F0382)	1:75

Immunolabelling for histone-3 and -4 acetylation degree in intestine cryosections

The degree of acetylation of histone 3 and 4 in intestinal epithelia was evaluated by indirect immunofluorescence in cryosections of intestine fragments. For that, intestine cryosections, previously fixed with acetone, were refixed with formalin for 30 minutes, washed with PBS, and then incubated with 0.1% Triton in PBS for 15 minutes. Subsequently, intestine cryosections were blocked with 5% BSA in PBS containing 0.1% Tween 20 for 1 h and, then, incubated overnight at 4 °C with the anti- acetylated H3 primary antibody (Invitrogen; cat number: PA516194; diluted 1:50 in 3% BSA solution) or anti- acetylated H4 primary antibody (Invitrogen; cat number PA532029; diluted 1:50 in 3% BSA solution). After washings with PBS, the intestine sections were incubated with the FITC-conjugated specific secondary antibody (Sigma) (dilution 1:100 in PBS plus 1% BSA solution) and DAPI (D 9542 Sigma) (dilution 1:1000) for 2h at room temperature (RT). All sections were mounted on coverslips with ProLong® Gold Antifade Mountant (Invitrogen P36930) and photographed using a digital camera coupled to an inverted fluorescence microscope (Observer.Z1; Zeiss – AxioCam, MRC, USA; or Leica DM5500 B; or Zeiss – LSM 510). Digital images of the intestine sections from all experimental groups were obtained and compared during the same session using identical microscope parameters (gain and time exposure). To evaluate the degree of fluorescence of the different histones, five (5) regions of the images were delimited, containing only nuclei of intestinal epithelial cells, and the degree of fluorescence and the delimited area were measured using the Image J program (http://rsbweb.nih.gov/ij/). The values were expressed as fluorescence intensity per area.

Immunoblotting of Claudins-2 and -3, ZO-1 in intestine epithelial homogenates

Fragments of jejunum, ileum, and colon were collected, the epithelium scraped off using a scalpel, and then added to antiprotease cocktail and sonicated. The epithelium homogenates were processed for immunoblotting using a standard protocol (Carvalho *et al.*, 2012; Oliveira *et al.*, 2014). Briefly, epithelium homogenate aliquots (containing 50μg of total proteins) were applied on 12% (Claudin-2,-3) or 6,5% (ZO-1) polyacrylamide gels and proteins were fractionated by electrophoresis and electrophoretically transferred onto nitrocellulose membranes (Bio-Rad). After, membranes were blocked for 4 h at RT with a basal solution (0.01M Trisma Base, 0.15M NaCl, 0.05% Tween 20; pH 7.4) containing 5% skimmed milk powder and then incubated overnight at 4°C with the primary antibody (Table II) diluted in the same basal solution but containing 3% skimmed milk powder.

Subsequently, the membranes were incubated with the specific secondary antibody conjugated with HRP (cat number A4914, Sigma) (dilution 1:600 in the basal solution containing 1% skimmed milk powder) for 2h at RT. Immunoreactive bands were detected using an enhanced chemiluminescence kit (Super Signal, Thermo Fisher Scientific, USA) and an imaging system (Genome Gene, Syngene Bio Imaging, UK). The relative size of the immunoreactive bands was quantified by densitometry using the ImageJ software. The same membranes were reincubated with anti-beta-actin antibody, used as an internal control. Optical densitometric values were expressed as a ratio of the respective proteins and beta-actin signals.

Table II. Antibody dilutions for Immunoblotting

PRIMARY ANTIBODY	
Anti Rabbit – Claudin -2 (Abcam ab53032)	1:300
Anti Rabbit – Claudin -3 (Invitrogen 1700)	1:400
Anti Rabbit– ZO-1 (Invitrogen 7300)	1:300
Anti Rabbit – Occludin (Abcam ab31721)	1:300
Anti Rabbit – β Actin (Uniscience 4970S)	1:400
SECONDARY ANTIBODY	
Goat anti-Rabbit HRP (Sigma A4914)	1:600

LPS, Zonulin and TNF-α plasma/serum/intestine concentrations and blood evaluation

Blood samples were collected in heparinized microtubes and centrifuged for 15 minutes at 3000 rpm (G = 503,1 - rotor radius = 5cm) using a refrigerated centrifuge (2-4° C) (Hettich, German) for plasma separation. To obtain the serum, blood samples (without heparin) remained at room temperature for 2 hours for clot formation, then were centrifuged for 15 minutes at 3000 rpm (G = 503,1 - rotor radius = 5cm) using a refrigerated centrifuge (Hettich). For homogenates, following the instructions of the respective kits, intestinal fragments (with no apparent presence of intestinal/fecal residues) were sonicated in 200 µL of LAL (LPS kit) or 500uL of sterile PBS (cat. number D8537, Sigma) (Zonulin and TNF-α kits).

The LPS concentration was determined using the Limulus Amebocyte Lysate (LAL) QCL-1000 ™ Endpoint Chromogenic kit (Lonza, Basel-SW). All endotoxin-free materials

and reagents were purchased from the same supplier of the kit (Lonza, Basel-SW). The zonulin concentration was measured using the Elisa Mouse Zonulin (MBS748504-MyBioSource). The TNF-α concentration was assessed using the ELISA MAX™ Deluxe Set Mouse TNF-α (Cat. No. 430904, BioLegend®). The absorbance measurements were performed in a microplate reader (Power Wave XS2, Biotek Inc., Winooski-US), at the wavelength of 405nm (LPS measurement) or 450nm (zonulin and TNF-α measurements).

The values were expressed as plasma or serum concentration in EU/mL for LPS, and ng/mL for zonulin. For the intestinal concentration, the values were expressed as the ratio of the marker concentration obtained and the respective total protein concentration (ug/mL), previously measured in an aliquot of the respective homogenates using Bradford's reagent (Protein Assay Dye Reagent Concentrate, cat. # 500-0006, Bio-Rad, Hercules-US).

Blood samples were also obtained for hematology/hematocrit analysis and biochemical parameters (such as amylase, alanine transferase (ALT), aspartate transferase (AST) and creatinine) performed by a specialized veterinary laboratory (VetPat, R. Cel. Manuel de Morais, 146 - Jardim Brasil, Campinas - SP, 13073-022).

Cell culture

Caco-2 cells (human colorectal adenocarcinoma) were cultured in Eagle medium modified by Dulbecco (high glucose) (DMEM), supplemented with 10% fetal bovine serum, 2% non-essential amino acids, 1% L-glutamine and 60 mg/L of gentamicin and kept in a humidified incubator at 37° C with 5% CO_2 (Incusafe Sanyo MCO-17A, Sanyo Electric Ltd., Japan). The medium was changed at least three times a week and the passages were performed by partial digestion with a trypsin/EDTA solution. Before cell seeding, cell culture inserts containing a membrane with a diameter of 12 or 30 mm (Millicell, Merck Millipore, German) were coated with collagen solution extracted from the Wistar rat tails (Hauschka and Konigsberg, 1966). Then cells were seeded at a density of $1.5x10^4$ cells/cm². After total confluence (approximately 10-11 days), the monolayers were exposed on both sides (apical + basal) to the luminal content of the small intestine obtained from mice of the different experimental groups.

In vitro exposure to the intestinal luminal content of mice

Mice from the different experimental groups (i.e. C, CB, HF, HFB) were euthanized, the small intestine removed under sterile conditions (within the laminar flow) and the luminal contents washed with 15 mL of sterile Krebs-bicarbonate buffer (concentration in mM: NaCl

115, KCl 5, $MgCl_2$ 1, $CaCl_2$ 1.24, $NaHCO_3$ 1, HEPES 15; pH = 7.4 equilibrated with 5% CO_2) containing 100 mg/dL of glucose. The small intestinal segment was chosen to obtain the luminal content for *in vitro* exposure since, in previous work (Oliveira *et al*., 2019), we have shown that the luminal content of the small intestine had a greater disruptive effect on the intestinal epithelial barrier, even at short period (6h), than that from the large intestine. The solution obtained by washing the intestinal luminal content was centrifuged in Falcon tubes at 2100 x g for 90 seconds, the supernatant was collected and diluted 1:5 ratio in sterile Krebs-bicarbonate. This dilution of the intestinal contents of the small intestine was necessary to eliminate/decrease the cytotoxic action on cells, as noted and described previously (Oliveira et al. 2019). Then, cell monolayers were exposed to the intestinal suspensions for 6 hours on both apical and basal surfaces

Transepithelial electrical resistance (TEER) and paracellular flux across Caco-2 cells

The TEER measurement was performed using two Ag/AgCl 'chopstick' electrodes coupled to a combined voltmeter and a constant current source (EVOM, World Precision Instruments, United Kingdom). TEER was measured every hour during the 6-hour interval after cell exposure to the intestinal luminal content. The final TEER was calculated as follows: the resistance of the blank membrane insert (without cells) was subtracted from the gross TEER value across Caco-2 monolayers and then multiplied by the membrane area (1.13 cm^2) to obtain the final TEER value (·Ω.cm²). The TEER data were depicted in the graph as a percentage of the initial mean value (at 0h, before exposure to luminal content).

To assess the paracellular permeability across Caco-2 monolayers, cells (cultured on 30 mm permeable culture inserts) were transferred to a new plate containing the suspension of intestinal luminal content (from the different experimental groups), or Krebs' solution, where the paracellular marker Lucifer Yellow (MW 457.25 Da) was added only to the basal solution at the final concentration of 100µM. In the apical environment, an identical solution was added, but without LY. After the incubation period (6h), samples of the apical and basolateral solutions were collected. The samples were read in triplicate (0.2mL) on a 96 well plate using the Synergy H1 microplate reader (Biotek Instruments, USA) at 428 nm (excitation wavelength) and 535 nm (emission wavelength). The transepithelial flux of LY (Ft), taken as an index of paracellular permeability, was calculated as follows: Ft = Apical fluorescence x 100/Apical fluorescence + Basal fluorescence.

Immunofluorescence and immunoblotting for junctional proteins in Caco-2 monolayers

Caco-2 monolayers were fixed and maintained in methanol at -20°C until the indirect immunofluorescence reaction. After washing with phosphate-buffered saline (PBS - 0.05M, pH = 7.4), the monolayers were incubated with 3% fetal bovine serum (FBS) in PBS for 30 min at room temperature (RT) and then incubated with the primary anti-Claudin-1 (Abcam ab15098, 1:30) or anti- ZO-1 (Invitrogen 7300, 1:50) antibodies diluted in PBS plus 3% SFB, overnight at 4 °C. Subsequently, the monolayers were incubated for 1 h with the FITC-conjugated specific secondary antibody FITC (Sigma- F0382, 1:75) and DAPI (Sigma, number of cat D9542) (dilution 1: 1000 in PBS plus 3% FBS) at room temperature. The monolayers were washed five times with PBS, mounted on coverslips with ProLong® Gold Antifade Medium (Invitrogen P36930) and photographed using a fluorescence microscope (Observer.Z1; Zeiss – AxioCam, MRC) at the same microscopic session, using the same gain/contrast parameters to compare the fluorescence degree between the treated and control groups.

For immunoblotting, Caco-2 monolayers were scraped using a cell scraper from 30 mm tissue inserts and added to 1 mL of PBS. After centrifugation at 1500 rpm (G = 125,77 – rotor = 5 cm), the supernatant was discarded and the cell pellet was resuspended in 20 µL of anti-protease cocktail and then sonicated [99]. Aliquots containing an equal amount of total proteins (20 µg) were processed for immunoblotting as described above for intestine homogenates. The membranes obtained were incubated sequentially overnight at 4° C with the primary antibody (Table III) and then with the specific secondary antibody conjugated with horseradish peroxidase (HRP-A4914-Sigma-1:600) for 2 h at room temperature. The immunoreactive bands were detected using the enhanced Super Signal chemiluminescence kit, the immunoreactive bands were quantified by densitometry, and expressed as a ratio of the respective proteins and beta-actin signals, as previously described (Oliveira *et al.*, 2019).

Table III. Primary antibody dilutions for Immunoblotting *In vitro*

Primary antibodies		
Anti Rabbit – Claudin-1	Abcam ab15098	1:300
Anti Rabbit – Claudin-3	Invitrogen 1700	1:500
Anti Rabbit – Occludin	Abcam ab31721	1:500
Anti Rabbit – ZO-1	Invitrogen 7300	1:300
Anti Rabbit – Beta actin	Uniscience 4970S	1:700

Statistical analysis

The One-way analysis of variance (ANOVA) followed by Bonferroni's post-test were used to compare the four experimental groups. The Student's t-test was used to determine the degree of statistical significance between two experimental groups. All statistical analyses were performed using the GraphPad *Prism* Software version 5.00 (GraphPad Software, USA). Results are expressed as means + SEM (Standard Error of the Mean), and the significance level was set at $P < 0.05$.

RESULTS AND DISCUSSION

Supplementation with sodium butyrate restores metabolic parameters and intestinal permeability compromised by the high-fat diet in prediabetic mice

Body weight and postprandial glycemia were evaluated to characterize the metabolic state of the animals after the intake of a high-fat diet. As expected, the ingestion of a high-fat diet for 60 days induced a significant increase in weight gain ($P<0.0001$) and in postprandial glycemia ($P<0.0001$), changes that are in line with previous studies of our group research (Oliveira *et al.*, 2015, 2019; Matheus *et al.*, 2017). Supplementation with sodium butyrate significantly reduced these effects induced by the high-fat diet, corroborating our previous data (Matheus *et al.*, 2017) (Chapter 3 of this Thesis). As also noted previously, there was no significant change in these parameters in the CB group that received the standard diet supplemented with 5% butyrate when compared to the C group (Matheus *et al*., 2017).

In a second step of the present work, we investigated the beneficial effect of butyrate on intestinal permeability in our type 2 prediabetes animal model. Previous data already indicated that butyrate has a protective effect on the intestinal barrier, as this SCFA induced a significant decrease in permeability intestinal to FITC-Dextran, as well as inhibiting the redistribution of claudin-1 in the intestinal epithelium in pre-diabetic animal (Matheus *et al.*, 2017) (Chapter 3 of this Thesis). Figure 1c shows the intestinal permeability to the LY marker in the different experimental groups studied (C, HF, CB HFB). The reason for using LY here was based on our previous work indicating that this molecule constituted a more adequate marker for the assessment of intestinal permeability *in vivo* than FITC-Dextran (Nascimento, 2019; Oliveira *et al.*, 2019). These studies demonstrated that the prediabetes state in our animal model involves selective regulation of the permeability of the paracellular barrier, favoring the transepithelial transport of small molecules (such as LY), and not of large

molecules (with an MW> 4000) such as FITC-Dextran, being the former often associated with modulation of the TJ permeability (Mongelli-Sabino *et al*., 2017; Oliveira *et al*., 2019) rather than involving general damage to the integrity of the epithelium (Cani *et al.*, 2008; Volynets *et al.*, 2015). In accordance with these results, we observed here a significant increase in the plasma concentration of the LY marker in animals wich were fed with a high-fat diet (HF group) ($P<0.0001$) compared to the control group (C), which indicates an increase in intestinal permeability for this marker in the prediabetic animals. Supplementation with sodium butyrate significantly reduced the presence of this marker in the plasma ($P<0.0001$) in animals from the HFB group compared to the HF group. Also, there was no difference in intestinal permeability to LY between animals that received a standard diet with butyrate (CB) compared to group that received a standard diet without butyrate (C), which reinforces the idea that butyrate seems to have its biological effect mainly in challenging situations, as after the administration of a high-fat diet.

The dysfunction of intestinal permeability has been linked to metabolic and intestinal diseases, such as celiac disease and Crohn's disease (Chang *et al.*, 2014; Bultman, 2017). Herein, we observed that after 60 days of exposure to the high-fat diet, the animals displayed systemic dysfunctions, typical of prediabetes, that were accompanied by increased intestinal permeability. Supplementation with sodium butyrate, in addition to significantly reducing the effects of the high-fat diet on weight gain and postprandial glycemia, also restored intestinal permeability to small molecules such as LY**.**

Sodium butyrate contributes to the maintenance of the intestinal epithelial barrier mediated by TJ proteins

Following the idea that sodium butyrate has a positive effect on the intestinal epithelial barrier (Matheus *et al.*, 2017), confirmed here by the paracellular permeability test, we have investigated the structural integrity of the intestinal epithelial barrier by immunodetection of proteins associated to TJ (claudin- 2, -3 and ZO-1) in cryosections of fragments of the small intestine (jejunum and ileum) and large intestine (colon) and posterior analysis of the degree of fluorescence in the digital photomicrographs obtained. As shown in Figures 2 to 4, exposure to HF diet induced significant changes in the junctional content of these proteins in the intestinal epithelium, which included a significant decrease in the intercellular labeling of claudin-2 in the jejunum and ileum ($P<0.0001$) and increased colon ($P<0.001$); decreased claudin-3 in the jejunum ($P<0.0001$), ileum ($P<0.0001$) and colon ($P<0.0001$); decreased ZO-

1 in the jejunum (P<0.0001), ileum (P<0.0001) and an increase in ZO-1 in the colon (P<0.0001). These changes in the junctional distribution of TJ proteins observed in prediabetic animals were similar to those previously reported by our group (Nascimento, 2019; Oliveira *et al.*, 2019). Surprisingly, sodium butyrate supplementation (HFB group) completely reversed or significantly inhibited these changes in the TJ protein content in intestinal epithelial cells, except for the ZO-1 protein in the colon, when compared to the HF group (Figures 2-4). In comparison with the CB group that received a standard diet + butyrate, the HFB group showed an increase in the ZO-1 junctional content in the three segments studied (P<0.0001 jejunum and colon, P<0.05 ileum), an increase in claudin-3 in the ileum and colon (P<0.0001), and decreased claudin-2 in the jejunum and ileum (P<0.0001), suggesting a greater reinforcement of the TJ-mediated paracellular barrier when butyrate was administered in conjunction with the high-fat diet. However, the CB group did not show a significant change in the junctional content of TJ proteins (Cld-2, -3 and ZO-1) in any of the intestinal segments studied (jejunum, ileum, and colon) when compared to C group. The protein content of these junctional proteins in homogenates of intestinal epithelium was evaluated by immunoblotting. As shown in Figure 5, no significant changes were observed in the protein expression of Cld-2, -3, occludin, and ZO-1 in the intestinal epithelium of the studied segments (jejunum, ileum, and colon) from the different experimental groups.

It is well known that the TJ protein complex is a dynamic cell structure, that can be regulated in response to various stimuli such as nutrients, humoral/neuronal signaling, or inflammatory mediators (De Kort *et al*., 2011; Mongelli-Sabino *et al*., 2017; Collares-Buzato, 2019). The regulation of the TJ structure/function can occur through alteration in the expression of TJ genes, in the protein content and/or cellular redistribution of its structural proteins, involving epigenetic regulation, the turnover process or post-translational modifications such as phosphorylation/dephosphorylation, palmitoylation and/or ubiquitination (Khan & Asif, 2015; Hichino *et al.*, 2017; Collares-Buzato, 2019). Another possibility of modulating the selective permeability of the tight junction is through the interaction between its main constitutive proteins, the claudins that can be barrier-forming (e.g.: Cld -1, -3, -4, -5, -8) or pore-forming (e.g.: Cld -2, -7, -12) proteins (Markov *et al.*, 2010; Gunzel & Yu, 2013; Krug *et al*., 2014). In the present work and previous one (Matheus *et al.*, 2017), we demonstrated, by indirect immunofluorescence, that exposure to a HF diet induced a significant decrease in the junctional content of claudins-1 and -3 (barrier-forming) in the epithelium from different intestinal segments (jejunum, ileum, and colon), associated

with a decrease in claudin-2 (pore-forming) and ZO-1 (anchoring protein) in the jejunum and ileum, and an increase in both proteins (Cld-2 and ZO-1) in the colon. These changes indicate significant disorganization of TJ structure in the intestinal epithelium of the prediabetic mice, which certainly can have a functional impact on the intestinal barrier properties (Garcia-Hernandez, Quiros & Nusrat, 2017; Buckley & Turner, 2018). In particular, the reduction in the junctional content of Cld-1 and 3 suggests a rupture of the intestinal epithelial barrier allowing the passage of molecules, which is in accordance with the data obtained from intestinal permeability to LY in prediabetic animals fed by HF diet.

Studies have reported that alteration of the intestinal microbiota is related to metabolic diseases and that patients with intestinal infection have a lower content of barrier-forming proteins and an increase in claudin-2 (Cani *et al.*, 2012; Spiljar *et al.*, 2017). In the present study, supplementation with sodium butyrate reversed or significantly inhibited the effects of the HF diet on the organization of proteins at TJ site in intestinal epithelia of prediabetic mice. Nevertheless, this effect of butyrate on the TJ structure was not associated with changes in the TJ protein expression, as assessed by Western Blot, which suggests that this SCFA has its action through post-translational regulation of junctional proteins, which would favor their transport from cytoplasmic pools to the TJ region at cell-cell contact (Utech *et al.*, 2010; Butt *et al.*, 2012; Stamatovic *et al.*, 2017). Future investigations may elucidate the mechanisms involved in the action of butyrate on the structure/function of the intestinal epithelial TJ.

Exposure to the intestinal luminal content from mice that received butyrate supplementation maintains the TJ structure in Caco-2 cells

In a pioneering work, Oliveira and coworkers have observed that *in vitro* exposure to the intestinal content of mice fed a high-fat diet induced disruption of the TJ-mediated epithelial barrier in Caco-2 monolayers, an intestine-derived cell line. This data suggest a possible involvement of a component of the intestinal lumen in the increased intestinal permeability seen *in vivo* after HF diet intake (Oliveira *et al.*, 2019). Following this idea, we investigated herein whether the intestinal luminal content of animals fed a diet supplemented with butyrate would have a protective effect on the epithelial barrier *in vitro*. As shown in Figure 6, the exposure of Caco-2 cells to the luminal content of prediabetic animals, fed a high-fat diet (HF), did not alter cell viability (Fig. 6a) but resulted in a tendency to a decrease of the transepithelial electrical resistance (TEER) ($P=0.06$) (Fig. 6b) associated with a significant increase in paracellular permeability to LY ($P<0.05$) (Fig. 6c) when compared to

cells exposed to the luminal content of animals that received a standard diet (C) or to Krebs. These changes, indicative of impairment of the paracellular barrier (Mongelli-Sabino *et al*., 2017; Canuto & Collares-Buzato, 2019; Oliveira *et al*., 2019), were accompanied by a significant decrease in the junctional labeling for TJ proteins (Claudin-1 and ZO-1) (Fig. 6d), suggesting a disruption of TJ in Caco-2 cells when exposed to the luminal content of HF-fed prediabetic animals compared to those exposed to the luminal content of control animals (C). In contrast, cells exposed to the luminal content of animals receiving butyrate (either with a high-fat diet (DB) or a standard diet (CB)) maintained the TEER values close to those of cells exposed to the luminal content of animals that received a standard diet (C), as well as showing the restoration of paracellular permeability at levels similar to cells exposed only to Krebs (Fig. 6 b, c). Following these functional data, immunofluorescence analyses showed that cells exposed to the luminal content of animals with butyrate supplementation reestablished the typical structure of TJ, with immunostaining for Cld-1 and ZO-1 similar to the cells that were exposed to the content luminal from control animals or Krebs (Fig. 6 d). In this context, the present work reinforces the idea, previously suggested, of a direct association between components of the intestinal luminal content and the modulation of the intestinal epithelial barrier during type 2 prediabetes (Oliveira *et al*., 2019).

Supplementation with sodium butyrate does not seem to have an epigenetic effect on enterocytes.

Taking into account the fact that sodium butyrate is a known inhibitor of the enzyme histone deacetylase (Della Ragione *et al.*, 2001), the degree of fluorescence of the histones H3 and H4, both acetylated in the respective lysine residues, was evaluated in cryosections of the intestinal segments (duodenum, jejunum, and ileum) by indirect immunofluorescence. As shown in Figure 7, no significant changes were observed in the degree of fluorescence of acetylated H3 and H4 in the intestinal epithelium from the different experimental groups, except in the case of H3 histone which showed a significant increase in its immunodetection in the colon of HFB mice compared to the C group (Fig. 7d).

It is known that the histone deacetylase enzyme removes acetyl groups from specific lysine residues that are added by a different set of enzymes known as histone acetyltransferases. This process is an important transcriptional regulatory mechanism since hyperacetylated histones enable or facilitate the transcription of certain genes and hypoacetylated histones prevent or hinder transcription (Haberland *et al*., 2009; Zhang *et al.*,

2017). The histone deacetylase enzyme has several isoforms that act on specific lysine residues (Della Ragione *et al.*, 2001; De Ruijter *et al.*, 2003). Some molecules, such as butyrate, are inhibitors of the histone deacetylase causing histone hyperacetylation and, as a consequence, can potentially facilitate or increase the cell gene expression. Khan & Jena (2014) observed an increase in histone deacetylase activity in diabetic rats, whereas, in rats treated with butyrate, the activity was significantly lower, both in the liver and in the pancreas, which was associated with increased cell proliferation and reduced apoptosis. Besides improving the metabolic dysfunctions induced by HF diet, butyrate supplementation also attenuated the apoptotic signs in the myocardium of diabetic mice, suggesting a reduction in the oxidative stress induced by HF diet via inhibition of histone deacetylase (Zhang *et al.*, 2017). In our type 2 prediabetes model, sodium butyrate does not seem to have an epigenetic action on enterocytes, showing that its epigenetic effect may be more related to genes associated with cell growth, proliferation, and apoptosis, as reported in the literature (Kumar *et al.*, 2007; Khan & Jena, 2014)rather than to the alteration of the gene expression of TJ proteins (Khan & Asif, 2015).

Sodium butyrate has no fundamental role in the plasma/serum and intestinal levels of LPS, zonulin or TNF-α at the prediabetic state

Based on evidence suggesting an anti-inflammatory effect of butyrate (Säemann *et al.*, 2000; Ohira *et al.*, 2013), we investigated whether this SCFA would have any effect on the systemic levels of some pro-inflammatory markers (i.e. LPS, zonulin, and TNF-α) in the context of T2DM.

The dysfunction of the intestinal epithelial barrier facilitates the paracellular passage of lipopolysaccharides (LPS), a component of the cell wall of gram-negative bacteria (Jayashree *et al.*, 2014; Odenwald & Turner, 2016; Gomes *et al*., 2017). This leads to an increase in the systemic concentration of LPS (endotoxemia), which can contribute to the development of insulin resistance in peripheral tissues (Jayashree *et al.*, 2014; Odenwald & Turner, 2016). It has been shown that mice exposed to HF diet have high levels of LPS associated with changes in the composition of the intestinal microbiota (Cani *et al.*, 2007). Zonulin, in turn, is an endogenous molecule that modulates intestinal permeability, being used as a marker of intestinal barrier dysfunction (Fasano, 2012; Jayashree *et al.*, 2014; Sturgeon & Fasano, 2016). The release of zonulin by different cells is stimulated after exposure to luminal

antigens such as bacteria or from the diet, such as gluten (Fasano, 2012; Suzuki, 2013). The dysfunction of the intestinal epithelial barrier facilitates the passage of luminal antigens, stimulating an immune response and the release of pro-inflammatory cytokines, such as TNF-α (Tang *et al.*, 2010; Ammon, 2019).

Although studies indicate an increase in the blood level of LPS in diabetic patients (Jayasheree *et al*., 2014), in the present study, the measurement of LPS concentrations in serum and lysates of intestinal fragments did not show significant differences among the experimental groups (C, HF, CB, and HFB) (Figures 8a-c). Similarly, no significant differences were observed in plasma concentrations and homogenates of intestinal fragments (from the small intestine) of zonulin in mice from the different experimental groups (Fig. 8 d, e). Furthermore, Fig. 8f shows that neither the administration of the HF diet for 60d nor the supplementation with butyrate significantly altered the concentration of the proinflammatory cytokine TNF-α in the large intestine. Normal plasma/intestinal LPS levels observed herein indicate that our type 2 prediabetes animal model did not develop endotoxemia (defined by high LPS blood concentrations), while normal plasma and intestinal levels of zonulin and TNF-α suggest an absence of a marked general systemic and intestinal inflammatory state mediated by these proteins in the animals. Similar data was also observed previously in another work by our group (Nascimento, 2019). Yet, the treatment with butyrate does not display any further effect on these parameters.

Butyrate supplementation does not present systemic toxicity and attenuates liver dysfunction marker and lymphocytosis induced by the high-fat diet.

To investigate possible systemic toxicity of sodium butyrate, an evaluation of the red and white blood cell count and the biochemical profile for markers of liver function (ALT and AST), pancreatic (amylase) and renal (creatinine) were done in mice from the different groups (C, HF, CB, and HFB). The hematology analysis showed no changes in the hematocrit, red blood cell and platelet count, and the concentration of total blood proteins in mice from the different groups (Table IV). However, the HF group showed a significant increase ($P<0.05$) in hemoglobin levels compared to the C group, with no changes in the other groups. There was also a significant increase in the total leukocyte count ($P<0.05$) and specifically in the lymphocytes ($P<0.05$) in the HF group compared to the C group, with no changes in the other groups (CB and HFB), indicating inhibition of lymphocytosis with treatment by sodium butyrate. In biochemical analyses, a significant increase in ALT was observed in the HF

group compared to the C group, and supplementation with sodium butyrate significantly reduced this change in the HFB group compared to the HF group. There were no significant alteration in the other investigated biochemical parameters (AST, creatinine, and amylase) among the groups (Table IV).

It is known that one of the characteristics of obesity is the inflammatory response triggered predominantly by adipose tissue (Tsalamandris *et al.*, 2019). Even though our results on inflammatory markers such as zonulin and TNF-α did not show significant alteration among the experimental groups, the leukocytes/lymphocytes count data point to an initial inflammatory process in mice that received the HF diet in comparison with those that received a standard diet (Table IV). Meanwhile, the animals that received supplementation with sodium butyrate showed a decrease in the lymphocyte count compared to the HF group (Table IV). The data showing increased ALT, a liver function marker, in HF diet fed-mice, compared to the control group, corroborates our results of hepatic steatosis assessment (Matheus *et al*., 2017) (Chapter 3 of this Thesis). Supplementation with sodium butyrate significantly decreased the serum concentration of ALT as well as decreased the condition of hepatic steatosis developed in our prediabetic animals (Matheus *et al*., 2017).

In conclusion, our data suggest a protective effect of sodium butyrate on the intestinal barrier mediated by TJ proteins. This effect is apparently not related to the recognized epigenetic and anti-inflammatory action of this SCFA. Future work will be needed to unravel the mechanisms of action of butyrate on the structure and function of TJ in the intestinal epithelium.

Table IV. Hematology analysis and biochemical parameters.

	Control	High-Fat Diet	Control+B	High-Fat+B
Creatinine (mg/dL)	0.37±0.10	0.24±0.12	0.34±0.08	0.39±0.08
ALT (U/L)	37±4.63	105±10.48***	33±3.80	46±7.86###
AST (U/L)	219±39	279±43	268±46	223±46
Amilase	1.00±0.12	1.05±0.12	0.99±0.15	0.95±0.08
Hematocrit (%)	36±0.82	38±0.63	38±0.90	37±0.36
PT/PL (g/dL)	5.45±0.19	5.78±0.16	5.26±0.22	5.68±0.17
Hemoglobin (g/dL)	11±0.52	13±0.24*	12±0.29	12±0.29
Erythrocytes ($x10^6$/μL)	8.44±0.40	9.02±0.15	9.08±0.26	8.90±0.19
Leucocytes (/μL)	3713±484	6160±446*	4057±889	4860±593
Neutrophils (/μL)	1080±175	1417±251	1181±311	1355±261
Lymphocytes (/μL)	2514±340	4566±410*	2771±603	3426±409
Platelets ($x10^6$/μL)	1.21±0.09	1.25±0.07	1.31±0.09	1.46±0.15

*P<0.05; ***P<0.0001 in relation to Control

###P<0.0001 in relation to HF

Values are expressed as mean ± SEM (n=6-10)

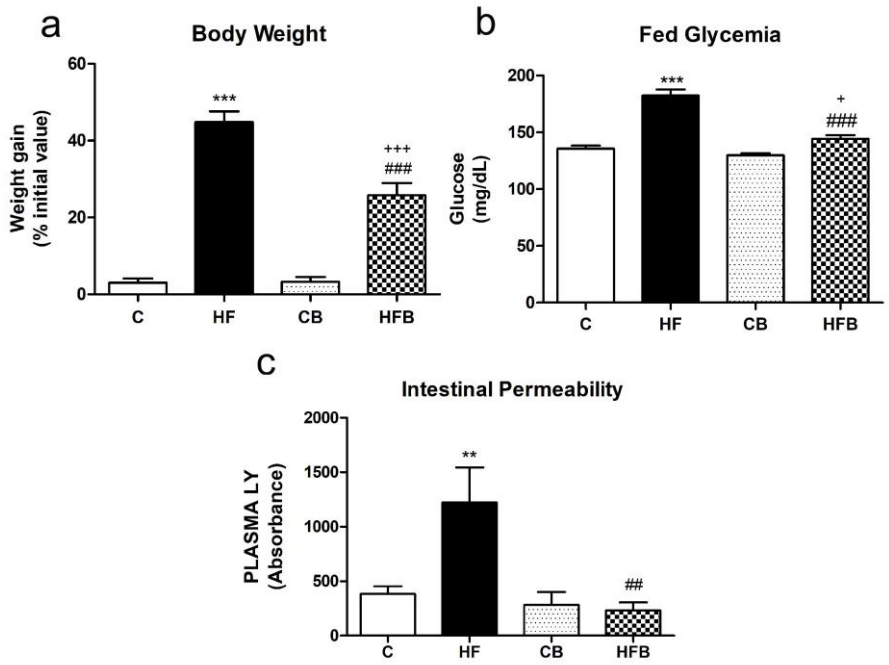

Figure 1. Effect of the dietary supplementation with sodium butyrate on body weight gain (a), fed glycemia (b) and intestinal permeability to the paracellular marker, Lucifer Yellow (LY) (c), in mice fed a standard or high-fat (HF) diet. HF diet induced a significant increase in weight gain **(a)**, fed glycemia **(b),** and in the intestinal permeability (that indicates possible dysfunction of the paracellular barrier) **(c)** as compared to the control group (C). The supplementation with sodium butyrate resulted in a significant decrease in the overweight (**a**), hyperglycemia (**b**), and increased intestinal permeability (**c**) induced by HF diet in HFB mice as compared to the HF group. As seen in the CB group, butyrate *per se* maintained these parameters at the level of the control group. The values represent the mean ± SEM. (n=12-17). **P<0.001, ***P<0.0001 compared to C group; ##P<0.001, ###P<0.0001 compared to HF group; +P<0.05, +++P<0.0001 compared to CB group.

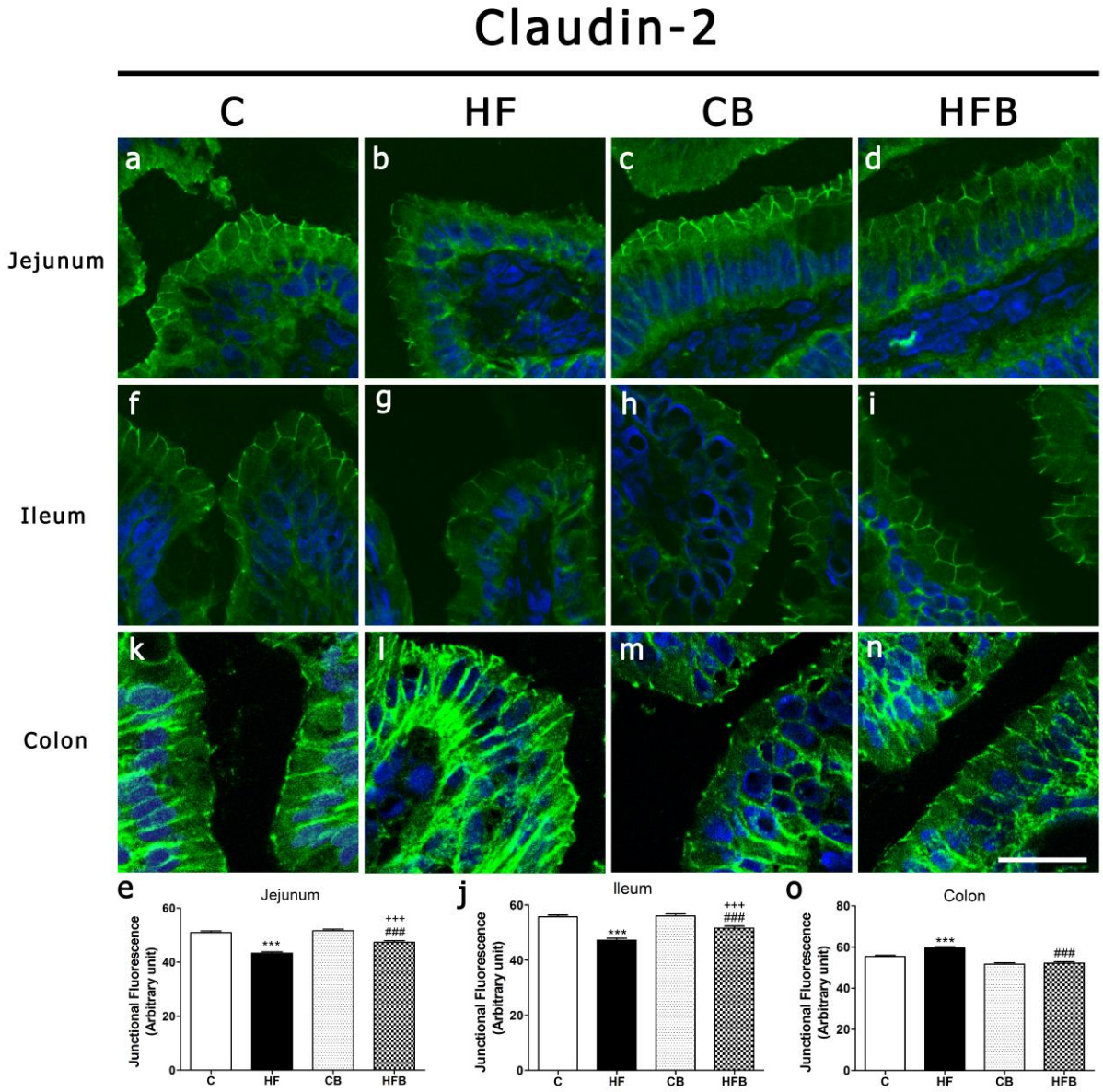

Figure 2: Effect of the dietary supplementation with sodium butyrate on the cellular distribution of Claudin-2 in the epithelium of small intestine (jejunum and ileum) and large intestine (colon) of mice fed a standard or high-fat (HF) diet. Images show the immunofluorescence detection of Cld-2 (in green, DAPI/nuclei in blue) in cryosections of intestine segments of mice from the different experimental groups (C/Control, HF/High-fat diet, CB/Control+Butyrate, and HFB/High-fat diet+Butyrate). The analysis of the degree of fluorescence at the cell-cell contact showed that HF diet induced a significant reduction of the Claudin-2 content at the intercellular region of the epithelial cells of jejunum **(e)** and ileum **(j)** but led to an increase in the junctional content of this protein in the colon epithelium **(o)**. Butyrate supplementation partially reversed the effects of the HF diet on the junctional content of this TJ protein in the three intestinal segments studied **(e,j,o)**. Bar, 25 µm. The values represent the mean ± SEM. ***P<0.0001 compared to C group; ###P<0.0001 compared to HF group; +++P<0.0001 compared to CB group.

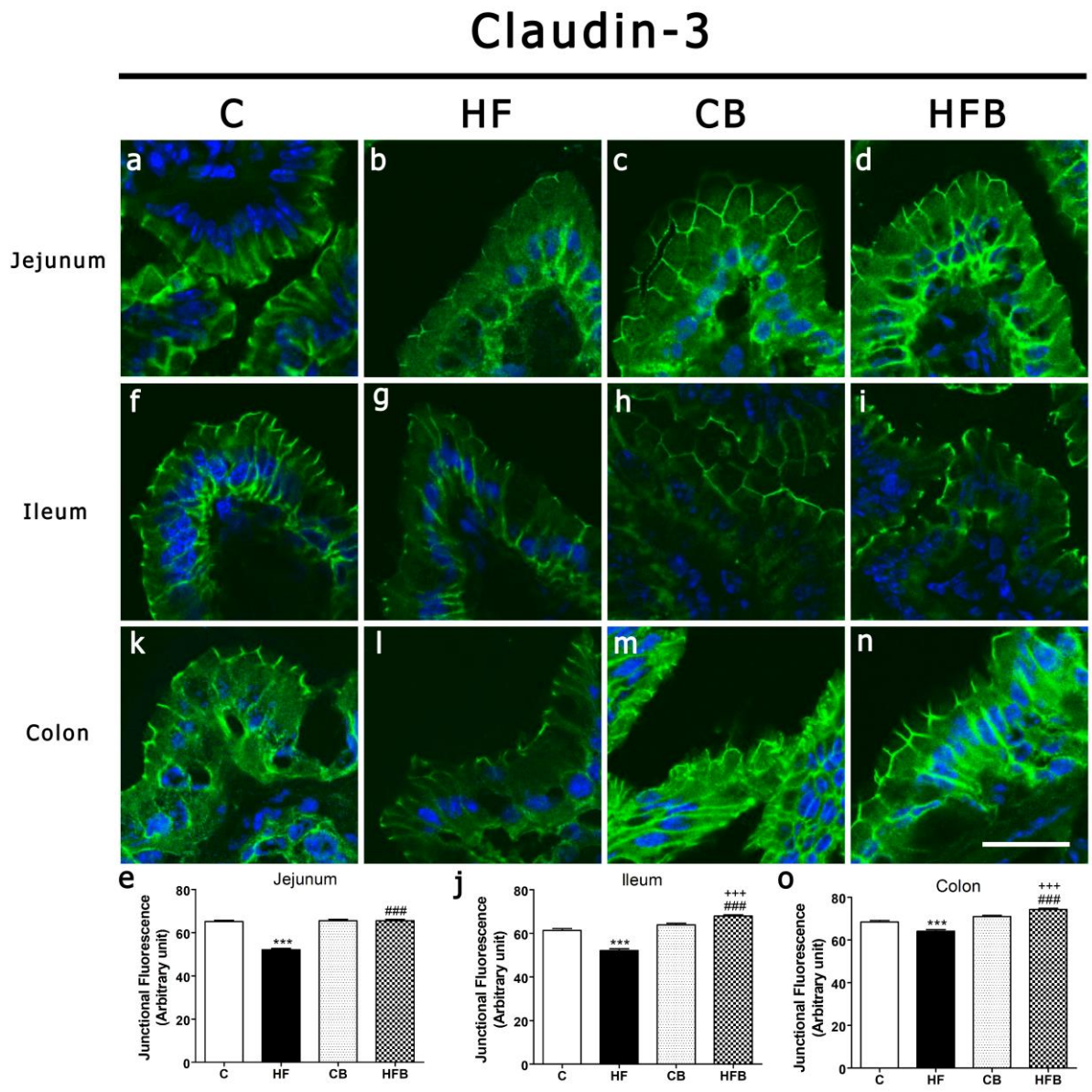

Figure 3: Effect of the dietary supplementation with sodium butyrate on the cellular distribution of Claudin-3 in the epithelium of small intestine (jejunum and ileum) and large intestine (colon) of mice fed a standard or high-fat (HF) diet. Images show the immunofluorescence detection of Cld-3 (in green, DAPI/nuclei in blue) in cryosections of intestine segments of mice from the different experimental groups (C/Control, HF/High-fat diet, CB/Control+Butyrate, and HFB/High-fat diet+Butyrate). The analysis of the degree of fluorescence at the cell-cell contact showed that Claudin-3 immunostaining at the intercellular region of the intestinal epithelium was significantly reduced in all the intestinal segments studied (jejunum-**e**, ileum-**j**, and colon-**o**) in mice after HF diet. The supplementation with sodium butyrate significantly reversed this effect in HFB group as compared to HF mice and even increased the Claudin-3 immunoreaction in the ileum (**j**) and colon (**o**) when compared to the CB group. Bar, 25 µm. The values represent the mean ± SEM. ***P<0.0001 compared to C group; ###P<0.0001 compared to HF group; +++P<0.0001 compared to CB group.

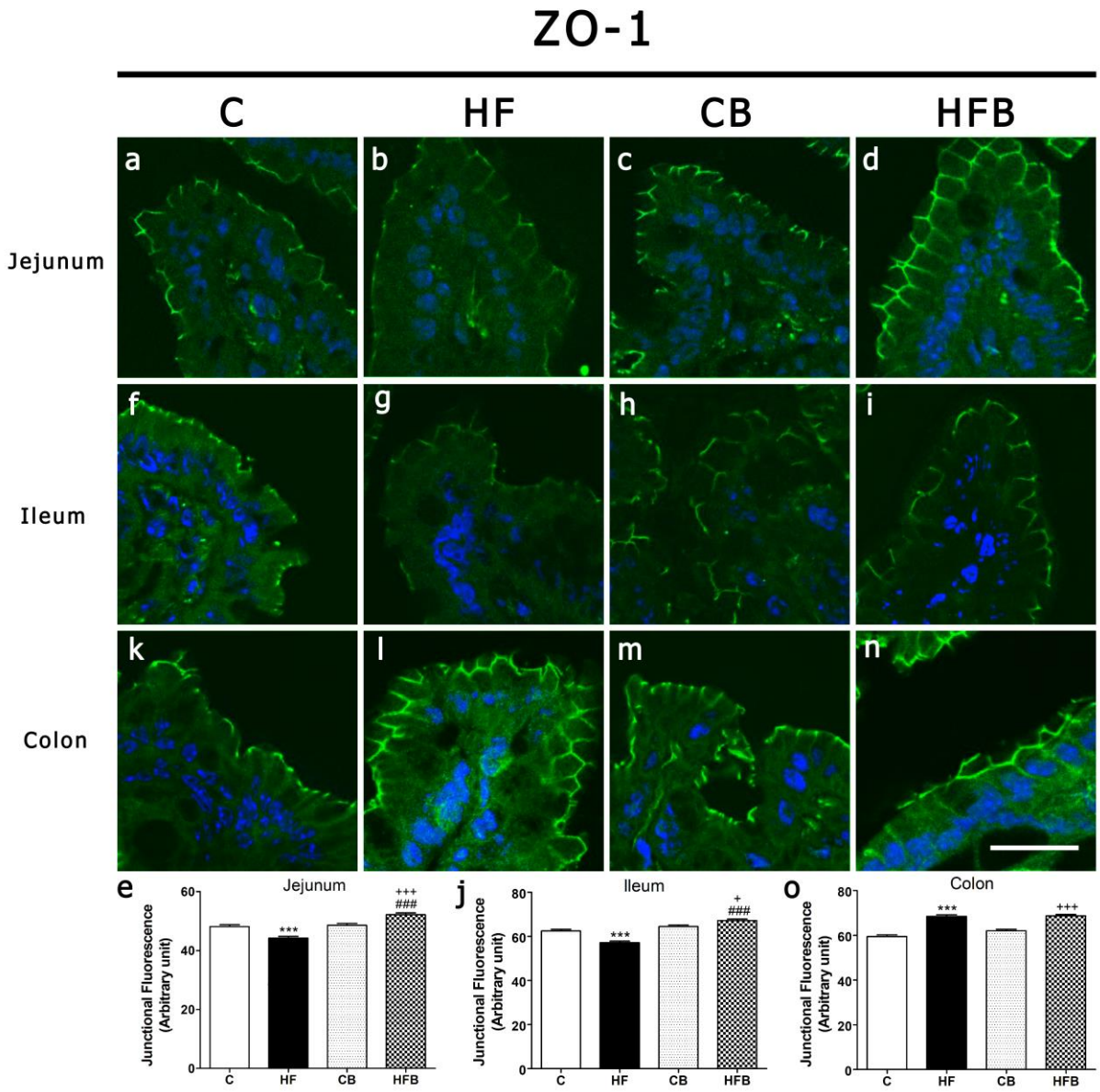

Figure 4: Effect of the dietary supplementation with sodium butyrate on the cellular distribution of ZO-1 in the epithelium of small intestine (jejunum and ileum) and large intestine (colon) of mice fed a standard or high-fat (HF) diet. Images show the immunofluorescence detection of ZO-1 (in green, DAPI/nuclei in blue) in cryosections of intestine segments of mice from the different experimental groups (C/Control, HF/High-fat diet, CB/Control+Butyrate, and HFB/High-fat diet+Butyrate). The analysis of the degree of fluorescence at the cell-cell contact showed that HF diet induced a significant reduction of the ZO-1 content at the intercellular region of the epithelial cells of jejunum **(e)** and ileum **(j)** but led to an increase in the junctional content of this protein in the colon epithelium **(o)**. Butyrate supplementation reversed the effects of the HF diet on the junctional content of this TJ protein in jejunum and ileum **(e,j)** but not in the colon **(o)**. Compared to the CB group, the HFB group showed a significant increase in ZO-1 in the three studied segments (jejunum-e, ileum-j, colon-o). Bar, 25 µm. The values represent the mean ± SEM.***P<0.0001 compared to C group, ###P<0.0001 compared to HF group, +P<0.05 +++P<0.0001 compared to CB group.

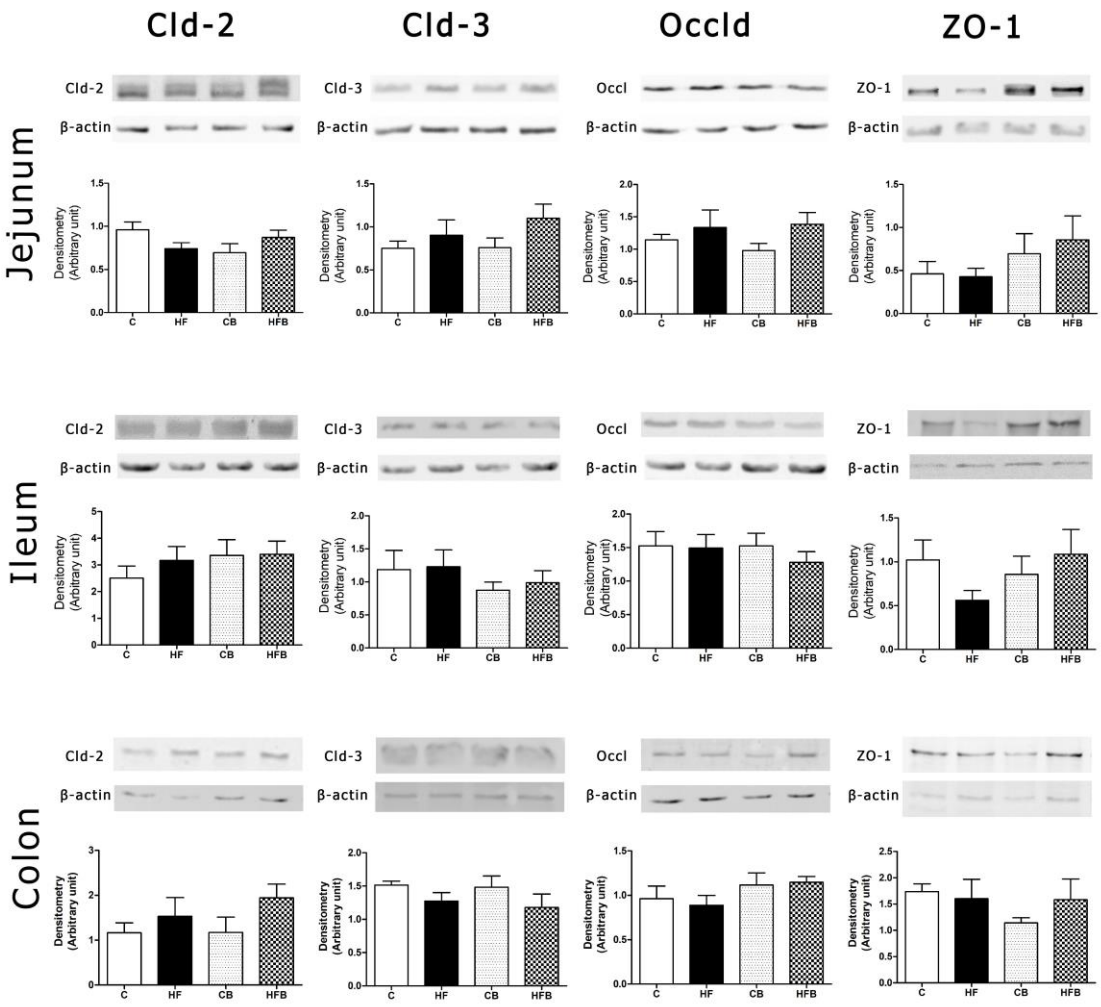

Figure 5: Effect of the dietary supplementation with sodium butyrate on the intestine epithelium content of TJ proteins in mice fed a standard or high-fat diet. The TJ protein expression was assessed by immunoblotting in homogenates of the epithelium obtained from the small intestine (jejunum and ileum) and large intestine (colon) from all the experimental groups (C, HF, CB, HFB). No significant difference was observed in total intestine epithelial content of TJ proteins (i.e. claudins-2, -3, occludin, and ZO-1) among the groups (C, HF, CB, and HFB). The values represent the mean ± SEM of the ratio between TJ protein signal/β-actin band densitometry.

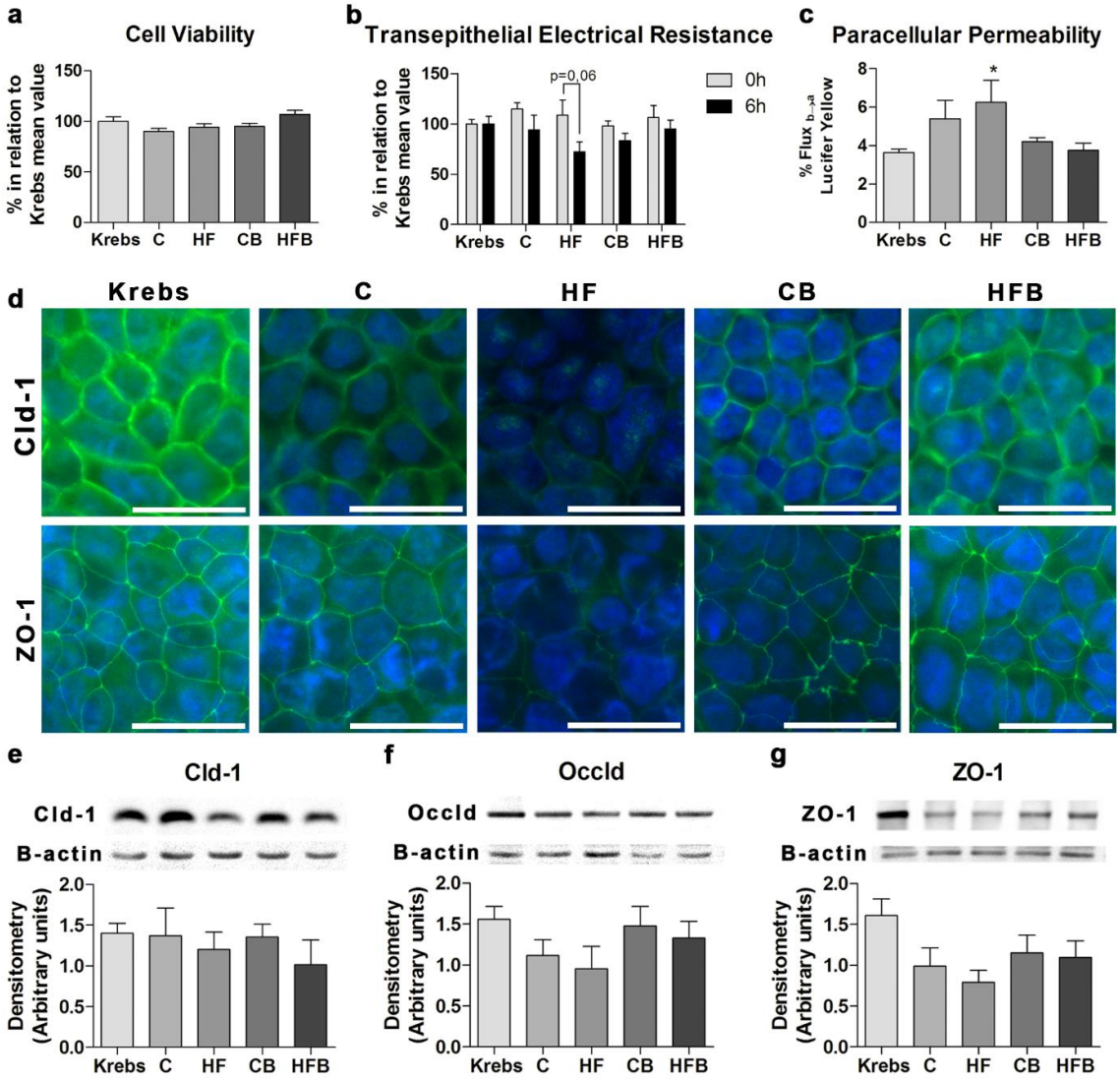

Figure 6: Caco-2 monolayers exposure to the luminal content of small intestine isolated from mice from the different experimental groups. (**a**) Cell viability, (**b**) transepithelial electrical resistance (TEER), (**c**) paracellular permeability to Lucifer Yellow (LY), and (**d**) intercellular distribution of tight junctional proteins (Claudin-1 and ZO-1) were evaluated in Caco-2 monolayers after 6h exposure to the luminal content of small intestine from mice of different groups (C, HF, CB, and HFB). Cell viability was assessed by the Neutral Red assay. The TEER was measured using a pair of electrodes coupled to EVOM and the values were expressed as a percentage of the mean TEER value of Caco-2 monolayers exposed to Krebs (taken as 100%). For the transepithelial flux, LY apical absorbance was expressed as a percentage of the apical+basal absorbance (taken as 100%) The images in (**d**) are representative of Caco-2 monolayers immunolabeled for claudin-1 and ZO-1 (in green - FITC; DAPI/nuclei in blue) (**e-f-g**) Immunoblotting for junctional proteins (Claudin-1, Occludin, and ZO-1) in homogenates of Caco-2 monolayers exposed to the luminal content of the small intestine for 6h. Graphs display the mean values (± SEM; 4 membranes/group) of the optical density analysis of the TJ protein bands. Beta-actin was employed as the loading control. Results are expressed as means ± SEM. *P < 0.05 in relation to Krebs.

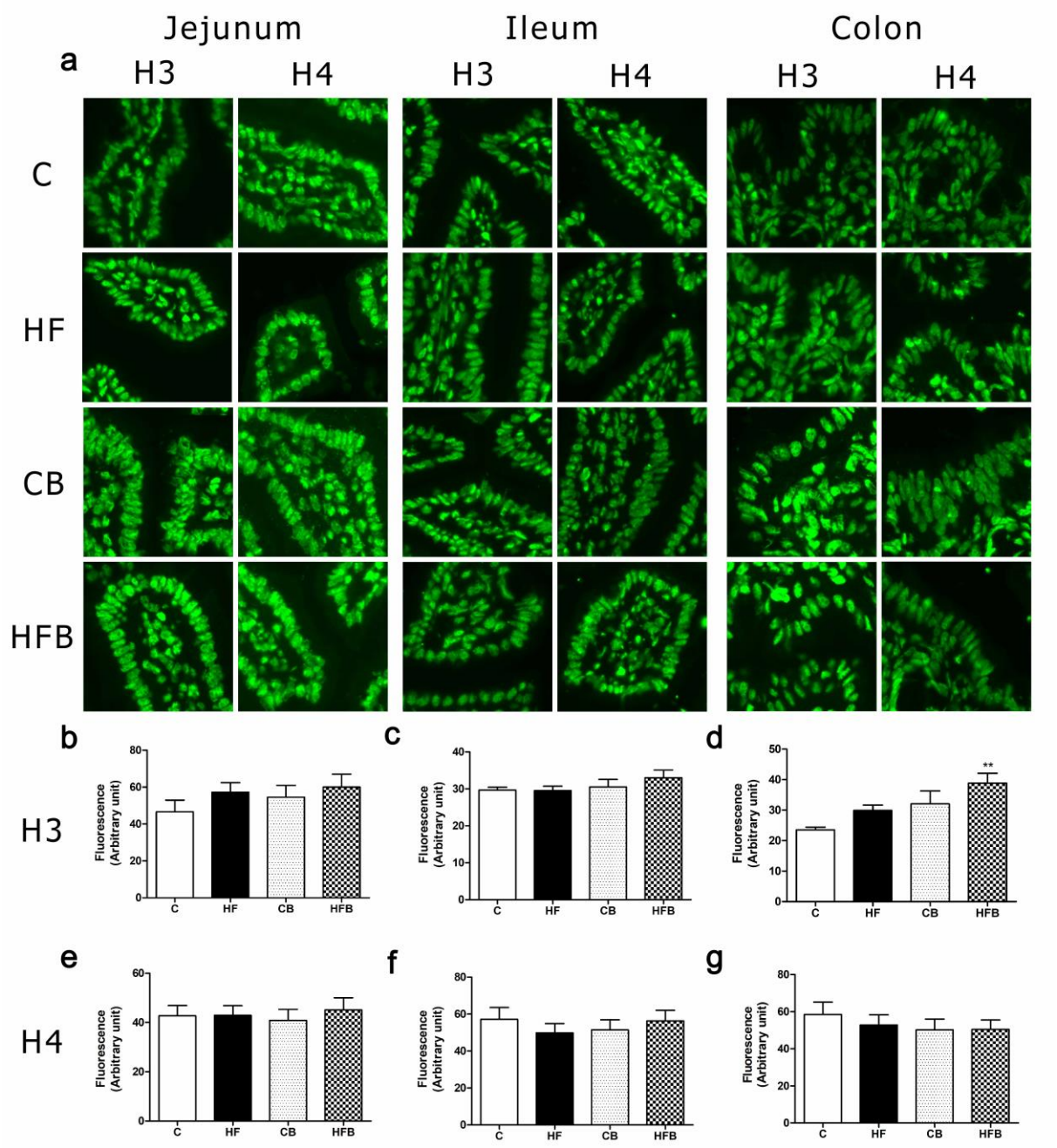

Figure 7: Effect of the dietary supplementation with sodium butyrate in the acetylation level of histones H3 and H4 on the intestine epithelium. The acetylated H3 and H4 were detected by immunofluorescence in cryosections of the epithelium obtained from the small intestine (jejunum and ileum) and large intestine (colon) from all the experimental groups (C, HF, CB, HFB) **(a)**. No significant difference was observed in the degree of acetylation of H3 and H4 among the groups (C, HF, CB, and HFB) (**b, c, e, f, g**), except in the colon that the degree of H3 acetylation in the HFB group was higher compared to C group (**d**). The values represent the mean ± SEM (fluorescence degree expressed as arbitrary units).

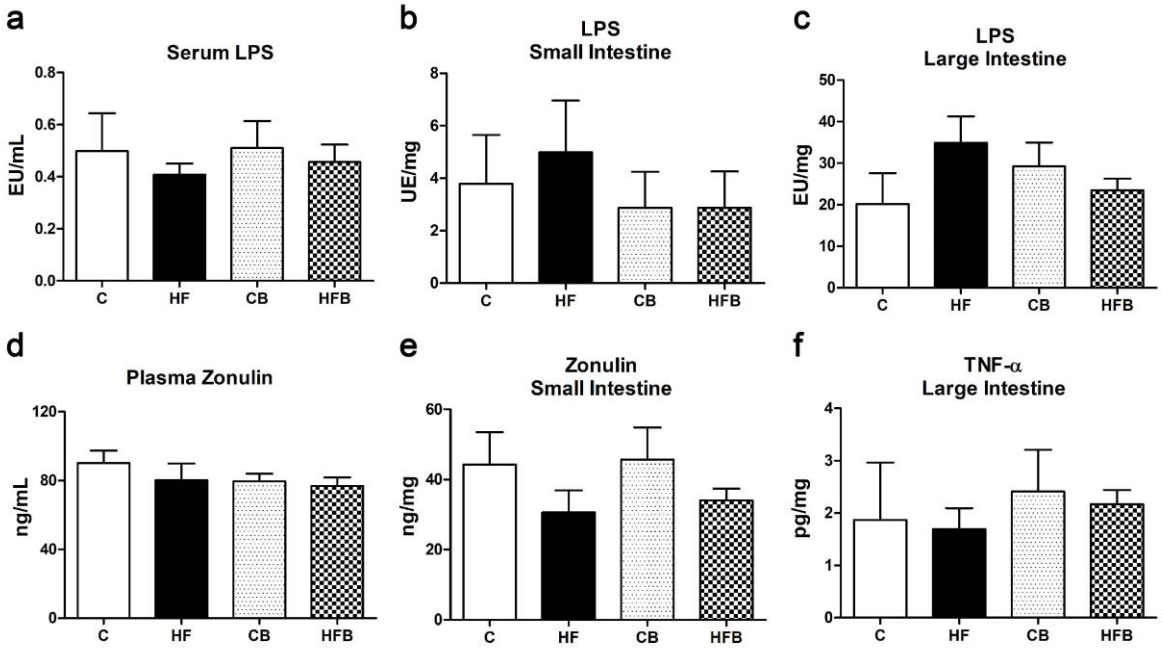

Figure 8: Effect of the dietary supplementation with sodium butyrate on LPS, zonulin, and TNF-α quantification in serum/plasma and intestinal homogenates of mice fed a standard or a high-fat diet. There was no significant change in the LPS concentration in serum **(a)**, either in the homogenates of small **(b)** and large intestines **(c)** among the experimental groups. No significant alteration in zonulin plasma (**d**) and small intestine (**e**) level was observed. Also, there was no significant difference in the concentration of TNF-α in large intestine homogenates between the groups (**f**). The values represent the mean ± SEM.

CAPITULO 6

CONSIDERAÇÕES FINAIS

Nessa Tese de Doutorado, avaliou-se o possível efeito anti-diabetogênico do butirato de sódio, utilizando, como modelo animal de pré-diabetes tipo 2, camundongos alimentados com DHL por 60 dias. Nossos resultados mostraram uma ação protetora do butirato nas alterações biométricas/metabólicas como menor ganho de peso, melhora na sensibilidade à insulina (ITT) e resposta à glicose (GTT). Esse AGCC teve também um efeito hepático benéfico pois inibiu significantemente o acúmulo de gordura nesse órgão, melhorando significativamente o quadro de esteatose hepática induzida pela DHL. Ainda, a administração de butirato foi associada com um aumento da secreção estática de insulina e inibição de depósito ectópico de tecido adiposo no pâncreas. O butirato também se mostrou eficiente no restabelecimento da proporção de massa gorda/magra, diminuindo a adiposidade e aumentando a massa muscular esquelética, além de minimizar a dislipidemia característica do estado pré-diabético tipo 2. Todos esses efeitos metabólicos e teciduais do butirato ocorreram na ausência de alteração da ingestão calórica diária ou da expressão de proteínas orexigênicas e anorexigênicas no hipotálamo dos animais.

A ação do butirato sobre o metabolismo basal celular foi avaliado em condições *in vivo* e *in vitro*. Nos testes *in vivo,* o butirato teve ação positiva sobre o metabolismo basal, aumentando o gasto energético nos camundongos após DHL, sem afetar a atividade basal motora. Ainda, esse AGCC teve ação protetora sobre o tecido adiposo marrom, preservando as suas características morfológicas e funcionais (esta última avaliada pelo nível da expressão de UCP-1). No entanto, o mesmo efeito sobre a bioenergética celular não foi observado nos experimentos *in vitro* empregando uma linhagem celular de adipócitos do tipo marrom (indiferenciados e diferenciados)

Outro objetivo dessa Tese foi avaliar o efeito do butirato sobre as alterações funcionais e estruturais da barreira intestinal mediada pela JO induzidas pela exposição à DHL. Como esperado, a exposição dos camundongos à DHL induziu alterações na estrutura da barreira epitelial intestinal, diminuindo a marcação juncional das proteínas Cld-1, Cld-2, Cld-3 e ZO-1 analisadas por imunofluorescência, bem como levou a uma disfunção desta barreira avaliada pelo teste de permeabilidade intestinal para marcadores paracelulares. A suplementação com

butirato de sódio reverteu os efeitos da DHL sobre as alterações estruturais e também funcionais da barreira epitelial intestinal nos camundongos pré-diabéticos. Entretanto, esses efeitos do butirato e da DHL sobre a barreira intestinal não parecem envolver regulação epigenética via hiperacetilação de histonas, nem alterações significativas nas concentrações séricas/plasmáticas e/ou intestinais de LPS, zonulina e TNF-α, conhecidos marcadores de endotoxemia e inflamação tecidual e sistêmica. A avaliação de toxicidade sistêmica do butirato foi realizada por meio da contagem de glóbulos vermelhos e brancos e pelo perfil bioquímico de marcadores da função hepática (ALT e AST), pancreática (amilase) e renal (creatinina). Essa análise mostra que não houve alterações significativas entre os grupos quanto aos resultados da série vermelha, porém, na série branca, os animais que receberam DHL tiveram aumento significativo no número de linfócitos e no perfil bioquímico aumento significativo do marcador de função hepática ALT, resultados que não foram observados em animais com suplementação com butirato.

Por fim, para as análises *in vitro*, células da linhagem intestinal Caco-2 foram expostas ao conteúdo luminal do intestino delgado de animais dos diferentes grupos afim de observar a influência de componentes do lúmen intestinal sobre as características funcionais e estruturais da barreira epitelial mediada pelas proteínas da JO. Como esperado, a exposição *in vitro* do conteúdo intestinal de animais que receberam DHL induziu ruptura da barreira paracelular associada com desarranjo da estrutura da JO observada por imunofluorescência para as proteínas Cld-1 e ZO-1. Em contraste, as monocamadas de Caco-2 expostas ao conteúdo luminal de animais que receberam a suplementação com butirato mostraram uma estrutura e função da da barreira epitelial preservada e semelhante àquela observada nas células controle (expostas à solução de Krebs). Esses dados corroboram os resultados *in vivo* que indicando um efeito protetor do butirato sobre a função de barreira epitelial e estrutura da JO.

CONCLUSÃO

Diante do exposto, podemos concluir que o butirato de sódio pode ter relevância clínica por notavelmente influenciar vias que medeiam tanto o metabolismo de lipídios e/ou carboidratos quanto vias que atuam sobre o possível endereçamento das proteínas da junção de oclusão sendo, assim, potencialmente sugerido para o tratamento e prevenção de distúrbios metabólicos e de doenças intestinais.

CAPÍTULO 7

REFERÊNCIAS

Al-Salami, H. *et al.* (2008) 'Probiotic treatment reduces blood glucose levels and increases systemic absorption of gliclazide in diabetic rats.', *European journal of drug metabolism and pharmacokinetics*, 33(2), pp. 101–106. doi: 10.1007/BF03191026.

Amar, Jacques *et al.* (2011) 'Intestinal mucosal adherence and translocation of commensal bacteria at the early onset of type 2 diabetes: Molecular mechanisms and probiotic treatment', *EMBO Molecular Medicine*, 3(9), pp. 559–572. doi: 10.1002/emmm.201100159.

Amar, J. *et al.* (2011) 'Involvement of tissue bacteria in the onset of diabetes in humans: Evidence for a concept', *Diabetologia*, 54(12), pp. 3055–3061. doi: 10.1007/s00125-011-2329-8.

American Diabetes Association (2014) 'Diagnosis and classification of diabetes mellitus', *Diabetes Care*, 37(SUPPL.1), pp. 81–90. doi: 10.2337/dc14-S081.

American Diabetes Association (2020) 'Standards of Medical Care in diabetes — 2020', *Diabetes Care*, 43(January), pp. S1–S212.

Ammon, H. P. T. (2019) 'Boswellic extracts and 11-keto-ß-boswellic acids prevent type 1 and type 2 diabetes mellitus by suppressing the expression of proinflammatory cytokines', *Phytomedicine*. Elsevier, 63(June), p. 153002. doi: 10.1016/j.phymed.2019.153002.

Anderson, J. M. and Van Itallie, C. M. (2009) 'Physiology and function of the tight junction.', *Cold Spring Harbor perspectives in biology*, 1(2). doi: 10.1101/cshperspect.a002584.

Aron-Wisnewsky, J. and Clément, K. (2016) 'The gut microbiome, diet, and links to cardiometabolic and chronic disorders', *Nature Reviews Nephrology*. Nature Publishing Group, 12(3), pp. 169–181. doi: 10.1038/nrneph.2015.191.

Arrieta, M. C., Bistritz, L. and Meddings, J. B. (2006) 'Alterations in intestinal permeability.', *Gut*, 55(10), pp. 1512–1520. doi: 10.1136/gut.2005.085373.

Asghar, Z. *et al.* (2006) 'Insulin resistance causes increased beta-cell mass but defective glucose-stimulated insulin secretion in a murine model of type 2 diabetes', *Diabetologia*, 49(1), pp. 90–99. doi: 10.1007/s00125-005-0045-y.

Asmat, U., Abad, K. and Ismail, K. (2016) 'Diabetes mellitus and oxidative stress—A concise review', *Saudi Pharmaceutical Journal*. King Saud University, 24(5), pp. 547–553. doi: 10.1016/j.jsps.2015.03.013.

Banerjee, S. *et al.* (2019) 'Review Type II diabetes mellitus and obesity : Common links , existing therapeutics and future developments', *J Biosci*, 44(150), pp. 1–13. doi: 10.1007/s12038-019-9962-7.

Berni Canani, R., Di Costanzo, M. and Leone, L. (2012) 'The epigenetic effects of butyrate:

potential therapeutic implications for clinical practice.', *Clinical epigenetics*. BioMed Central Ltd, 4(1), p. 4. doi: 10.1186/1868-7083-4-4.

Björnholm, M. and Zierath, J. R. (2005) 'Insulin signal transduction in human skeletal muscle: identifying the defects in Type II diabetes.', *Biochemical Society transactions*, 33(Pt 2), pp. 354–357. doi: 10.1042/BST0330354.

Bosi, E. *et al.* (2006) 'Increased intestinal permeability precedes clinical onset of type 1 diabetes', *Diabetologia*, 49(12), pp. 2824–2827. doi: 10.1007/s00125-006-0465-3.

Branco, R. C. S. *et al.* (2019) 'Protein malnutrition mitigates the effects of a high-fat diet on glucose homeostasis in mice', *Journal of Cellular Physiology*, 234(5), pp. 6313–6323. doi: 10.1002/jcp.27361.

Brinton, E. A. (2003) 'Lipid abnormalities in the metabolic syndrome', *Current Diabetes Reports*, 3(1).

Bron, P. A. *et al.* (2017) 'Can probiotics modulate human disease by impacting intestinal barrier function?', *British Journal of Nutrition*, 117(1), pp. 93–107. doi: 10.1017/S0007114516004037.

Brunzell, J. D. and Ayyobi, A. F. (2003) 'Dyslipidemia in the metabolic syndrome and type 2 diabetes mellitus', *American Journal of Medicine*, 115(8 SUPPL. 1), pp. 24–28. doi: 10.1016/j.amjmed.2003.08.011.

Buckley, A. and Turner, J. R. (2018) 'Cell biology of tight junction barrier regulation and mucosal disease', *Cold Spring Harbor Perspectives in Biology*, 10(1). doi: 10.1101/cshperspect.a029314.

Bultman, S. J. (2017) 'Interplay between diet, gut microbiota, epigenetic events, and colorectal cancer', *Molecular Nutrition and Food Research*, 61(1), pp. 1–12. doi: 10.1002/mnfr.201500902.

Butt, A. M. *et al.* (2012) 'Role of post translational modifications and novel crosstalk between phosphorylation and O-beta-GlcNAc modifications in human claudin-1, -3 and -4', *Molecular Biology Reports*, 39(2), pp. 1359–1369. doi: 10.1007/s11033-011-0870-7.

Byrne, C. D. *et al.* (2009) 'Metabolic disturbances in non-alcoholic fatty liver disease.', *Clinical science (London, England : 1979)*, 116(7), pp. 539–64. doi: 10.1042/CS20080253.

Caminhotto, R. O. *et al.* (2019) 'Physiological concentrations of β-hydroxybutyrate do not promote adipocyte browning', *Life Sciences*, 232(July). doi: 10.1016/j.lfs.2019.116683.

Canani, R. B. *et al.* (2004) 'Butyrate as an effective treatment of congenital chloride diarrhea', *Gastroenterology*, 127(2), pp. 630–634. doi: 10.1053/j.gastro.2004.03.071.

Canani, R. B. *et al.* (2011) 'Potential beneficial effects of butyrate in intestinal and extraintestinal diseases', *World Journal of Gastroenterology*, 17(12), pp. 1519–1528. doi: 10.3748/wjg.v17.i12.1519.

Cani, Patrice D *et al.* (2007) 'Metabolic endotoxemia initiates obesity and insulin resistence', *Diabetes*, 56(July), pp. 1761–1772. doi: 10.2337/db06-1491.P.D.C.

Cani, P. D. *et al.* (2007) 'Selective increases of bifidobacteria in gut microflora improve high-fat-diet-induced diabetes in mice through a mechanism associated with endotoxaemia', *Diabetologia*, 50(11), pp. 2374–2383. doi: 10.1007/s00125-007-0791-0.

Cani, P. D. *et al.* (2008) 'Changes in gut microbiota control metabolic diet–induced obesity and diabetes in mice', *Diabetes*, 57(6), pp. 1470–81. doi: 10.2337/db07-1403.Additional.

Cani, P. D. *et al.* (2012) 'Involvement of gut microbiota in the development of low-grade inflammation and type 2 diabetes associated with obesity', *Gut microbes*, (August), pp. 279–288.

Canivell, S. and Gomis, R. (2014) 'Diagnosis and classification of autoimmune diabetes mellitus', *Autoimmunity Reviews*, 13(4), pp. 403–407. doi: 10.1016/j.autrev.2014.01.020.

Canuto, L. P. and Collares-Buzato, C. B. (2019) 'Increased osmolality enhances the tight junction-mediated barrier function in a cultured renal epithelial cell line', *Cell Biology International*, 43(1), pp. 73–82. doi: 10.1002/cbin.11074.

Cao, M. *et al.* (2013) 'Amelioration of IFN-γ and TNF-α-Induced Intestinal Epithelial Barrier Dysfunction by Berberine via Suppression of MLCK-MLC Phosphorylation Signaling Pathway', *PLoS ONE*, 8(5). doi: 10.1371/journal.pone.0061944.

Carvalho, C. P. F. *et al.* (2010) 'Beta cell coupling and connexin expression change during the functional maturation of rat pancreatic islets', *Diabetologia*, 53(7), pp. 1428–1437. doi: 10.1007/s00125-010-1726-8.

Carvalho, C. P. F. *et al.* (2012) 'Impaired β-cell-β-cell coupling mediated by Cx36 gap junctions in prediabetic mice.', *American journal of physiology. Endocrinology and metabolism*, 303(1), pp. E144-51. doi: 10.1152/ajpendo.00489.2011.

Castro, A. V. B. *et al.* (2015) 'Obesity, insulin resistance and comorbidities – Mechanisms of association', *Arq Bras Endocrinol Metabol*, 58(6), pp. 600–609. doi: 10.1590/0004-2730000003223.

Catta-Preta, M. *et al.* (2011) 'A critical analysis of three quantitative methods of assessment of hepatic steatosis in liver biopsies', *Virchows Arch*, 459(5), pp. 477–485. doi: 10.1007/s00428-011-1147-1.

Chang, P. V. *et al.* (2014) 'The microbial metabolite butyrate regulates intestinal macrophage function via histone deacetylase inhibition', *Proceedings of the National Academy of Sciences*, 111(6), pp. 2247–2252. doi: 10.1073/pnas.1322269111.

Chaudhury, A. *et al.* (2017) 'Clinical Review of Antidiabetic Drugs: Implications for Type 2 Diabetes Mellitus Management', *Front Endocrinol (Lausanne)*, 8(January), p. 6. doi: 10.3389/fendo.2017.00006.

Collares-buzato, C. B. (2015) 'High-fat diets and β-cell dysfuntion: molecular aspects. In:

Molecular Nutrition and Diabetes.', in Elsevier (ed.) *Molecular Nutrition and Diabetes.* San Diego, USA, pp. 115-130.

Collares-Buzato, C. B. *et al.* (1994) 'Paracellular barrier and junctional protein distribution depend on basolateral extracellular Ca2+ in cultured epithelia', *BBA - Molecular Cell Research*, 1222(2), pp. 147–158. doi: 10.1016/0167-4889(94)90163-5.

Collares-Buzato, C. B. *et al.* (1998) 'Increased tyrosine phosphorylation causes redistribution of adherens junction and tight junction proteins and perturbs paracellular barrier function in MDCK epithelia', *European Journal of Cell Biology*. Gustav Fischer Verlag GmbH & Co. KG, 76(2), pp. 85–92. doi: 10.1016/S0171-9335(98)80020-4.

Collares-Buzato, C. B. (2019) 'Junções Celulares', in *A Célula*. 4ª. Manole, pp. 145–169.

Cypess, A. M. and Kahn, C. R. (2010) 'Brown fat as a therapy for obesity and diabetes Aaron', *Curr Opin Endocrinol Diabetes Obes*, 17(2), pp. 143–149. doi: 10.1097/MED.0b013e328337a81f.Brown.

Dangelo, J. and Fattini, C. (2011) *Anatomia Humana - Sistêmica e Segmentar*. 3ª edição. Edited by Atheneu.

Dankner, R. *et al.* (2009) 'Basal-state hyperinsulinemia in healthy normoglycemic adults is predictive of type 2 diabetes over a 24-year follow-up: A preliminary report', *Diabetes Care*, 32(8), pp. 1464–1466. doi: 10.2337/dc09-0153.

Ding, S. *et al.* (2010) 'High-fat diet: Bacteria interactions promote intestinal inflammation which precedes and correlates with obesity and insulin resistance in mouse', *PLoS ONE*, 5(8). doi: 10.1371/journal.pone.0012191.

Doerrier, C. *et al.* (2018) *High-Resolution FluoRespirometry and OXPHOS Protocols for Human Cells, Permeabilized Fibers from Small Biopsies of Muscle, and Isolated Mitochondria*.

Dudakovic, A. *et al.* (2013) 'Histone deacetylase inhibition promotes osteoblast maturation by altering the histone H4 epigenome and reduces akt phosphorylation', *Journal of Biological Chemistry*, 288(40), pp. 28783–28791. doi: 10.1074/jbc.M113.489732.

Everard, A. and Cani, P. (2013) 'Diabetes, obesity and gut microbiota.', *Best practice & research. Clinical gastroenterology*. Elsevier Ltd, 27(1), pp. 73–83. doi: 10.1016/j.bpg.2013.03.007.

Falcão, V. T. F. L. *et al.* (2016) 'Reduced insulin secretion function is associated with pancreatic islet redistribution of cell adhesion molecules (CAMs) in diabetic mice after prolonged high-fat diet', *Histochemistry and Cell Biology*. Springer Berlin Heidelberg, 146(1), pp. 13–31. doi: 10.1007/s00418-016-1428-5.

Fasano, A. (2008) 'Physiological, pathological, and therapeutic implications of zonulin-mediated intestinal barrier modulation: living life on the edge of the wall.', *The American journal of pathology*, 173(5), pp. 1243–52. doi: 10.2353/ajpath.2008.080192.

Fasano, A. (2011) ‘Zonulin and its regulation of intestinal barrier function: the biological door to inflammation, autoimmunity, and cancer.’, *Physiological reviews*, 91(1), pp. 151–175. doi: 10.1152/physrev.00003.2008.

Fasano, A. (2012) ‘Zonulin, regulation of tight junctions, and autoimmune diseases’, *Annals of the New York Academy of Sciences*, 1258(1), pp. 25–33. doi: 10.1111/j.1749-6632.2012.06538.x.

Fasano, A. and Shea-Donohue, T. (2005) ‘Mechanisms of Disease: the role of intestinal barrier function in the pathogenesis of gastrointestinal autoimmune diseases’, *Nature Clinical Practice Gastroenterology & Hepatology*, 2(9), pp. 416–422. doi: 10.1038/ncpgasthep0259.

Forbes, J. M. and Cooper, M. E. (2013) ‘Mechanisms of diabetic complications.’, *Physiological reviews*, 93(1), pp. 137–88. doi: 10.1152/physrev.00045.2011.

Fukui, H. (2016) ‘Increased Intestinal Permeability and Decreased Barrier Function: Does It Really Influence the Risk of Inflammation?’, *Inflammatory Intestinal Diseases*, 1(3), pp. 135–145. doi: 10.1159/000447252.

Furuse, M. (2010) ‘Molecular basis of the core structure of tight junctions.’, *Cold Spring Harbor perspectives in biology*, 2(1). doi: 10.1101/cshperspect.a002907.

Gao, Z. *et al.* (2009) ‘Butyrate improves insulin sensitivity and increases energy expenditure in mice’, *Diabetes*, 58(7), pp. 1509–1517. doi: 10.2337/db08-1637.

Garcia-Hernandez, V., Quiros, M. and Nusrat, A. (2017) ‘Intestinal epithelial claudins: Expression and regulation in homeostasis and inflammation’, *Annals of the New York Academy of Sciences*, 1397(1), pp. 66–79. doi: 10.1111/nyas.13360.

Garrett, W. S., Gordon, J. I. and Glimcher, L. H. (2010) ‘Homeostasis and Inflammation in the Intestine’, *Cell*. Elsevier Inc., 140(6), pp. 859–870. doi: 10.1016/j.cell.2010.01.023.

Geurts, L. *et al.* (2014) ‘Gut microbiota controls adipose tissue expansion, gut barrier and glucose metabolism: Novel insights into molecular targets and interventions using prebiotics’, *Beneficial Microbes*, 5(1), pp. 3–17. doi: 10.3920/BM2012.0065.

Ghaisas, S., Maher, J. and Kanthasamy, A. (2015) ‘Gut microbiome in health and disease: Linking the microbiome-gut-brain axis and environmental factors in the pathogenesis of systemic and neurodegenerative diseases.’, *Pharmacology & therapeutics*, 158, pp. 52–62. doi: 10.1016/j.pharmthera.2015.11.012.

Gill, R. K. and Dudeja, P. K. (2011) ‘A novel facet to consider for the effects of butyrate on its target cells. Focus on “The short-chain fatty acid butyrate is a substrate of breast cancer resistance protein”’, *Am J Physiol Cell Physiol*, 301, pp. C977–C979. doi: 10.1152/ajpcell.00290.2011.

Gomes, J. M. G., Costa, J. de A. and Alfenas, R. de C. G. (2017) ‘Metabolic endotoxemia and diabetes mellitus: A systematic review’, *Metabolism: Clinical and Experimental*. Elsevier Inc., 68, pp. 133–144. doi: 10.1016/j.metabol.2016.12.009.

Gómez-Dumm, L. A., Semino, M. C. and Gagliardino, J. J. (1990) 'Sequential Morphological Changes in Pancreatic Islets of Spontaneously Diabetic Rats', 5(5), pp. 533–539.

Groschwitz, K. R. and Hogan, S. P. (2009) 'Intestinal barrier function: Molecular regulation and disease pathogenesis', *Journal of Allergy and Clinical Immunology*. Elsevier Ltd, 124(1), pp. 3–20. doi: 10.1016/j.jaci.2009.05.038.

Gunzel, D. and Yu, A. S. L. (2013) 'Claudins and the Modulation of Tight Junction Permeability', *Physiological Reviews*, 93(2), pp. 525–569. doi: 10.1152/physrev.00019.2012.

Haberland, M., Montgomery, R. L. and Olson, E. N. (2009) 'The many roles of histone deacetylases in development and physiology: Implications for disease and therapy', *Nature Reviews Genetics*, 10(1), pp. 32–42. doi: 10.1038/nrg2485.

Hadjiagapiou, C. *et al.* (2000) 'Mechanism (s) of butyrate transport in Caco-2 cells : role of monocarboxylate transporter 1', *Am J Physiol Gastrointest Liver Physiol*, 279, pp. 775–780.

Halpern, M. D. and Denning, P. W. (2015) 'The role of intestinal epithelial barrier function in the development of NEC', *Tissue Barriers*, 3(1). doi: 10.1080/21688370.2014.1000707.

Hamer, H. M. *et al.* (2008) 'Review article: The role of butyrate on colonic function', *Alimentary Pharmacology and Therapeutics*, 27(2), pp. 104–119. doi: 10.1111/j.1365-2036.2007.03562.x.

Hauschka, S. D. and Konigsberg, I. R. (1966) 'The influence of collagen on the development of muscle clones.', *Proceedings of the National Academy of Sciences of the United States of America*, 55(1), pp. 119–126. doi: 10.1073/pnas.55.1.119.

Henagan, T. M. *et al.* (2015) 'Sodium butyrate epigenetically modulates high-fat diet-induced skeletal muscle mitochondrial adaptation, obesity and insulin resistance through nucleosome positioning', *British Journal of Pharmacology*, 172, pp. 2782–2798. doi: 10.1111/bph.13058.

Hichino, A. *et al.* (2017) 'Down-regulation of claudin-2 expression and proliferation by epigenetic inhibitors in human lung adenocarcinoma A549 cells', *Journal of Biological Chemistry*, 292(6), pp. 2411–2421. doi: 10.1074/jbc.M116.762807.

Hillebrand, J. J. G., De Wied, D. and Adan, R. A. H. (2002) 'Neuropeptides, food intake and body weight regulation: A hypothalamic focus', *Peptides*, 23(12), pp. 2283–2306. doi: 10.1016/S0196-9781(02)00269-3.

Horton, F. *et al.* (2014) 'Increased intestinal permeability to oral chromium (51Cr) -EDTA in human Type 2 diabetes', *Diabetic Medicine*, 31(5), pp. 559–563. doi: 10.1111/dme.12360.

Hossain, Z. and Hirata, T. (2008) 'Molecular mechanism of intestinal permeability: interaction at tight junctions.', *Molecular bioSystems*, 4(12), pp. 1181–1185. doi: 10.1039/b800402a.

Huang, C. *et al.* (2015) 'Dietary Sodium Butyrate Decreases Postweaning Diarrhea by Modulating Intestinal Permeability and Changing the Bacterial Communities in Weaned Piglets 1 – 3', (C), pp. 1–7. doi: 10.3945/jn.115.217406.The.

Inan, M. S. *et al.* (2000) 'The luminal short-chain fatty acid butyrate modulates NF-κB activity in a human colonic epithelial cell line', *Gastroenterology*, 118(4), pp. 724–734. doi: 10.1053/gg.2000.5967.

Issekutz, B., Birkhead, N. C. and Rodahl, K. (1962) 'Use of respiratory quotients in assessment of aerobic work capacity', *Journal of Applied Physiology*, 17(1), pp. 47–50. doi: 10.1152/jappl.1962.17.1.47.

Van Itallie, C. M. and Anderson, J. M. (2014) 'Architecture of tight junctions and principles of molecular composition', *Seminars in Cell and Developmental Biology*. Elsevier Ltd, 36, pp. 157–165. doi: 10.1016/j.semcdb.2014.08.011.

Jayashree, B. *et al.* (2014) 'Increased circulatory levels of lipopolysaccharide (LPS) and zonulin signify novel biomarkers of proinflammation in patients with type 2 diabetes', *Molecular and Cellular Biochemistry*, 388(1–2), pp. 203–210. doi: 10.1007/s11010-013-1911-4.

Jepson, M. A., Schlecht, H. B. and Collares-Buzato, C. B. (2000) 'Localization of Dysfunctional Tight Junctions in Salmonella enterica Serovar Typhimurium-Infected Epithelial Layers Localization of Dysfunctional Tight Junctions in Salmonella enterica Serovar Typhimurium-Infected Epithelial Layers', *Infection and immunity*, 68(12), pp. 7202–7208. doi: 10.1128/IAI.68.12.7202-7208.2000.Updated.

Jkobsdottira, G. *et al.* (2013) 'High-fat diet reduces the formation of butyrate, but increases succinate, inflammation, liver fat and cholesterol in rats, while dietary fibre counteracts these effects', *PLoS ONE*, 8(11), pp. 1–15. doi: 10.1371/journal.pone.0080476.

Johnson, A. M. F. *et al.* (2015) 'High fat diet causes depletion of intestinal eosinophils associated with intestinal permeability', *PLoS ONE*, 10(4), pp. 1–15. doi: 10.1371/journal.pone.0122195.

Judex, S. *et al.* (2010) 'Quantification of adiposity in small rodents using micro-CT', *Methods*. Elsevier Inc., 50(1), pp. 14–19. doi: 10.1016/j.ymeth.2009.05.017.

Junqueira, L.C & Carneiro, J. (2013) *Histologia Básica*. 12ª edição. Edited by G. Koogan.

Kahn, S. E., Hull, R. L. and Utzschneider, K. M. (2006) 'Mechanisms linking obesity to insulin resistance and type 2 diabetes', *Nature*, 444(7121), pp. 840–846. doi: 10.1038/nature05482.

Kaiko, G. E. *et al.* (2016) 'The Colonic Crypt Protects Stem Cells from Microbiota-Derived Metabolites', *Cell*. Elsevier Inc., 165(7), pp. 1708–1720. doi: 10.1016/j.cell.2016.05.018.

Kato, S. *et al.* (1996) 'Alterations in basal and glucose-stimulated voltage-dependent Ca2+ channel activities in pancreatic β-cells of non-insulin-dependent diabetes mellitus GK rats', *Journal of Clinical Investigation*, 97(11), pp. 2417–2425. doi: 10.1172/JCI118688.

Kespohl, M. *et al.* (2017) 'The microbial metabolite butyrate induces expression of Th1-associated factors in cD4+ T cells', *Frontiers in Immunology*, 8(AUG), pp. 1–12. doi: 10.3389/fimmu.2017.01036.

Khan, N. and Asif, A. R. (2015) 'Transcriptional Regulators of Claudins in Epithelial Tight Junctions', *Hindawi Publishing Corporation*, 2015(1), pp. 1–6. doi: 10.1155/2015/219843.

Khan, S. and Jena, G. (2016) 'Sodium butyrate reduces insulin-resistance, fat accumulation and dyslipidemia in type-2 diabetic rat: A comparative study with metformin', *Chemico-Biological Interactions*. Elsevier Ltd, 254, pp. 124–134. doi: 10.1016/j.cbi.2016.06.007.

Khan, S. and Jena, G. B. (2014) 'Protective role of sodium butyrate, a HDAC inhibitor on beta-cell proliferation, function and glucose homeostasis through modulation of p38/ERK MAPK and apoptotic pathways: Study in juvenile diabetic rat', *Chemico-Biological Interactions*. Elsevier Ireland Ltd, 213(1), pp. 1–12. doi: 10.1016/j.cbi.2014.02.001.

Kierszenbaum, A. L. & Tres, L. L. (2012) *Histologia e Biologia Celular - Uma Introdução à Patologia*. 3ª edição. Edited by Saunders.

Kim, A. *et al.* (2009) 'Islet architecture: A comparative study.', *Islets*, 1(2), pp. 129–136. doi: 10.4161/isl.1.2.9480.

Kootte, R. S. *et al.* (2012) 'The therapeutic potential of manipulating gut microbiota in obesity and type 2 diabetes mellitus', *Diabetes, Obesity and Metabolism*, 14(2), pp. 112–120. doi: 10.1111/j.1463-1326.2011.01483.x.

De Kort, S., Keszthelyi, D. and Masclee, A. A. M. (2011) 'Leaky gut and diabetes mellitus: What is the link?', *Obesity Reviews*, 12(6), pp. 449–458. doi: 10.1111/j.1467-789X.2010.00845.x.

Krauss, S., Zhang, C. Y. and Lowell, B. B. (2005) 'The mitochondrial uncoupling-protein homologues', *Nature Reviews Molecular Cell Biology*, 6(3), pp. 248–261. doi: 10.1038/nrm1592.

Krug, S. M., Schulzke, J. D. and Fromm, M. (2014) 'Tight junction, selective permeability, and related diseases', *Seminars in Cell and Developmental Biology*. Elsevier Ltd, 36, pp. 166–176. doi: 10.1016/j.semcdb.2014.09.002.

Kruh, J. (1982) 'Effects of sodium butyrate , a new pharmacological agent , on cells in culture', *Molecular and Cellular Biochemistry*, 42, pp. 65–82. doi: 10.1007/BF00222695.

Kumar, M. *et al.* (2007) 'Effect of histone acetylation modification with sodium butyrate, a histone deacetylase inhibitor, on cell cycle, apoptosis, ploidy and gene expression in porcine fetal fibroblasts.', *The Journal of reproduction and development*, 53(4), pp. 903–13. doi: 10.1262/jrd.18180.

Lapa, C. *et al.* (2017) 'Whitening and Impaired Glucose Utilization of Brown Adipose Tissue in a Rat Model of Type 2 Diabetes Mellitus', *Scientific Reports*, 7(1), pp. 5–10. doi: 10.1038/s41598-017-17148-w.

Larsen, N. *et al.* (2010) 'Gut microbiota in human adults with type 2 diabetes differs from non-diabetic adults', *PLoS ONE*, 5(2). doi: 10.1371/journal.pone.0009085.

Lee, B. C. and Lee, J. (2014) 'Cellular and molecular players in adipose tissue inflammation

in the development of obesity-induced insulin resistance', *Biochimica et Biophysica Acta - Molecular Basis of Disease*. Elsevier B.V., 1842(3), pp. 446–462. doi: 10.1016/j.bbadis.2013.05.017.

Ley, R. E. *et al.* (2005) 'Obesity alters gut microbial ecology.', *Proceedings of the National Academy of Sciences of the United States of America*, 102(31), pp. 11070–5. doi: 10.1073/pnas.0504978102.

Li, C. J. *et al.* (2016) 'Transcriptomic sequencing reveals a set of unique genes activated by butyrate-induced histone modification', *Gene Regulation and Systems Biology*, 10, pp. 1–8. doi: 10.4137/GRSB.S35607.

Li, H. P., Chen, X. and Li, M. Q. (2013) 'Butyrate alleviates metabolic impairments and protects pancreatic β cell function in pregnant mice with obesity', *International Journal of Clinical and Experimental Pathology*, 6(8), pp. 1574–1584.

Li, Z. *et al.* (2018) 'Butyrate reduces appetite and activates brown adipose tissue via the gut-brain neural circuit', *Gut*, 67(7), pp. 1269–1279. doi: 10.1136/gutjnl-2017-314050.

Lin, Y. *et al.* (2005) 'The hyperglycemia-induced inflammatory response in adipocytes: The role of reactive oxygen species', *Journal of Biological Chemistry*, 280(6), pp. 4617–4626. doi: 10.1074/jbc.M411863200.

Lin, Y. and Sun, Z. (2010) 'Current views on type 2 diabetes', *Journal of Endocrinology*, 204(1), pp. 1–11. doi: 10.1677/JOE-09-0260.

Liu, J. *et al.* (2020) 'Beneficial effects of butyrate in intestinal injury', *Journal of Pediatric Surgery*, (xxxx), pp. 6–11. doi: 10.1016/j.jpedsurg.2020.02.036.

Lu, Z. *et al.* (2013) 'Claudins in intestines: Distribution and functional significance in health and diseases', *Tissue barriers*, 1(3), p. e24978. doi: 10.4161/tisb.24978.

Luo, H. M. *et al.* (2013) 'Valproic Acid Treatment Inhibits Hypoxia-Inducible Factor 1α Accumulation and Protects against Burn-Induced Gut Barrier Dysfunction in a Rodent Model', *PLoS ONE*, 8(10), pp. 1–13. doi: 10.1371/journal.pone.0077523.

Mao, J. *et al.* (2013) 'Overnutrition stimulates intestinal epithelium proliferation through beta-catenin signaling in obese mice', *Diabetes*, 62(11), pp. 3736–3746. doi: 10.2337/db13-0035.

Markov, A. G. *et al.* (2010) 'Segmental expression of claudin proteins correlates with tight junction barrier properties in rat intestine', *Journal of Comparative Physiology B: Biochemical, Systemic, and Environmental Physiology*, 180(4), pp. 591–598. doi: 10.1007/s00360-009-0440-7.

Maschio, D. A. *et al.* (2016) 'Biochemical and Biophysical Research Communications Activation of the Wnt/b -catenin pathway in pancreatic beta cells during the compensatory islet hyperplasia in prediabetic mice', *Biochemical and Biophysical Research Communications*. Elsevier Ltd, 478(4), pp. 1534–1540. doi: 10.1016/j.bbrc.2016.08.146.

Maschio, D. A., Matheus, V. A. and Collares-Buzato, C. B. (2019) 'Islet cells are the source

of Wnts that can induce beta-cell proliferation in vitro', *Journal of Cellular Physiology*, 234(11). doi: 10.1002/jcp.28584.

Matheus, V. A. (2016) *Efeito do butirato de sódio sobre os parâmetros metabólicos e a barreira epitelial intestinal de animais pré-diabéticos*.

Matheus, V. A. *et al.* (2017) 'Butyrate reduces high-fat diet-induced metabolic alterations, hepatic steatosis and pancreatic beta cell and intestinal barrier dysfunctions in prediabetic mice', *Experimental Biology and Medicine*, 242(12), pp. 1214–1226. doi: 10.1177/1535370217708188.

Mátis, G. *et al.* (2015) 'Effects of oral butyrate application on insulin signaling in various tissues of chickens', *Domestic Animal Endocrinology*. Elsevier Inc, 50, pp. 26–31. doi: 10.1016/j.domaniend.2014.07.004.

Matsuzaki, T. *et al.* (1997) 'Prevention of onset in an insulin-dependent diabetes mellitus model, NOD mice, by oral feeding of Lactobacillus casei.', *Apmis*, 105(8), pp. 643–9. doi: 10.1111/j.1699-0463.1997.tb05066.x.

Meddings, J. B. *et al.* (1999) 'Increased gastrointestinal permeability is an early lesion in the spontaneously diabetic BB rat.', *The American journal of physiology*, 276(4 Pt 1), pp. G951-7. Available at: http://www.ncbi.nlm.nih.gov/pubmed/10198339.

Miao, W. *et al.* (2016) 'Sodium butyrate promotes reassembly of tight junctions in Caco-2 monolayers involving inhibition of MLCK/MLC2 pathway and phosphorylation of PKCβ2', *International Journal of Molecular Sciences*, 17(10), pp. 1–12. doi: 10.3390/ijms17101696.

Milatz, S. *et al.* (2010) 'Claudin-3 acts as a sealing component of the tight junction for ions of either charge and uncharged solutes', *Biochimica et Biophysica Acta - Biomembranes*. Elsevier B.V., 1798(11), pp. 2048–2057. doi: 10.1016/j.bbamem.2010.07.014.

Mitic, L. L., Itallie, C. M. Van and Anderson, J. M. (2000) 'Tight junction struture and function: lessons from mutant animals and proteins', *American Journal of Physiology. Gastrointestinal and liver physiology*, 279, pp. G250–G254.

Mollica, M. P. *et al.* (2017) 'Butyrate regulates liver mitochondrial function, efficiency, and dynamics in insulin-resistant obese mice', *Diabetes*, 66(5), pp. 1405–1418. doi: 10.2337/db16-0924.

Mongelli-Sabino, B. M., Canuto, L. P. and Collares-Buzato, C. B. (2017) 'Acute and chronic exposure to high levels of glucose modulates tight junction-associated epithelial barrier function in a renal tubular cell line', *Life Sciences*. Elsevier, 188(May), pp. 149–157. doi: 10.1016/j.lfs.2017.09.004.

Montanya, E. (2014) 'Insulin resistance compensation: not just a matter of β-cells?', *Diabetes*, 63(3), pp. 832–834. doi: 10.2337/db13-1843.

Mooradian, A. (2009) 'Dyslipidemia in type 2 diabetes mellitus', *Nature clinical practice endocrinology & metabolism*, 5(3), pp. 150–9. doi: 10.1038/ncpendmet.

Mori, M. A. *et al.* (2012) 'Role of MicroRNA Processing in Adipose Tissue in Stress Defense and Longevity', *Cell Metabolism*. Elsevier Inc., 16(3), pp. 336–347. doi: 10.1016/j.cmet.2012.07.017.

Mukiza, C. N. and Dubreuil, D. J. (2013) 'Escherichia coli heat-stable toxin b impairs intestinal epithelial barrier function by altering tight junction proteins', *Infection and Immunity*, 81(8), pp. 2819–2827. doi: 10.1128/IAI.00455-13.

Nagaraj, V. *et al.* (2016) 'Elevated basal insulin secretion in type 2-diabetes caused by reduced plasma membrane cholesterol.', *Molecular endocrinology (Baltimore, Md.)*, 30(November), p. me20161023. doi: 10.1210/me.2016-1023.

Nascimento, J. C. P. (2019) *Mecanismos moleculares e funcionais envolvidos na quebra de barreira epitelial intestinal mediada pela junção de oclusão e sua possível contribuição para a evolução do diabetes melito tipo 2 experimental*. Unicamp.

Neu, J. *et al.* (2005) 'Changes in Intestinal Morphology and Permeability in the BioBreeding Rat Before the Onset of Type 1 Diabetes', (May), pp. 589–595.

Odenwald, M. A. and Turner, J. R. (2016) 'The intestinal epithelial barrier: a therapeutic target?', *Nature Reviews Gastroenterology & Hepatology*. Nature Publishing Group, 14(1), pp. 9–21. doi: 10.1038/nrgastro.2016.169.

Ohira, H. *et al.* (2013) 'Butyrate attenuates inflammation and lipolysis generated by the interaction of adipocytes and macrophages.', *Journal of atherosclerosis and thrombosis*, 20(5), pp. 425–42. doi: 10.5551/jat.15065.

Oliveira, R. B. *et al.* (2014) 'Impaired compensatory beta-cell function and growth in response to high-fat diet in LDL receptor knockout mice', *International Journal of Experimental Pathology*, 95(4), pp. 296–308. doi: 10.1111/iep.12084.

Oliveira, R. B. *et al.* (2015) 'Influence of gender and time diet exposure on endocrine pancreas remodeling in response to high fat diet-induced metabolic disturbances in mice', *Annals of Anatomy*. Elsevier GmbH., 200, pp. 88–97. doi: 10.1016/j.aanat.2015.01.007.

Oliveira, R. B. *et al.* (2019) 'Time-dependent alteration to the tight junction structure of distal intestinal epithelia in type 2 prediabetic mice', *Life Sciences*. Elsevier, 238(116971), pp. 1–14. doi: 10.1016/j.lfs.2019.116971.

Oliveira, R. B., Canuto, L. P. and Collares-Buzato, C. B. (2019) 'Intestinal luminal content from high-fat-fed prediabetic mice changes epithelial barrier function in vitro', *Life Sciences*. Elsevier, 216(October 2018), pp. 10–21. doi: 10.1016/j.lfs.2018.11.012.

de Oliveira, R. B. *et al.* (2019) 'Time-dependent alteration to the tight junction structure of distal intestinal epithelia in type 2 prediabetic mice', *Life Sciences*, 238. doi: 10.1016/j.lfs.2019.116971.

Olokoba, A. B., Obateru, O. A. and Olokoba, L. B. (2012) 'Type 2 diabetes mellitus: A review of current trends', *Oman Medical Journal*, 27(4), pp. 269–273. doi: 10. 5001/omj.2012.68.

Pappan, K. L. *et al.* (2005) 'Pancreatic β-cell lipoprotein lipase independently regulates islet glucose metabolism and normal insulin secretion', *Journal of Biological Chemistry*, 280(10), pp. 9023–9029. doi: 10.1074/jbc.M409706200.

Patnala, R. *et al.* (2017) 'HDAC Inhibitor Sodium Butyrate-Mediated Epigenetic Regulation Enhances Neuroprotective Function of Microglia During Ischemic Stroke', *Molecular Neurobiology*, 54(8), pp. 6391–6411. doi: 10.1007/s12035-016-0149-z.

Peixoto, E. B. M. I. and Collares-Buzato, C. B. (2005) 'Protamine-induced epithelial barrier disruption involves rearrangement of cytoskeleton and decreased tight junction-associated protein expression in cultured MDCK strains.', *Cell structure and function*, 29(5–6), pp. 165–78. doi: 10.1247/csf.29.165.

Pessin, J. E. and Saltiel, A. R. (2000) 'Signaling pathways in insulin action : molecular targets of insulin resistance', *The Journal of clinical investigation*, 106(2), pp. 165–169. doi: 10.1172/JCI10582.

Pinnick, K. E. *et al.* (2008) 'Pancreatic ectopic fat is characterized by adipocyte infiltration and altered lipid composition.', *Obesity (Silver Spring, Md.)*, 16(3), pp. 522–530. doi: 10.1038/oby.2007.110.

Prentki, M. and Nolan, C. J. (2006) 'Islet b cell failure in type 2 diabetes', *The Journal of Clinical Investigation*, 116(7), pp. 1802–1812. doi: 10.1172/JCI29103.1802.

Rabbani, G. H. *et al.* (1999) 'Short-chain fatty acids inhibit fluid and electrolyte loss induced by cholera toxin in proximal colon of rabbit in vivo', *Digestive Diseases and Sciences*, 44(8), pp. 1547–1553. doi: 10.1023/A:1026650624193.

Rabbani, G. H. *et al.* (2001) 'Clinical studies in persistent diarrhea: dietary management with green banana or pectin in Bangladeshi children.', *Gastroenterology*, 121, pp. 554–560. doi: 10.1053/gast.2001.27178.

Della Ragione, F. *et al.* (2001) 'Genes modulated by histone acetylation as new effectors of butyrate activity', *FEBS Letters*, 499(3), pp. 199–204. doi: 10.1016/S0014-5793(01)02539-X.

Raposo, H. F. *et al.* (2015) 'Apolipoprotein CIII overexpression exacerbates diet-induced obesity due to adipose tissue higher exogenous lipid uptake and retention and lower lipolysis rates', *Nutrition & Metabolism*. Nutrition & Metabolism, pp. 1–10. doi: 10.1186/s12986-015-0058-6.

Rhodes, C. J. (2005) 'Type 2 Diabetes-a Matter of β-Cell Life and Death?', *Science*, 307(5708), pp. 380–4. doi: 10.1126/science.1104345.

Ricquier, D. (2017) 'UCP1, the mitochondrial uncoupling protein of brown adipocyte: A personal contribution and a historical perspective', *Biochimie*. Elsevier B.V, 134, pp. 3–8. doi: 10.1016/j.biochi.2016.10.018.

Rojczyk, E., Pałasz, A. and Wiaderkiewicz, R. (2015) 'Effect of short and long-term treatment with antipsychotics on orexigenic/anorexigenic neuropeptides expression in the rat hypothalamus', *Neuropeptides*. Elsevier Ltd, 51, pp. 31–42. doi: 10.1016/j.npep.2015.04.001.

De Ruijter, A. J. M. *et al.* (2003) 'Histone deacetylases (HDACs): Characterization of the classical HDAC family', *Biochemical Journal*, 370(3), pp. 737–749. doi: 10.1042/BJ20021321.

Sabatino, A. *et al.* (2017) 'Protein-energy wasting and nutritional supplementation in patients with end-stage renal disease on hemodialysis', *Clinical Nutrition*. Elsevier Ltd, 36(3), pp. 663–671. doi: 10.1016/j.clnu.2016.06.007.

Säemann, M. D. *et al.* (2000) 'Anti-inflammatory effects of sodium butyrate on human monocytes: potent inhibition of IL-12 and up-regulation of IL-10 production', *The FASEB Journal*, 14(15), pp. 2380–2382. doi: 10.1096/fj.00-0359fje.

Salvador, E., Burek, M. and Förster, C. Y. (2016) 'Tight Junctions and the Tumor Microenvironment', *Current Pathobiology Reports*, 4(3), pp. 135–145. doi: 10.1007/s40139-016-0106-6.

Santos, R. D. S. *et al.* (2018) 'Diet - induced glucose homeostasis dysregulation is enhanced by taurine supplementation in ovariectomized mice', *Amino Acids*. Springer Vienna, 50(3), pp. 469–477. doi: 10.1007/s00726-017-2533-z.

Sapone, A. *et al.* (2006) 'Zonulin upregulation is associated with increased gut permeability in subjects with type 1 diabetes and their relatives', *Diabetes*, 55(5), pp. 1443–1449. doi: 10.2337/db05-1593.

Scheithauer, T. P. M. *et al.* (2016) 'Causality of small and large intestinal microbiota in weight regulation and insulin resistance', *Molecular Metabolism*. Elsevier GmbH, 5(9), pp. 759–770. doi: 10.1016/j.molmet.2016.06.002.

Schultz, M. and Sartor, R. B. (2000) 'Probiotics and inflammatory bowel diseases', *The American journal of gastroenterology*, 95(1), pp. S19–S21. doi: https://doi.org/10.1016/S0002-9270(99)00812-6.

Shoelson, S. E. *et al.* (2006) 'Inflammation and insulin resistance', *The Journal of Clinical Investigation*, 116(7), pp. 1793–1801. doi: https://doi.org/10.1172/JCI29069.

Shulman, G. I. (2014) 'Ectopic Fat in Insulin Resistance, Dyslipidemia, and Cardiometabolic Disease', *The New England journal of medicine*, 31, pp. 1131–1141. doi: 10.1056/NEJMra1011035.

Singh, B., Halestrap, A. P. and Paraskeva, C. (1997) 'Butyrate can act as a stimulator of growth or inducer of apoptosis in human colonic epithelial cell lines depending on the presence of alternative energy sources', *Carcinogenesis*, 18(6), pp. 1265–1270. doi: 10.1093/carcin/18.6.1265.

Soares, G. M. *et al.* (2019) 'Whole-body ArhGAP21-deficiency improves energetic homeostasis in lean and obese mice', *Frontiers in Endocrinology*, 10(MAY), pp. 1–9. doi: 10.3389/fendo.2019.00338.

Sohail, M. U. *et al.* (2017) 'Role of the Gastrointestinal Tract Microbiome in the Pathophysiology of Diabetes Mellitus', *Journal of Diabetes Research*, 2017. doi:

10.1155/2017/9631435.

Sone, H. and Kagawa, Y. (2005) 'Pancreatic beta cell senescence contributes to the pathogenesis of type 2 diabetes in high-fat diet-induced diabetic mice', *Diabetologia*, 48(1), pp. 58–67. doi: 10.1007/s00125-004-1605-2.

Spiljar, M., Merkler, D. and Trajkovski, M. (2017) 'The immune system bridges the gut microbiota with systemic energy homeostasis: Focus on TLRs, mucosal barrier, and SCFAs', *Frontiers in Immunology*, 8(OCT), pp. 1–10. doi: 10.3389/fimmu.2017.01353.

Stamatovic, S. M. *et al.* (2017) 'Endocytosis of tight junction proteins and the regulation of degradation and recycling', *Annals of the New York Academy of Sciences*, 1397(1), pp. 54–65. doi: 10.1111/nyas.13346.

Stanford, K. I. *et al.* (2013) 'Brown adipose tissue regulates glucose homeostasis and insulin sensitivity', *Journal of Clinical Investigation*, 123(1), pp. 215–223. doi: 10.1172/JCI62308.

Sturgeon, C. and Fasano, A. (2016) 'Zonulin, a regulator of epithelial and endothelial barrier functions, and its involvement in chronic inflammatory diseases', *Tissue Barriers*. Taylor & Francis, 4(4), pp. 1–19. doi: 10.1080/21688370.2016.1251384.

Suzuki, T. (2013) 'Regulation of intestinal epithelial permeability by tight junctions', *Cellular and Molecular Life Sciences*, 70(4), pp. 631–659. doi: 10.1007/s00018-012-1070-x.

Suzuki, T. and Hara, H. (2010) 'Dietary fat and bile juice, but not obesity, are responsible for the increase in small intestinal permeability induced through the suppression of tight junction protein expression in LETO and OLETF rats', *Nutr Metab (Lond)*, 7, p. 19. doi: 10.1186/1743-7075-7-19.

Tang, Y. *et al.* (2010) 'Epithelial NF-κB enhances transmucosal fluid movement by altering tight junction protein composition after T cell activation', *American Journal of Pathology*. American Society for Investigative Pathology, 176(1), pp. 158–167. doi: 10.2353/ajpath.2010.090548.

Tang, Y. *et al.* (2011) 'G-protein-coupled receptor for short-chain fatty acids suppresses colon cancer', *International Journal of Cancer*, 128(4), pp. 847–856. doi: 10.1002/ijc.25638.

Tangvarasittichai, S. (2015) 'Oxidative stress, insulin resistance, dyslipidemia and type 2 diabetes mellitus.', *World journal of diabetes*, 6(3), pp. 456–80. doi: 10.4239/wjd.v6.i3.456.

Thomas, C. C. and Philipson, L. H. (2015) 'Update on Diabetes Classification', *Medical Clinics of North America*, 99(1), pp. 1–16. doi: 10.1016/j.mcna.2014.08.015.

Tremaroli, V. and Bäckhed, F. (2012) 'Functional interactions between the gut microbiota and host metabolism', *Nature*, 489(7415), pp. 242–249. doi: 10.1038/nature11552.

Tripathy, D. and Chavez, A. O. (2010) 'Defects in insulin secretion and action in the pathogenesis of type 2 diabetes mellitus', *Current Diabetes Reports*, 10(3), pp. 184–191. doi: 10.1007/s11892-010-0115-5.

Tsalamandris, S. *et al.* (2019) 'The role of inflammation in diabetes: Current concepts and future perspectives', *European Cardiology Review* , 14(1), pp. 50–59. doi: 10.15420/ecr.2018.33.1.

Ulluwishewa, D. *et al.* (2011) 'Regulation of tight junction permeability by intestinal bacteria and dietary components.', *The Journal of nutrition*, 141(5), pp. 769–776. doi: 10.3945/jn.110.135657.

Utech, M., Mennigen, R. and Bruewer, M. (2010) 'Endocytosis and recycling of tight junction proteins in inflammation', *Journal of Biomedicine and Biotechnology*, 2010. doi: 10.1155/2010/484987.

Valladares, R. *et al.* (2010) 'Lactobacillus johnsonii N6.2 mitigates the development of type 1 diabetes in BB-DP rats', *PLoS ONE*, 5(5). doi: 10.1371/journal.pone.0010507.

Veshnyakova, A. *et al.* (2012) 'Determinants contributing to claudin ion channel formation', *Annals of the New York Academy of Sciences*, 1257(1), pp. 45–53. doi: 10.1111/j.1749-6632.2012.06566.x.

Vijayaraghavan, K. (2010) 'Treatment of dyslipidemia in patients with type 2 diabetes', *Lipids in Health and Disease*, 9, pp. 1–12. doi: 10.1186/1476-511X-9-144.

Vinken, M. *et al.* (2009) 'Epigenetic regulation of gap junctional intercellular communication: More than a way to keep cells quiet?', *Biochimica et Biophysica Acta - Reviews on Cancer*. Elsevier B.V., 1795(1), pp. 53–61. doi: 10.1016/j.bbcan.2008.08.002.

Volynets, V. *et al.* (2015) 'Assessment of the Intestinal Barrier with Five Different Permeability Tests in Healthy C57BL/6J and BALB/cJ Mice', *Digestive Diseases and Sciences*. doi: 10.1007/s10620-015-3935-y.

Wang, H. B. *et al.* (2012) 'Butyrate enhances intestinal epithelial barrier function via up-regulation of tight junction protein claudin-1 transcription', *Digestive Diseases and Sciences*, 57(12), pp. 3126–3135. doi: 10.1007/s10620-012-2259-4.

Wang, L. *et al.* (2017) 'Fetal DNA hypermethylation in tight junction pathway is associated with neural tube defects: A genome-wide DNA methylation analysis', *Epigenetics*. Taylor & Francis, 12(2), pp. 157–165. doi: 10.1080/15592294.2016.1277298.

Wang, X. *et al.* (2015) 'Sodium butyrate alleviates adipocyte inflammation by inhibiting NLRP3 pathway'. doi: 10.1038/srep12676.

Wellen, K. E. and Hotamisligil, G. S. (2005) 'Inflammation , stress , and diabetes', 115(5), pp. 1111–1119. doi: 10.1172/JCI200525102.The.

Weyer, C. *et al.* (2000) 'Enlarged subcutaneous abdominal adipocyte size, but not obesity itself, predicts type II diabetes independent of insulin resistance', *Diabetologia*, 43(12), pp. 1498–1506. doi: 10.1007/s001250051560.

Wilcox, G. (2005) 'Insulin and insulin resistance', *Clin Biochem Rev*, 26(2), pp. 19–39. Available at:

http://www.ncbi.nlm.nih.gov/entrez/query.fcgi?cmd=Retrieve&db=PubMed&dopt=Citation&list_uids=16278749.

Willebrords, J. *et al.* (2016) 'Europe PMC Funders Group Strategies , models and biomarkers in experimental non- alcoholic fatty liver disease research', pp. 106–125. doi: 10.1016/j.plipres.2015.05.002.Strategies.

World Health Organization (2016) 'Global Report on Diabetes', *Isbn*, 978, p. 88. doi: ISBN 978 92 4 156525 7.

Wu, Y. *et al.* (2014) 'Risk factors contributing to type 2 diabetes and recent advances in the treatment and prevention', *International journal of medical sciences*, 11(11), pp. 1185–1200. doi: 10.7150/ijms.10001.

Xiong, Y. *et al.* (2004) 'Short-chain fatty acids stimulate leptin production in adipocytes through the G protein-coupled receptor GPR41.', *Proceedings of the National Academy of Sciences of the United States of America*, 101(4), pp. 1045–50. doi: 10.1073/pnas.2637002100.

Y Lee, C. (2013) 'The Effect of High-Fat Diet-Induced Pathophysiological Changes in the Gut on Obesity: What Should be the Ideal Treatment?', *Clinical and translational gastroenterology*. Nature Publishing Group, 4(7), p. e39. doi: 10.1038/ctg.2013.11.

Ye, J. (2008) 'Regulation of PPARγ function by TNF-α', *Biochemical and Biophysical Research Communications*, 374(3), pp. 405–408. doi: 10.1038/jid.2014.371.

Yki-Järvinen, H. (2015) 'Nutritional modulation of non-alcoholic fatty liver disease and insulin resistance', *Nutrients*, 7(11), pp. 9127–9138. doi: 10.3390/nu7115454.

Zhang, L. *et al.* (2017) 'Sodium Butyrate Protects Against High Fat Diet-Induced Diabetic Mice', *Journal of Cellular Biochemistry*, 118, pp. 2395–2408. doi: 10.1002/jcb.25902.

Zhang, W.-Q. *et al.* (2019) 'Sodium Butyrate Improves Liver Glycogen Metabolism in Type 2 Diabetes Mellitus', *Journal of Agricultural and Food Chemistry*, 67, pp. 7694–7705. doi: 10.1021/acs.jafc.9b02083.

ANEXO I

UNICAMP

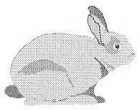

CEUA/Unicamp

Comissão de Ética no Uso de Animais
CEUA/Unicamp

C E R T I F I C A D O

Certificamos que o projeto de pesquisa intitulado "**Regulação epigenética de proteínas da junção de oclusão pelo Butirato: emprego de modelos in vivo e in vitro de quebra de barreira epitelial intestinal na pré-diabetes e após exposição a ácidos graxos.**", (protocolo CEUA/UNICAMP nº **4185-1**), de responsabilidade da **Profª. Drª. Carla Beatriz Collares Buzato** e da aluna **Valquíria Aparecida Matheus**, teve o título alterado para "**Ação anti-diabetogênica do butirato de sódio e seu efeito protetor sobre a barreira epitelial intestinal em camundongos alimentados com dieta hiperlipídica**".

Este documento é válido apenas se apresentado junto com o certificado emitido originalmente pela CEUA/UNICAMP em 02/06/2016.

Campinas, 19 de novembro de 2019.

Prof. Dr. Wagner José Fávaro
Presidente da CEUA/UNICAMP

Rosangela dos Santos
Secretária Executiva

CEUA/UNICAMP
Caixa Postal 6109
13083-970 Campinas, SP – Brasil

Telefone: (19) 3521-6359
E-mail: comisib@unicamp.br
http://www.ib.unicamp.br/ceea/

ANEXO II

DECLARAÇÃO

Declaro para os devidos fins que o conteúdo de minha **Tese de Doutorado** intitulada " Ação anti-diabetogênica do butirato de sódio e seu efeito protetor sobre a barreira epitelial intestinal em camundongos alimentados com dieta hiperlipídica ":

( ) não se enquadra no § 4º do Artigo 1º da Informação CCPG 002/13, referente a bioética e biossegurança.

Tem autorização da(s) seguinte(s) Comissão(ões):

( ) CIBio – Comissão Interna de Biossegurança , projeto No. _____, Instituição: _____.

(X) CEUA – Comissão de Ética no Uso de Animais , projeto No. 3439-1, Instituição: Instituto de Biologia, Universidade Estadual de Campinas.

_____.

( ) CEP - Comissão de Ética em Pesquisa, protocolo No. _____, Instituição: _____

** Caso a Comissão seja externa ao IB/UNICAMP, anexar o comprovante de autorização dada ao trabalho. Se a autorização não tiver sido dada diretamente ao trabalho de tese ou dissertação, deverá ser anexado também um comprovante do vínculo do trabalho do aluno com o que constar no documento de autorização apresentado.*

Aluna: Valquiria Aparecida Matheus

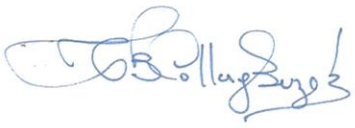

Orientadora: Carla Beatriz Collares Buzato

Para uso da Comissão ou Comitê pertinente:
( ) Deferido ( ) Indeferido

Carimbo e assinatura

Para uso da Comissão ou Comitê pertinente:
( ) Deferido ( ) Indeferido

Carimbo e assinatura

ANEXO III

Declaração

As cópias de artigos de minha autoria ou de minha co-autoria, já publicados ou submetidos para publicação em revistas científicas ou anais de congressos sujeitos a arbitragem, que constam da minha Tese de Doutorado, intitulada **" Ação anti-diabetogênica do butirato de sódio e seu efeito protetor sobre a barreira epitelial intestinal em camundongos alimentados com dieta hiperlipídica"**, não infringem os dispositivos da Lei nº 9.610/98, nem o direito autoral de qualquer editora.

Campinas, 06 de Junho de 2020.

Autora: Valquiria Aparecida Matheus
RG nº 29.019.958-X

Orientadora: Profa. Dra. Carla Beatriz Collares Buzato
RG nº 15.281.910